ENCLOSURE 3

TENNESSEE VALLEY AUTHORITY
BROWNS FERRY NUCLEAR PLANT (BFN)
UNITS 1, 2, AND 3

TECHNICAL SPECIFICATIONS (TS) CHANGES TS-431 AND TS-418 -
EXTENDED POWER UPRATE (EPU) - REPLACEMENT DOCUMENTATION
(TAC NOS. MC3812, MC3743, AND MC3744)

CDI REPORT NO. 05-28P, REV. 1, "BOUNDING METHODOLOGY TO PREDICT
FULL SCALE STEAM DRYER LOADS FROM IN-PLANT MEASUREMENTS"

(REDACTED VERSION)

This enclosure provides CDI Report No. 05-28P, Rev. 1, "Bounding Methodology to Predict Full Scale Steam Dryer Loads from In-Plant Measurements" (redacted version).

This Report Does Not Contain Continuum Dynamics, Inc. Proprietary Information

C.D.I. Report No. 05-28P

Bounding Methodology to Predict Full Scale Steam Dryer Loads from In-Plant Measurements (C.D.I. Proprietary)

Revision 1

Prepared by

Continuum Dynamics, Inc.
34 Lexington Avenue
Ewing, NJ 08618

Approved by

Alan J. Bilanin

May 2006

Executive Summary

Measured in-plant pressure time-history data in the four main steam lines of Quad Cities Unit 2 (QC2), inferred from strain gage data collected at two positions upstream of the ERV standpipes on each of the main steam lines, were used with Continuum Dynamics, Inc.'s acoustic model of the QC2 steam dome and steam lines to predict steam dryer loads. The strain gage data were first converted to pressures, and were then used to extract acoustic sources in the system. Once these sources were obtained, the model was used to predict the pressure time histories at 27 locations on the steam dryer, where pressure sensors were positioned. These predictions were then compared against data from the pressure sensors, and the model was modified to meet acceptance criteria based on degree of conservatism in the predictive loads.

These results provide an acoustic circuit model that bounds the pressure loads on a steam dryer, thereby enabling the dryer to be analyzed structurally for its fitness during power ascension and EPU operations.

Analysis of QC2 at power levels of 790, 842, and 930 MWe, which correspond to main steam line Mach numbers of 0.113, 0.122, and 0.135, respectively, show that the predictions are most conservative for lower Mach numbers. Since QC1 and QC2 have the highest main steam line Mach numbers in the domestic fleet at EPU conditions, the model can be confidently used with data taken from other plants to conservatively compute steam dryer loads during power ascension.

The recommended model for EPU conditions, as discussed in the report, is shown to have the following conservatism, defined as the relative standard deviation averaged over 20 pressure sensors on the QC2 steam dryer, in percentage:

Plant	EPU Mach number	Minimum Peak Pressure	Maximum Peak Pressure	RMS	Maximum PSD
Browns Ferry	0.097	[[			
Hope Creek	0.113				
Quad Cities 2	0.135				
Susquehanna	0.113				
Vermont Yankee	0.113				[3]]]

Table of Contents

I. Introduction

In the spring of 2005, Exelon Generation LLC installed new steam dryers into its Quad Cities Unit 2 (QC2) and Quad Cities Unit 1 nuclear power plants. The replacement design, developed by General Electric, sought to improve dryer performance and overcome structural inadequacies identified on the original dryers. The design had been previously analyzed by extrapolating acoustic circuit model predictions from the original dryer to produce expected full-scale vulnerability loads [1] and from modeling the new dryer in the SMT (subscale model test) to produce corresponding loads from subscale data [2]. The QC2 dryer was instrumented with pressure sensors at 27 locations, and these data could be used to validate the acoustic circuit model. These pressure data formed the set of data to be first predicted (blind evaluation) and then corrected (modified evalution) utilizing only data measured on the main steam lines. Data collection was undertaken at 790 MWe (2493 MWt), just short of Original Licensed Thermal Power (OLTP) conditions, and at 930 MWe (2885 MWt), near Extended Power Uprate (EPU) conditions. At QC2, OLTP is rated at 2511 MWt, while EPU is rated at 2957 MWt.

These results, encompassing (1) a blind evaluation at 790 MWe, (2) a modified evaluation at 790 MWe, (3) a blind evaluation at 930 MWe, (4) a modified evaluation at 930 MWe, (5) a pressure sensor evaluation at 930 MWe, and (6) a strain gage and pressure sensor evaluation at 930 MWe, are described in [3]. A later blind evaluation at 912 MWe (2831 MWt) and an evaluation at 842 MWe (2493 MWt) are described in [4]. The accuracy of these model predictions was judged by model agreement with data at six of the pressure sensors mounted on the steam dryer. Following further review, it became clear that, although model evaluations (4) and (6) tracked the data well for most pressure sensors, the data from several of the pressure sensors were underpredicted in the critical frequency range of 145 Hz to 165 Hz. Thus, Exelon requested that model parameters be re-examined to see whether a better comparison with the pressure sensor data could be achieved. That effort resulted in a model that matched the mean of the root mean square (RMS) of the pressure data at the 26 operational sensors on the QC2 dryer [5].

The work reported herein develops acoustic circuit model parameters which result in dryer pressure load predictions on the outside of the steam dryer that bound the pressure loads measured there, and therefore provide steam dryer load predictions that are even more conservative than those reported above.

II. Overview of Methodology

The QC2 steam supply system is broken into two distinct analyses: a Helmholtz solution within the steam dome and an acoustic circuit analysis in the main steam lines. This section of the report highlights the two approaches taken here. All analysis is undertaken in frequency space and the pressure P used here is the Fourier transformed pressure.

2.1 Helmholtz Analysis

The three-dimensional geometry of a steam dome and steam dryer is rendered onto a uniformly-spaced rectangular grid, and a solution is obtained for the Helmholtz equation

$$\frac{\partial^2 P}{\partial x^2}+\frac{\partial^2 P}{\partial y^2}+\frac{\partial^2 P}{\partial z^2}+\frac{\omega^2}{a^2}P=\nabla^2 P+\frac{\omega^2}{a^2}P=0 \qquad (2.1)$$

where P is the pressure at a grid point, ω is frequency, and a is acoustic speed. This equation is solved for incremental frequencies from 0 to 200 Hz, subject to the boundary conditions

$$\frac{dP}{dn}=0 \qquad (2.2)$$

normal to all solid surfaces (the steam dome wall and interior and exterior surfaces of the dryer),

$$\frac{dP}{dn}\propto\frac{i\omega}{a}P \qquad (2.3)$$

normal to the nominal water level surface, and unit pressure applied to one inlet to a main steam line and zero applied to the other three. In all of the equations presented here, $i=\sqrt{-1}$, and time dependence of the form $e^{i\omega t}$ is implied.

2.2 Acoustic Circuit Analysis

The Helmholtz solution within the steam dome is coupled to an acoustic circuit solution in the main steam lines. Pulsation in a single-phase compressible medium, where acoustic wavelengths are long compared to component dimensions, and in particular long compared to transverse dimensions (directions perpendicular to the primary flow directions), lend themselves to application of the acoustic circuit methodology. If the analysis is restricted to frequencies below 200 Hz, acoustic wavelengths are approximately eight feet in length, and wavelengths are therefore long compared to most components of interest, such as branch junctions.

Acoustic circuit analysis divides the main steam lines into elements which are each characterized by a length L, a cross-sectional area A, a fluid mean density ρ, a fluid mean flow velocity $\overline{U}$, and a fluid acoustic speed a.

Application of acoustic circuit methodology generates solutions for the fluctuating pressure P_n and velocity u_n in the n^{th} element of the form

$$P_n = \left[A_n e^{ik_{1n}X_n} + B_n e^{ik_{2n}X_n}\right] e^{i\omega t} \tag{2.4}$$

$$u_n = -\frac{1}{\rho a^2}\left[\frac{(\omega + \overline{U}_n k_{1n})}{k_{1n}} A_n e^{ik_{1n}X_n} + \frac{(\omega + \overline{U}_n k_{2n})}{k_{2n}} B_n e^{ik_{2n}X_n}\right] e^{i\omega t} \tag{2.5}$$

where harmonic time dependence of the form $e^{i\omega t}$ has been assumed. The wave numbers k_{1n} and k_{2n} are the two complex roots of the equation

$$k_n^2 + i\frac{f_n|\overline{U}_n|}{D_n a^2}(\omega + \overline{U}_n k_n) - \frac{1}{a^2}(\omega + \overline{U}_n k_n)^2 = 0 \tag{2.6}$$

where f_n is the pipe friction factor for element n and D_n is the hydrodynamic diameter for element n. A_n and B_n are complex constants which are a function of frequency and are determined by satisfying continuity of pressure and mass conservation at element junctions.

2.3 Modeling Parameters

When the steam dryer geometry is defined and the physical parameters at the power level of interest are provided (such as the mean steam flow in the main steam lines), the Helmholtz and acoustic circuit analyses are driven by five modeling parameters: (1) the damping in the steam dome, (2) the proportionality constant in Equation 2.3 at the steam-froth interface beneath the steam dryer, (3) the proportionality constant in Equation 2.3 at the steam-water interface between the dryer skirt and steam dome, (4) the damping in the main steam lines, and (5) the main steam line friction factor. The purpose of this evaluation is modify these parameters to build conservatism into model predictions when compared against full-scale test data.

2.4 Model Assembly and Algorithm

[[

[3]]]

[[

_____[3]]]

[[

[3]]]

III. Quad Cities Unit 2 Instrumentation and Plant Data

Strain gage pairs were mounted at two locations on the main steam lines, upstream of the ERV standpipes, as summarized in Table 3.1. These data proved reliable throughout the QC2 startup. Pressure sensors were positioned at 27 locations inside and outside the dryer, and were designated P1 to P27. The locations of the transducers can be found in [7]. Sensor P19 failed during the startup and was not used for comparisons. The strain gage data were taken at 2000 samples/second, while the pressure sensor data were taken at 2048 samples/second, on different recorders. Thus, the two data sets each included a channel for a trigger. In this way a common zero time could be established for the strain gage pairs and the pressure sensors, so as to eliminate any phasing difficulties. The sampling rate was sufficient, as the analysis was conducted to 200 Hz.

Data used in this analysis were taken at the power level of 930 MWe (test condition TC41, at EPU).

Table 3.1. Location of strain gage pairs on main steam lines [3].

Main Steam Line	N	Strain Gage Designation	Orientation	Elevation (ft)	Distance from Steam Dome (ft)
A	1	S1/S3	In Plane	651	9.5
		S2/S4	Out of Plane	651	9.5
A	2	S5/S5A	In Plane	624	41.0
		S6/S6A	Out of Plane	624	41.0
B	3	S7/S9	In Plane	651	9.5
		S8/S10	Out of Plane	651	9.5
B	4	S11/S11A	In Plane	624	41.3
		S12/S12A	Out of Plane	624	41.3
C	5	S31/S33	In Plane	651	9.5
		S32/S34	Out of Plane	651	9.5
C	6	S35/S35A	In Plane	624	41.3
		S36/S36A	Out of Plane	624	41.3
D	7	S37/S39	In Plane	651	9.5
		S38/S40	Out of Plane	651	9.5
D	8	S41/S41A	In Plane	624	41.0
		S42/S42A	Out of Plane	624	41.0

IV. Model Predictions and Comparisons

Previous model evaluation predictions [3, 4, 5] demonstrated comparison with pressure sensor data at all 26 locations, as seen in Figures 4.1 and 4.2. Figure 4.1 was generated by subtracting the data pressure range at each operational pressure sensor from the predicted pressure range at each sensor (pressure range is the sum of the maximum pressure and the absolute value of the minimum pressure over the time interval analyzed). Figure 4.2 was generated by subtracting the data RMS at each operational pressure sensor from the predicted RMS at each sensor. Pressure differences below zero mean that the model underpredicts the data there.

The acceptance criterion for the Modified Prediction and Minimum Error predictions was that the pressure predictions at P3, P6, P9, and P12 had to be within 90% of the data. These models achieved this criterion, but did not give bounding comparisons with the other sensors (as seen by examination of Figure 4.1). Model parameters (described in Section II) were therefore modified to improve model predictions substantially at the rest of the pressure sensors. Principally, it was determined that a reduction in the proportionality constant in Equation 2.3 at the steam-water interface between the dryer and the steam dome improved model performance, but that the greatest effect was a further reduction in the damping in the steam dome. Damping in the steam dome controls the magnitude of the pressure predictions on the steam dryer, and lower values of damping had the general effect of increasing the pressure across the dryer. The criterion followed was to find the damping factor that most improved the pressure predictions.

The reduction in steam dome damping then required an adjustment to the damping in the main steam line. The criterion here was to minimize the sum of the squares of the difference between predicted RMS and data RMS, for the 26 pressure sensors. Table 4.1 summarizes the normalized model parameter changes that result in the Minimum RMS prediction.

Table 4.1. Acoustic Circuit Model Parameter Factors.

[[

$^{(3)}$]]

With these improvements it may be seen that not all of the pressure sensor data are bounded (if the acoustic circuit model bounds the data, all of the ΔPressure Range and ΔRMS green dots would be at or above zero in Figures 4.1 and 4.2). This is especially true when a comparison is made with the maximum ΔPSD predicted by the three models (Figure 4.3); here it may be seen that nearly all PSD peaks from measured data are underpredicted by these three models.

[[

(3)]]

Figure 4.1. Modified Prediction (red curve), Minimum Error (black curve), and Minimum RMS (green curve) – with 930 MWe data subtracted – for Pressure Range. A value of zero or larger indicates a conservative Pressure Range prediction at that sensor.

[[

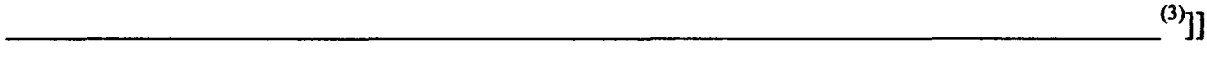

(3)]]

Figure 4.2. Modified Prediction (red curve), Minimum Error (black curve), and Minimum RMS (green curve) – with 930 MWe data subtracted – for RMS Pressure. A value of zero or larger indicates a conservative RMS prediction at that sensor.

[[

$^{(3)}$]]

Figure 4.3. Modified Prediction (red curve), Minimum Error (black curve), and Minimum RMS (green curve) – with 930 MWe data subtracted – for Maximum PSD. A value of zero or larger indicates a conservative Maximum PSD prediction at that sensor.

Note that sensors P13, P14, P16, P23, and P27 are positioned inside the dryer, that P26 is on a mast above the dryer, and that P19 is inoperative.

The Modified Prediction solution just matches the acceptance criterion on P3, P6, P9, and P12, while the Minimum Error solution improves the skirt loads on P22 and P25 and the Minimum RMS solution bounds nearly all pressure sensors on the outside of the dryer. However, none of these predictions bounds all of the pressure data on the outside of the dryer.

It is with this background that more conservative acoustic circuit model parameters were developed.

4.1 Bounding Pressure

The first solution extends the Minimum RMS solution so that the minimum and maximum pressure predictions at all pressure sensors on the outside of the dryer bound the data. This extension required an increase in the main steam line damping (model parameters summarized in Table 4.2). Model comparisons with data show the results (Figure 4.4), while the RMS pressure and Maximum PSD are not all bounded (Figures 4.5 and 4.6, respectively). The acoustic circuit model using these modeling parameters is denoted as the "Bounding Pressure" model.

4.2 Bounding RMS

The second solution modifies the Bounding Pressure solution so that the RMS of the pressure at all pressure sensors on the outside of the dryer bound the data. This extension required nearly a doubling in the main steam line damping (Table 4.2). Model comparisons with data show that the minimum and maximum values of nearly all of the outside pressure sensors are bounded by the prediction (Figure 4.7), while RMS pressures are bounded (Figure 4.8) but Maximum PSD values are still not (Figure 4.9). The acoustic circuit model using these modeling parameters is denoted as the "Bounding RMS" model.

4.3 Bounding PSD

The third solution modifies the Bounding RMS pressure solution so that the Maximum PSD of the pressure at all pressure sensors on the outside of the dryer bound the data. This extension required nearly a 50% increase in the main steam line damping (Table 4.2). Model comparisons with data show that the minimum and maximum values of all of the outside pressure sensors are bounded by the prediction (Figure 4.10), as are RMS pressures (Figure 4.11), except for P27, and Maximum PSD values (Figure 4.12), except for P16 and P27 as well. The acoustic circuit model using these modeling parameters is denoted as the "Bounding PSD" model.

Table 4.2. Additional Acoustic Circuit Model Parameter Factors.

[[

[3]]]

Direct comparisons may be made for the values plotted in Figures 4.4 to 4.12 in Table 4.3 (minimum pressure), Table 4.4 (maximum pressure), Table 4.5 (RMS), and Table 4.6 (maximum PSD). The conservatism built into the model may be summarized by computing the relative standard deviation across the pressure sensors. The relative standard deviation as used here is defined as

$$RSD = \frac{\sqrt{\frac{1}{N}\sum_{n=1}^{N}[P_P - P_D]^2}}{\frac{1}{N}\sum_{n=1}^{N}|P_D|} \qquad (4.1)$$

where P_P is the predicted pressure (or RMS or PSD), P_D is the measured pressure (or RMS or PSD), and N is the number of outside pressure sensors (N = 20). A PSD comparison at all pressure sensors is shown in Appendix C for 930 MWe.

[[

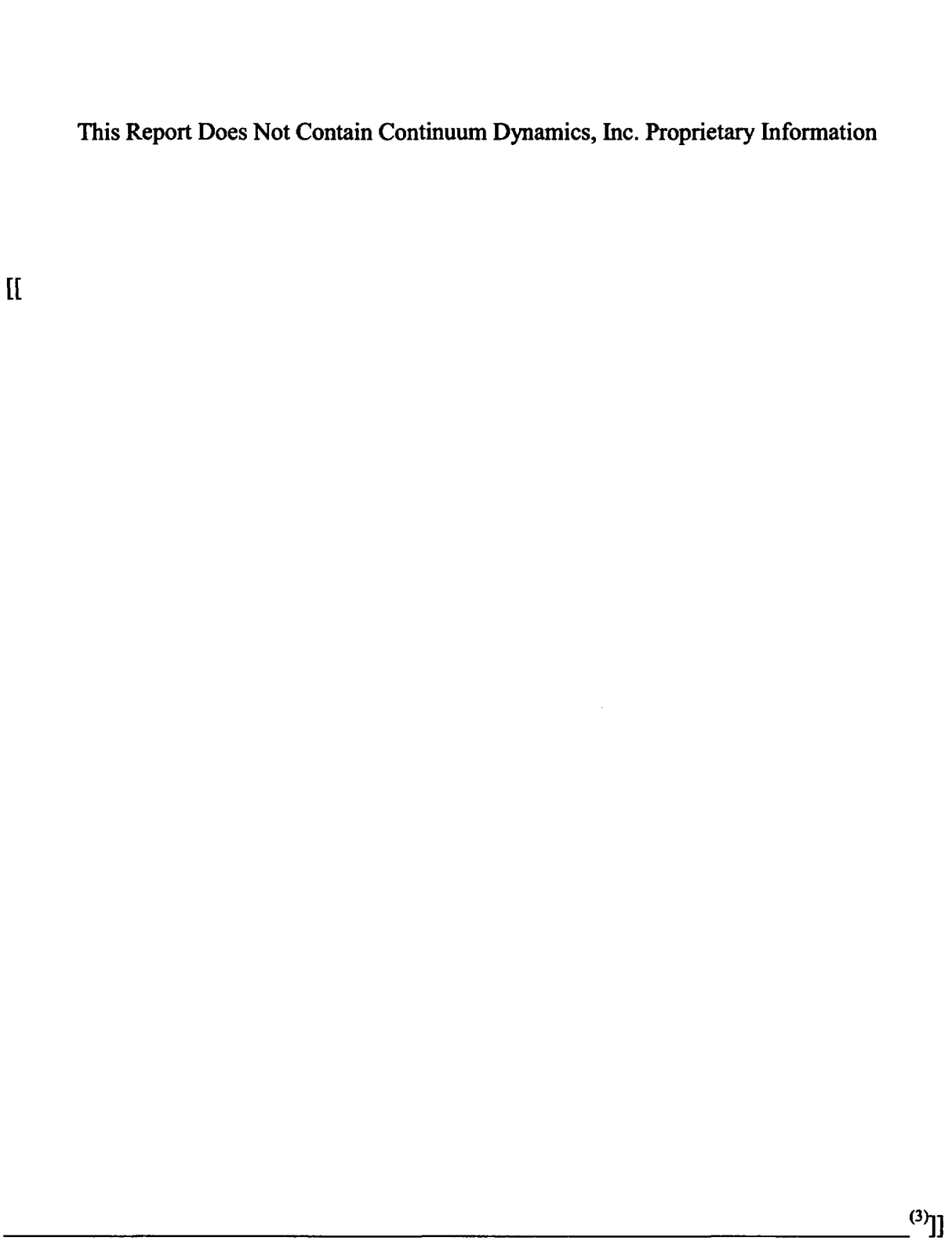

(3)]]

Figure 4.4. Bounding Pressure predictions at 930 MWe at the operational pressure sensors: peak minimum (top) and peak maximum (bottom) pressure levels, with data (red), outside predictions (black), and inside predictions (blue). Sensors P13, P14, P16, P23, and P27 are inside the dryer, while P26 is on a mast above the dryer, and P19 is inoperative.

[[

(3)]]

Figure 4.5. Corresponding RMS predictions at 930 MWe for Bounding Pressure at the operational pressure sensors, with data (red), outside predictions (black), and inside predictions (blue).

[[

(3)]]

Figure 4.6. Corresponding PSD predictions at 930 MWe for Bounding Pressure at the operational pressure sensors, with data (red), outside predictions (black), and inside predictions (blue).

[[

(3)]]

[[

(3)]]

Figure 4.7. Bounding RMS predictions at 930 MWe at the operational pressure sensors: peak minimum (top) and peak maximum (bottom) pressure levels, with data (red), outside predictions (black), and inside predictions (blue). Sensors P13, P14, P16, P23, and P27 are inside the dryer, while P26 is on a mast above the dryer, and P19 is inoperative.

[[

(3)]]

Figure 4.8. Corresponding RMS predictions at 930 MWe for Bounding RMS pressure at the operational pressure sensors, with data (red), outside predictions (black), and inside predictions (blue).

[[

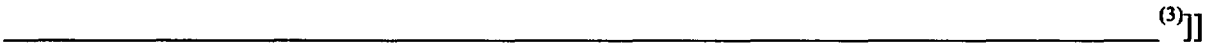

(3)]]

Figure 4.9. Corresponding PSD predictions at 930 MWe for Bounding RMS pressure at the operational pressure sensors, with data (red), outside predictions (black), and inside predictions (blue).

[[

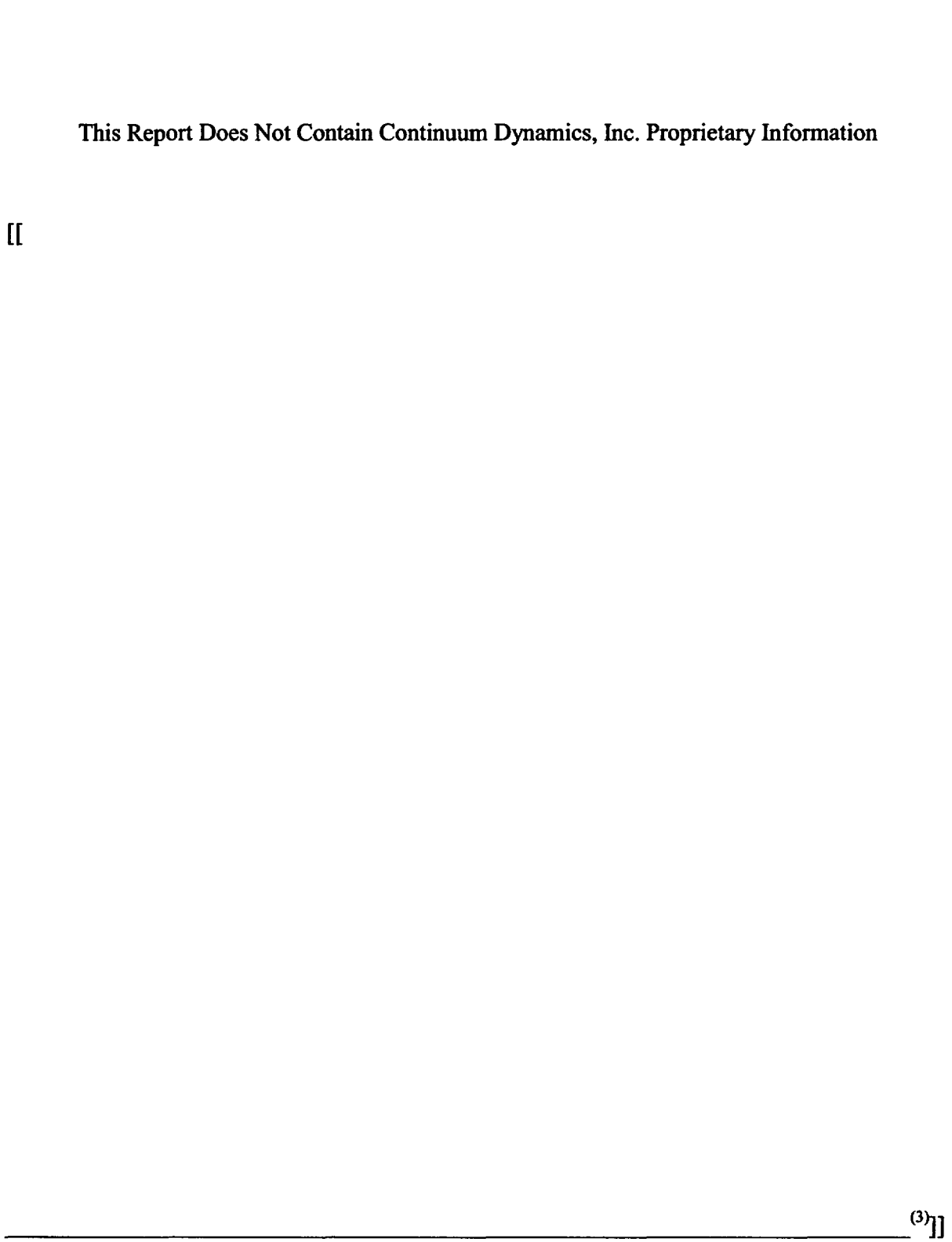

[3]]]

Figure 4.10. Bounding PSD predictions at 930 MWe at the operational pressure sensors: peak minimum (top) and peak maximum (bottom) pressure levels, with data (red), outside predictions (black), and inside predictions (blue). Sensors P13, P14, P16, P23, and P27 are inside the dryer, while P26 is on a mast above the dryer, and P19 is inoperative.

[[

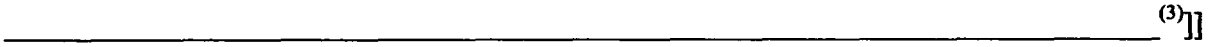

(3)]]

Figure 4.11. Corresponding RMS predictions at 930 MWe for Bounding PSD at the operational pressure sensors, with data (red), outside predictions (black), and inside predictions (blue).

[[

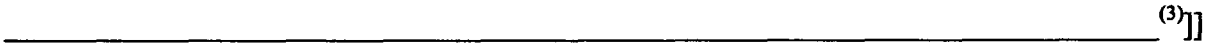

(3)]]

Figure 4.12. Corresponding PSD predictions at 930 MWe for Bounding PSD pressure at the operational pressure sensors, with data (red), outside predictions (black), and inside predictions (blue).

Table 4.3. Comparison between the 930 MWe data and the Bounding Pressure, Bounding RMS, and Bounding PSD predictions for minimum pressure. The data have been filtered to include the frequencies from 0 Hz to 200 Hz only. Standard deviation and relative standard deviation do not include P13, P14, P16, P23, P26, or P27.

[[

]](3)]]

Table 4.4. Comparison between the 930 MWe data and the Bounding Pressure, Bounding RMS, and Bounding PSD predictions for maximum pressure. The data have been filtered to include the frequencies from 0 Hz to 200 Hz only. Standard deviation and relative standard deviation do not include P13, P14, P16, P23, P26, or P27.

[[

[3]]

Table 4.5. Comparison between the 930 MWe data and the Bounding Pressure, Bounding RMS, and Bounding PSD predictions for RMS pressure. The data have been filtered to include the frequencies from 0 Hz to 200 Hz only. Standard deviation and relative standard deviation do not include P13, P14, P16, P23, P26, or P27.

[[

[3]]]

Table 4.6. Comparison between the 930 MWe data and the Bounding Pressure, Bounding RMS, and Bounding PSD predictions for maximum PSD. The data have been filtered to include the frequencies from 0 Hz to 200 Hz only. Standard deviation and relative standard deviation do not include P13, P14, P16, P23, P26, or P27.

[[

(3)]]

V. Comparison with Additional Power Levels

Two additional power levels were examined with the bounding models determined from the previous analysis of the 930 MWe data. These power levels are summarized in Table 5.1.

Table 5.1. Summary of the Power Levels Examined with the Bounding Methodology.

Exelon Test Condition	Electric Power Level (MWe)	Thermal Power Level (MWt)	MSL Flow Velocity (ft/sec)	Mach Number
TC32B (OLTP)	790	2430	168	0.113
TC35	842	2626	181	0.122
TC41 (EPU)	930	2887	200	0.135

The 790 MWe data were considered first, with summary results shown in Figures 5.1 to 5.6. Here it may be seen that the Bounding Pressure parameters bound all outside pressure sensors for both minimum and maximum pressure (Figure 5.1) and for RMS (Figure 5.2). In fact, nearly all outside pressure sensors are bounded for PSD maximum by the Bounding Pressure parameters (Figure 5.3). Direct comparisons may be made for the values plotted in Figures 5.1 to 5.3 in Table 5.2 (minimum pressure), Table 5.3 (maximum pressure), Table 5.4 (RMS), and Table 5.5 (maximum PSD). A PSD comparison at all pressure sensors is shown in Appendix A for 790 MWe.

The 842 MWe data were considered next, with summary results shown in Figures 5.7 to 5.12. Here it may be seen that the Bounding Pressure parameters indeed bound all outside pressure sensors for both minimum and maximum pressure (Figure 5.7) and for RMS (Figure 5.8), but not PSD Maximum (Figure 5.9). Bounding RMS parameters bound pressures, RMS, and PSD (Figures 5.10 to 5.12). Direct comparisons may be made for the values plotted in Figures 5.7 to 5.9 in Table 5.6 (minimum pressure), Table 5.7 (maximum pressure), Table 5.8 (RMS), and Table 5.9 (maximum PSD). A PSD comparison at all pressure sensors is shown in Appendix B for 842 MWe.

The Bounding Pressure parameters could therefore be used with lower values of main steam line flow velocity, below 180 ft/sec, to bound pressures, RMS, and maximum PSD. The conservatism that exists at these lower main stream line flow velocities has been built into the model by underestimating the main steam line damping that is velocity dependent (see Equation 2.6) at 930 MWe (M = 0.135).

[[

[3]]]

[[

[3]]]

Figure 5.1. Bounding Pressure predictions (790 MWe) at the operational pressure sensors: peak minimum (top) and peak maximum (bottom) pressure levels, with data (red), outside predictions (black), and inside predictions (blue). Sensors P13, P14, P16, P23, and P27 are inside the dryer, while P26 is on a mast above the dryer, and P19 is inoperative.

[[

[3]]]

Figure 5.2. Corresponding RMS predictions (790 MWe) for Bounding Pressure at the operational pressure sensors, with data (red), outside predictions (black), and inside predictions (blue).

[[

[3]]]

Figure 5.3. Corresponding PSD predictions (790 MWe) for Bounding Pressure at the operational pressure sensors, with data (red), outside predictions (black), and inside predictions (blue).

Table 5.2. Comparison between the 790 MWe data and the Bounding Pressure predictions for minimum pressure. The data have been filtered to include the frequencies from 0 Hz to 200 Hz only. Standard deviation and relative standard deviation do not include P13, P14, P16, P23, P26, or P27.

[[

(3)]]

Table 5.3. Comparison between the 790 MWe data and the Bounding Pressure predictions for maximum pressure. The data have been filtered to include the frequencies from 0 Hz to 200 Hz only. Standard deviation and relative standard deviation do not include P13, P14, P16, P23, P26, or P27.

[[

(3)]]

Table 5.4. Comparison between the 790 MWe data and the Bounding Pressure predictions for RMS pressure. The data have been filtered to include the frequencies from 0 Hz to 200 Hz only. Standard deviation and relative standard deviation do not include P13, P14, P16, P23, P26, or P27.

[[

]]$^{(3)}$

Table 5.5. Comparison between the 790 MWe data and the Bounding Pressure predictions for maximum PSD. The data have been filtered to include the frequencies from 0 Hz to 200 Hz only. Standard deviation and relative standard deviation do not include P13, P14, P16, P23, P26, or P27.

[[

(3)]]

[[

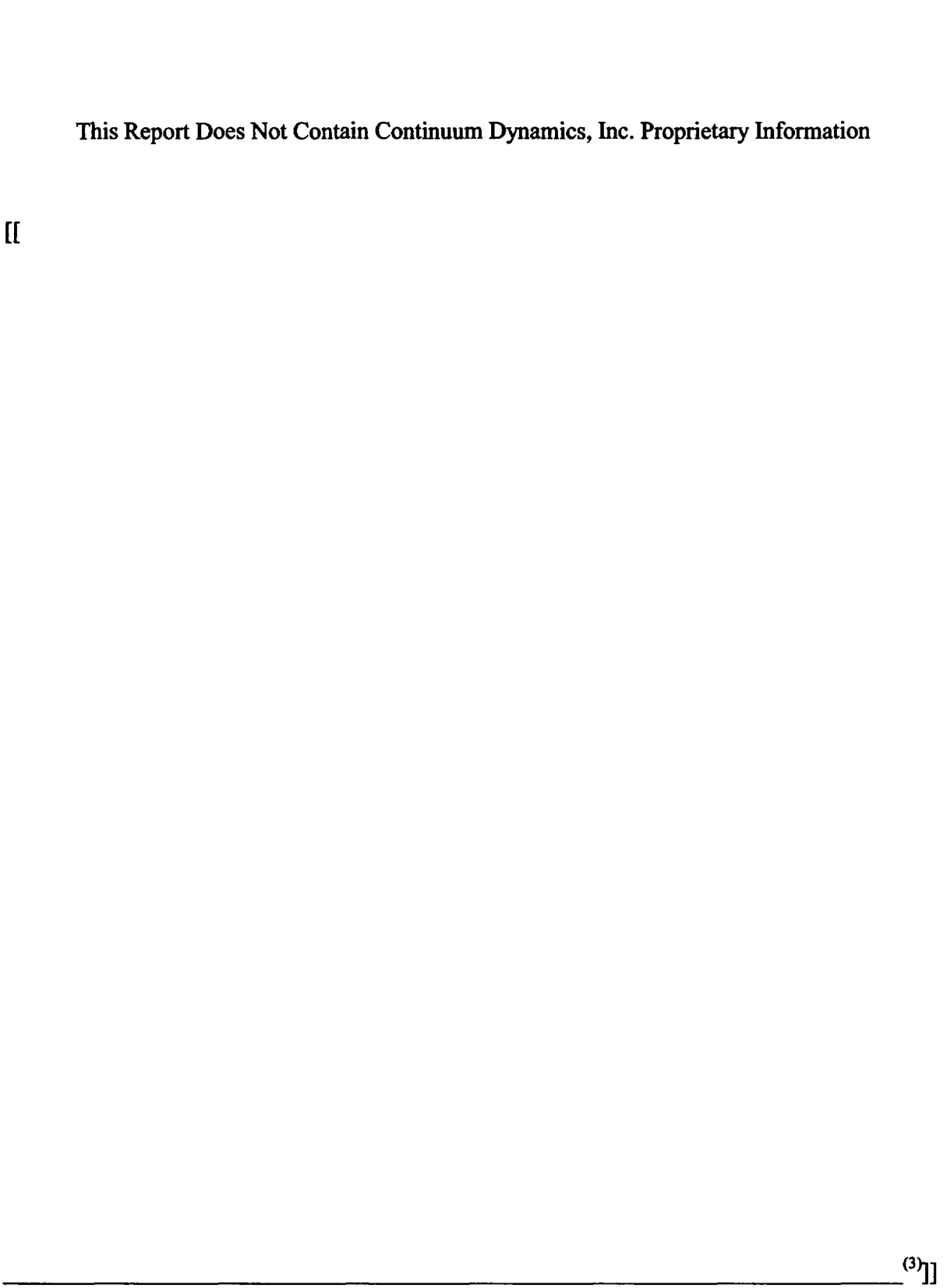

(3)]]

Figure 5.7. Bounding Pressure predictions (842 MWe) at the operational pressure sensors: peak minimum (top) and peak maximum (bottom) pressure levels, with data (red), outside predictions (black), and inside predictions (blue). Sensors P13, P14, P16, P23, and P27 are inside the dryer, while P26 is on a mast above the dryer, and P19 is inoperative.

[[

(3)]]

Figure 5.8. Corresponding RMS predictions (842 MWe) for Bounding Pressure at the operational pressure sensors, with data (red), outside predictions (black), and inside predictions (blue).

[[

(3)]]

Figure 5.9. Corresponding PSD predictions (842 MWe) for Bounding Pressure at the operational pressure sensors, with data (red), outside predictions (black), and inside predictions (blue).

[[

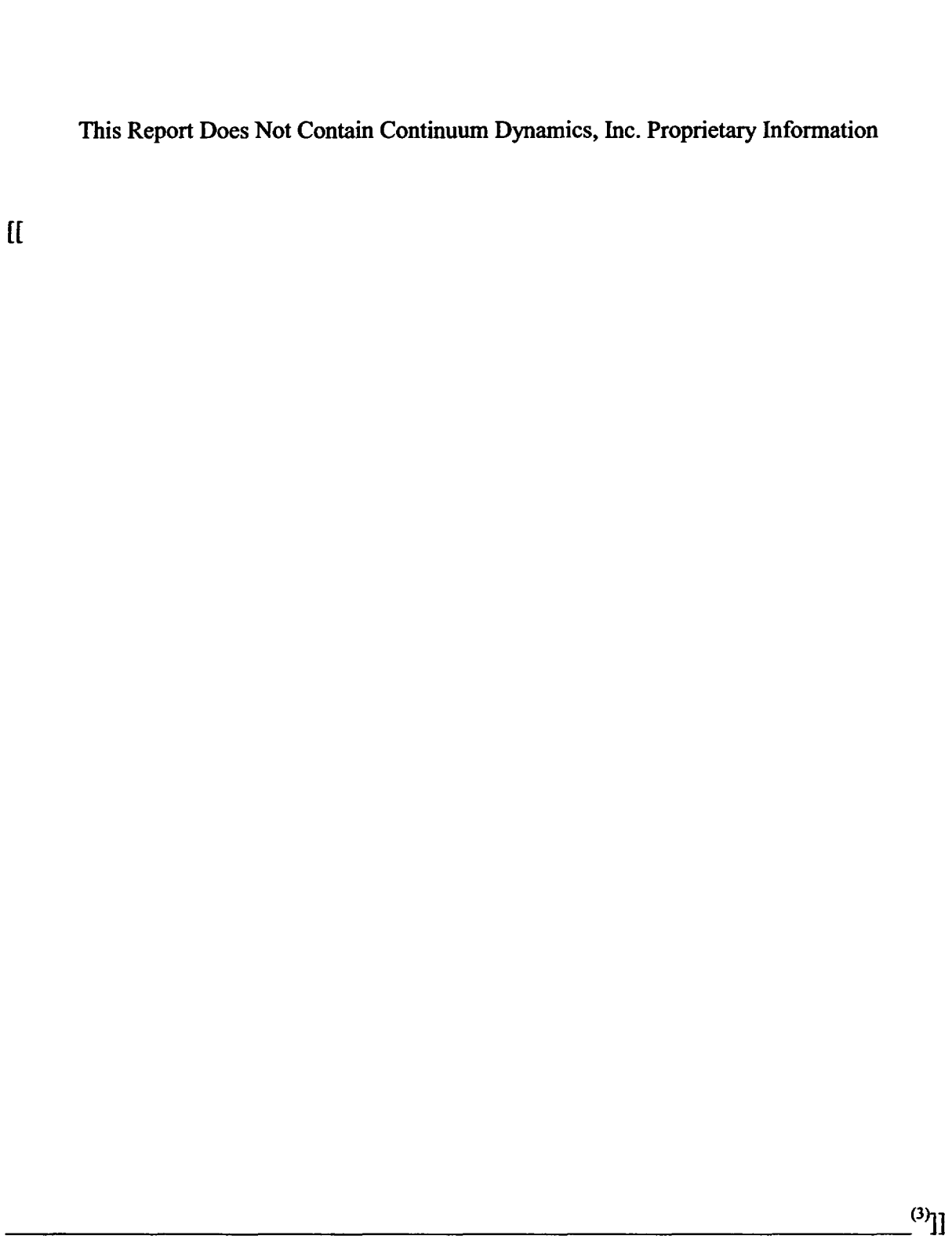

]]$^{(3)}$

Figure 5.10. Bounding RMS predictions (842 MWe) at the operational pressure sensors: peak minimum (top) and peak maximum (bottom) pressure levels, with data (red), outside predictions (black), and inside predictions (blue). Sensors P13, P14, P16, P23, and P27 are inside the dryer, while P26 is on a mast above the dryer, and P19 is inoperative.

[[

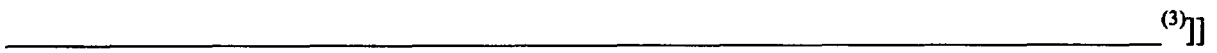

(3)]]

Figure 5.11. Corresponding RMS predictions (842 MWe) for Bounding RMS at the operational pressure sensors, with data (red), outside predictions (black), and inside predictions (blue).

[[

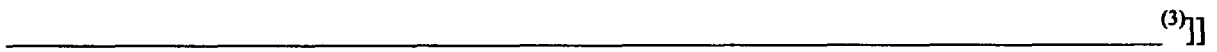

(3)]]

Figure 5.12. Corresponding PSD predictions (842 MWe) for Bounding RMS at the operational pressure sensors, with data (red), outside predictions (black), and inside predictions (blue).

Table 5.6. Comparison between the 842 MWe data and the Bounding Pressure and Bounding RMS predictions for minimum pressure. The data have been filtered to include the frequencies from 0 Hz to 200 Hz only. Standard deviation and relative standard deviation do not include P13, P14, P16, P23, P26, or P27.

[[

]]$^{(3)}$

Table 5.7. Comparison between the 842 MWe data and the Bounding Pressure and Bounding RMS predictions for maximum pressure. The data have been filtered to include the frequencies from 0 Hz to 200 Hz only. Standard deviation and relative standard deviation do not include P13, P14, P16, P23, P26, or P27.

[[

(3)]]

Table 5.8. Comparison between the 842 MWe data and the Bounding Pressure and Bounding RMS predictions for RMS pressure. The data have been filtered to include the frequencies from 0 Hz to 200 Hz only. Standard deviation and relative standard deviation do not include P13, P14, P16, P23, P26, or P27.

[[

[3]]]

Table 5.9. Comparison between the 842 MWe data and the Bounding Pressure and Bounding RMS predictions for maximum PSD. The data have been filtered to include the frequencies from 0 Hz to 200 Hz only. Standard deviation and relative standard deviation do not include P13, P14, P16, P23, P26, or P27.

[[

]]$^{(3)}$

[[

[3]]

Figure 5.13. Relative standard deviation.

VI. Statistical Analysis of Bounding Model Predictions

The three acoustic circuit model solutions developed here (Bounding Pressure, Bounding RMS, and Bounding PSD) can be further examined at EPU conditions to determine the level of conservatism in their predictions. For this, we follow a procedure used previously to analyze Modified Prediction model results [8], by plotting the data at the pressure sensors against the predictions at the pressure sensors. These results are shown in Figures 6.1 to 6.6. Table 6.1 summarizes the results in relation to the three previous benchmark models, by comparing the mean ratios (defined here as the average of the ratio of predicted pressure, RMS, or maximum PSD to measured pressure, RMS, or maximum PSD).

Table 6.1. Mean conservatism built into the various acoustic circuit model predictions, for minimum and maximum pressure, RMS, and maximum PSD. The data have been filtered to include the frequencies from 0 Hz to 200 Hz only. Mean ratio does not include P13, P14, P16, P19 (failed), P23, P26, or P27.

[[

[3]]

[[

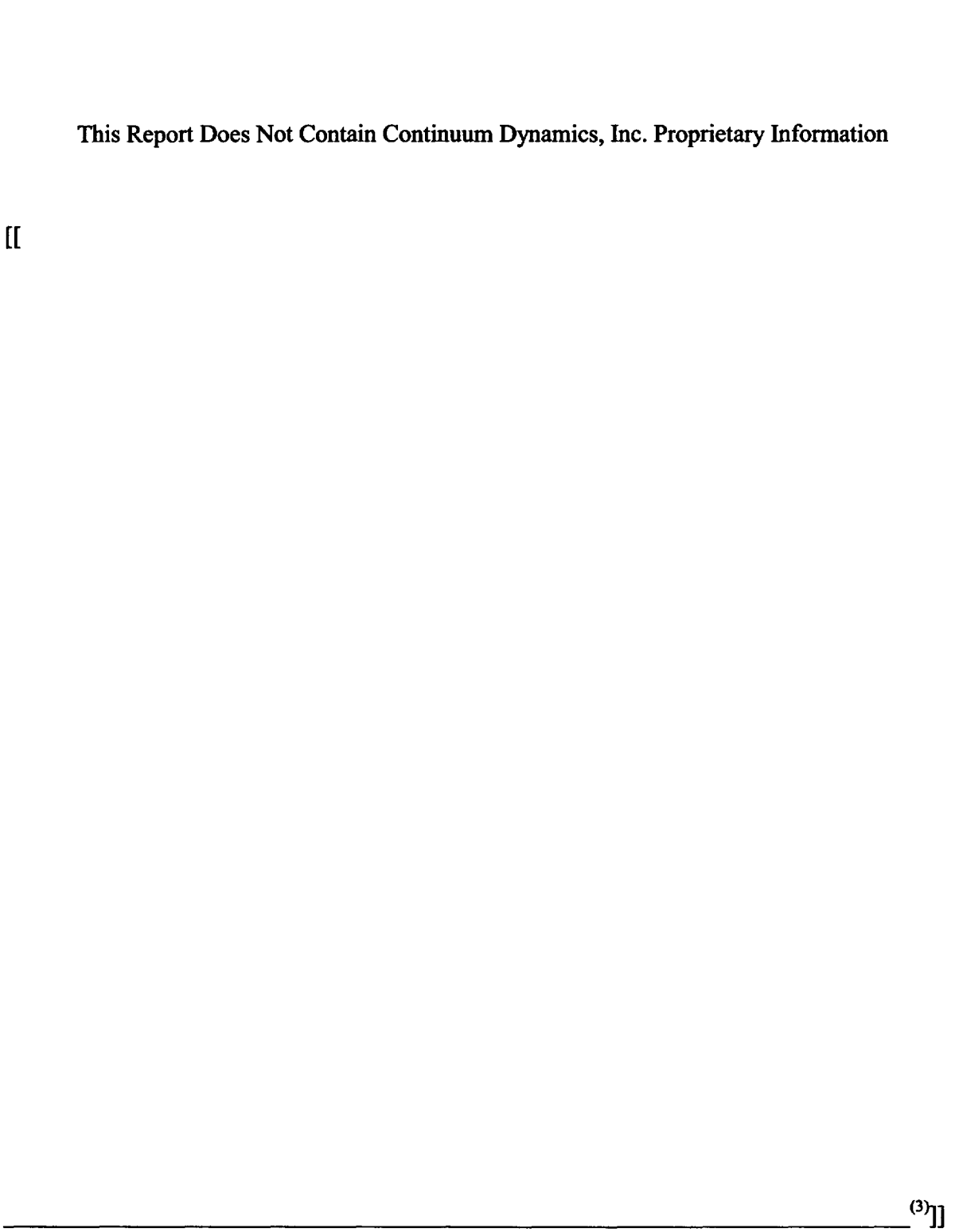

(3)]]

Figure 6.1. Bounding Pressure predictions at the operational pressure sensors, when plotted against the measured data at the sensors: peak minimum (top) and peak maximum (bottom) pressure levels. Sensors P13, P14, P16, P23, and P27 are inside the dryer, while P26 is on a mast above the dryer, and P19 is inoperative. Outside sensors (black); inside sensors (blue).

[[

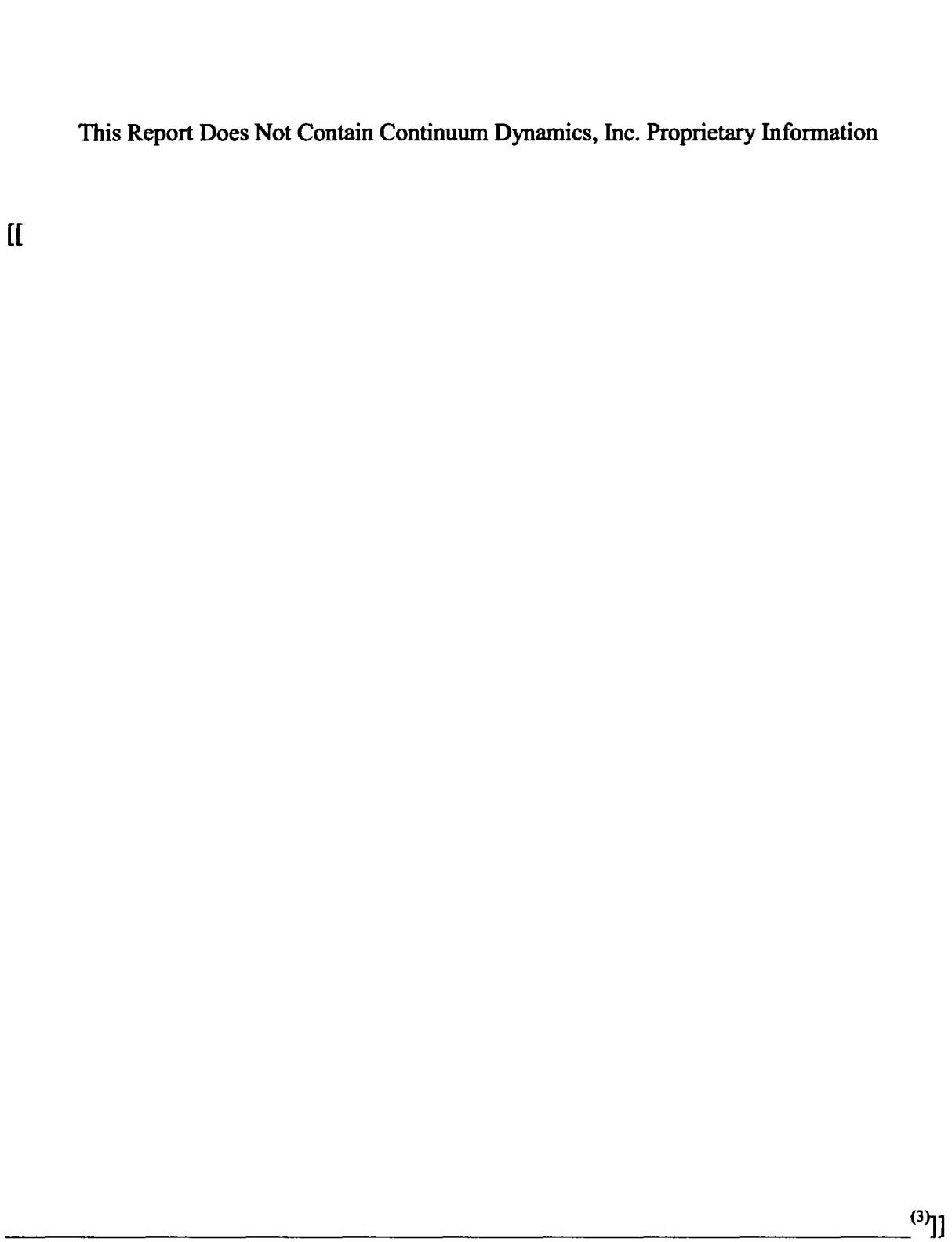

]]$^{(3)}$

Figure 6.2. Bounding RMS predictions at the operational pressure sensors, when plotted against the measured data at the sensors: peak minimum (top) and peak maximum (bottom) pressure levels. Sensors P13, P14, P16, P23, and P27 are inside the dryer, while P26 is on a mast above the dryer, and P19 is inoperative. Outside sensors (black); inside sensors (blue).

[[

(3)]]

Figure 6.3. Corresponding RMS predictions for Bounding RMS at the operational pressure sensors, when plotted against the measured RMS at the sensors. Outside sensors (black); inside sensors (blue).

[[

(3)]]

Figure 6.4. Bounding PSD predictions at the operational pressure sensors, when plotted against the measured data at the sensors: peak minimum (top) and peak maximum (bottom) pressure levels. Sensors P13, P14, P16, P23, and P27 are inside the dryer, while P26 is on a mast above the dryer, and P19 is inoperative. Outside sensors (black); inside sensors (blue).

[[

[3]]]

Figure 6.5. Corresponding RMS predictions for Bounding PSD at the operational pressure sensors, when plotted against the measured RMS at the sensors. Outside sensors (black); inside sensors (blue).

[[

[3]]]

Figure 6.6. Corresponding PSD predictions for Bounding PSD at the operational pressure sensors, when plotted against the measured PSD at the sensors. Outside sensors (black); inside sensors (blue).

VII. Model Uncertainty

As shown in this report, model comparisons with data demonstrate the high degree of correlation found in the application of the acoustic circuit model to the QC2 steam dryer, steam dome, and main steam lines. It is natural then to ask about the applicable range of the model and where model uncertainty is anticipated.

7.1 Uncertainty in the Proposed Analytical Model

To understand errors in the model, it is necessary to discuss the approximations that have been made during model formulation. These approximations then lead to the errors that are introduced and limit applicability of the model.

[[

_____ [(3)]]

[[

_____ (3)]]

7.2 Uncertainty as a Function of Instrument Placement

The acoustic circuit model has been benchmarked with data taken by strain gages on the main steam lines of QC2, located at average distances of 9.50 and 41.16 feet from the steam dome. Should instruments be placed at locations other than these distances, it is natural to ask what error may be introduced.

[[

_____ (3)]]

[[

(3)]]

Figure 7.1. PSD comparison at 930 MWe for pressure sensor data (blue curve), Bounding Pressure prediction (red curve), Bounding RMS prediction (black curve), and Bounding PSD prediction (green curve), for P1: 0 to 200 Hz. A solid horizontal line (magenta) indicates the suggested noise floor.

VIII. Low Resolution Pressure Load Predictions

The six acoustic circuit model results at EPU can be used to develop low resolution loads on the replacement QC2 dryer, as a means of further investigating the conservation built into the various acoustic circuit models. The dryer is represented by nodes as detailed in Figure 8.1. The predictions for Modified Prediction, Minimum Error, and Minimum RMS are shown in Figure 8.2, while the corresponding predictions for Bounding Pressure, Bounding RMS, and Bounding PSD are shown in Figure 8.3. Table 8.1 summarizes the predictions for all six load cases. These loads are further normalized by the Minimum Error values in Table 8.2.

Table 8.1. Pressure statistics on acoustic circuit model solutions.

[[

_____ [(3)]]

Table 8.2. Normalized acoustic circuit model solutions.

[[

_____ [(3)]]

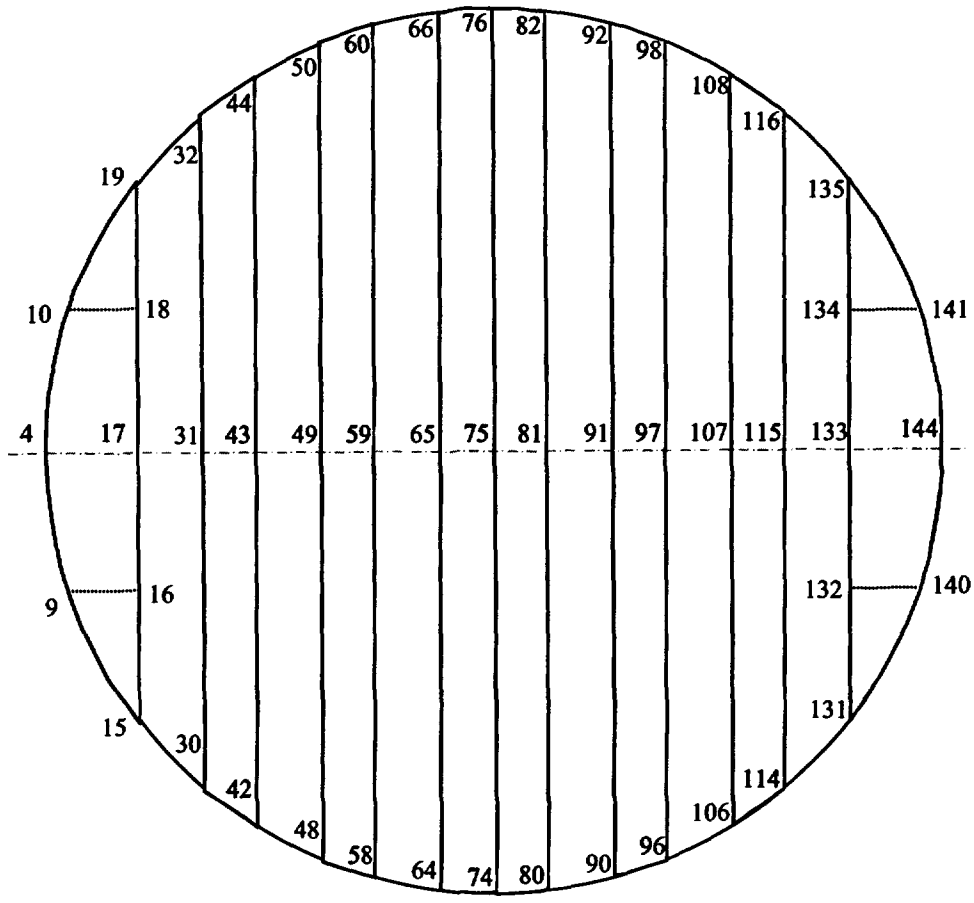

Figure 8.1a. Bottom plates pressure node locations.

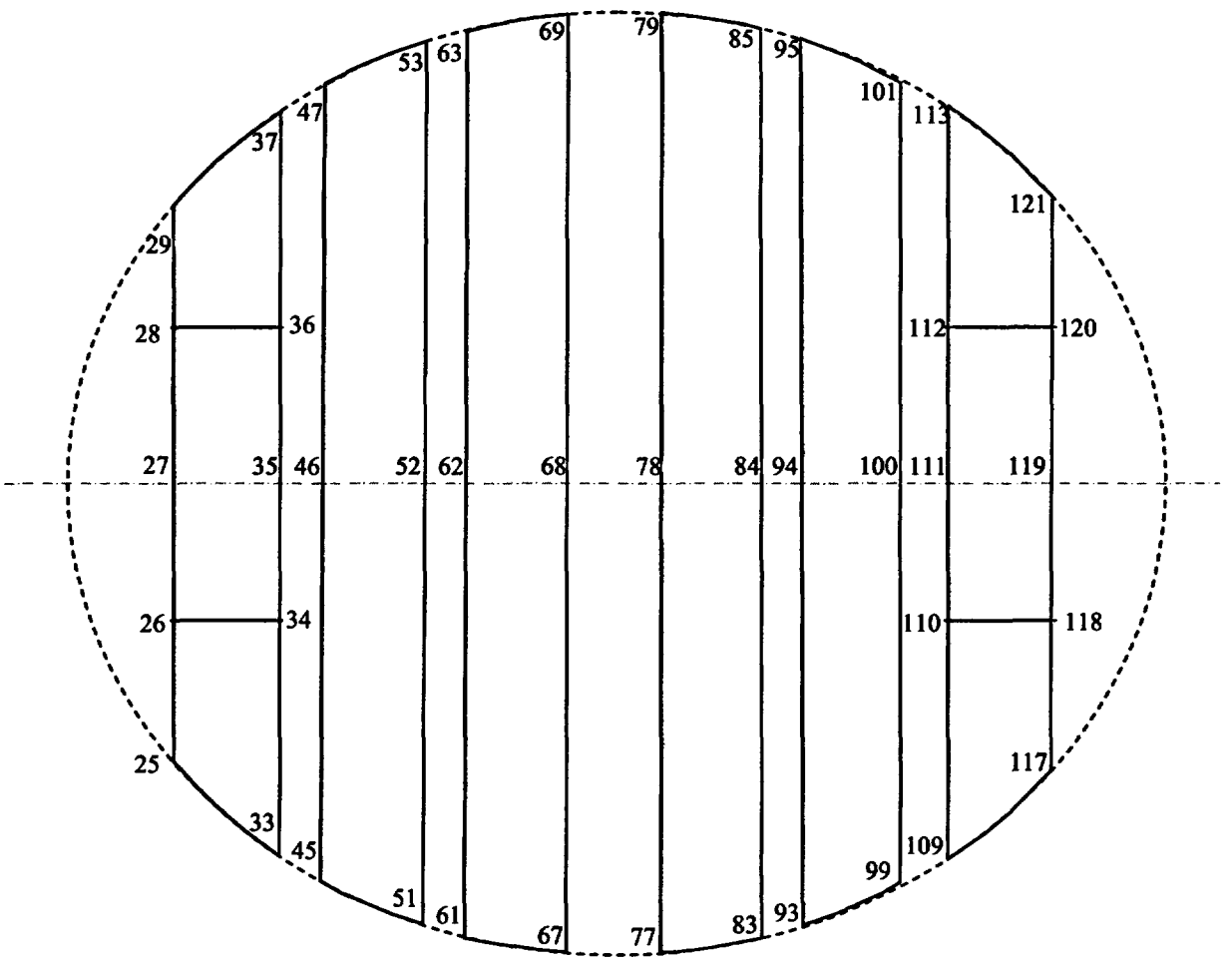

Figure 8.1b. Top plates pressure node locations.

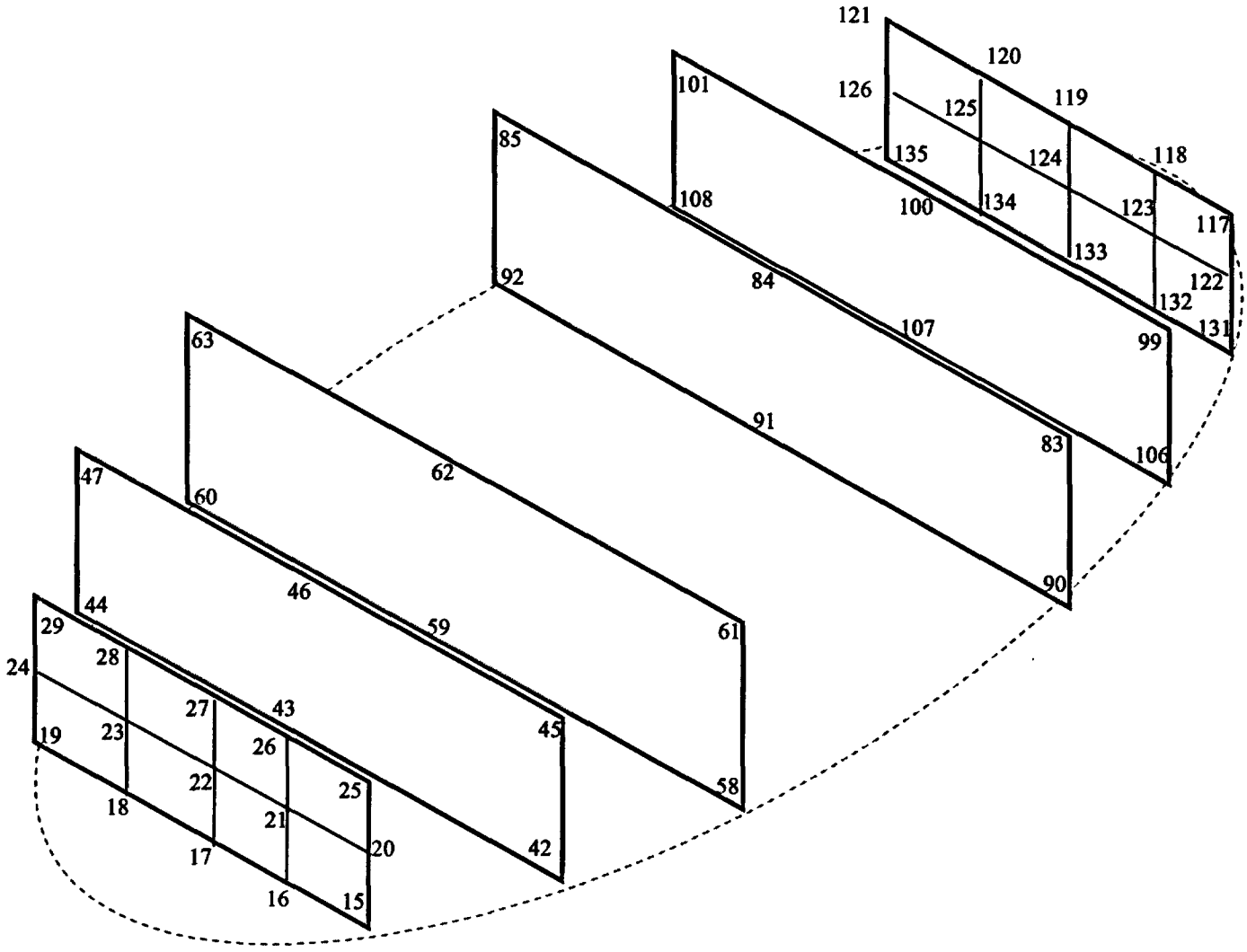

Figure 8.1c. Slanted plates pressure node locations.

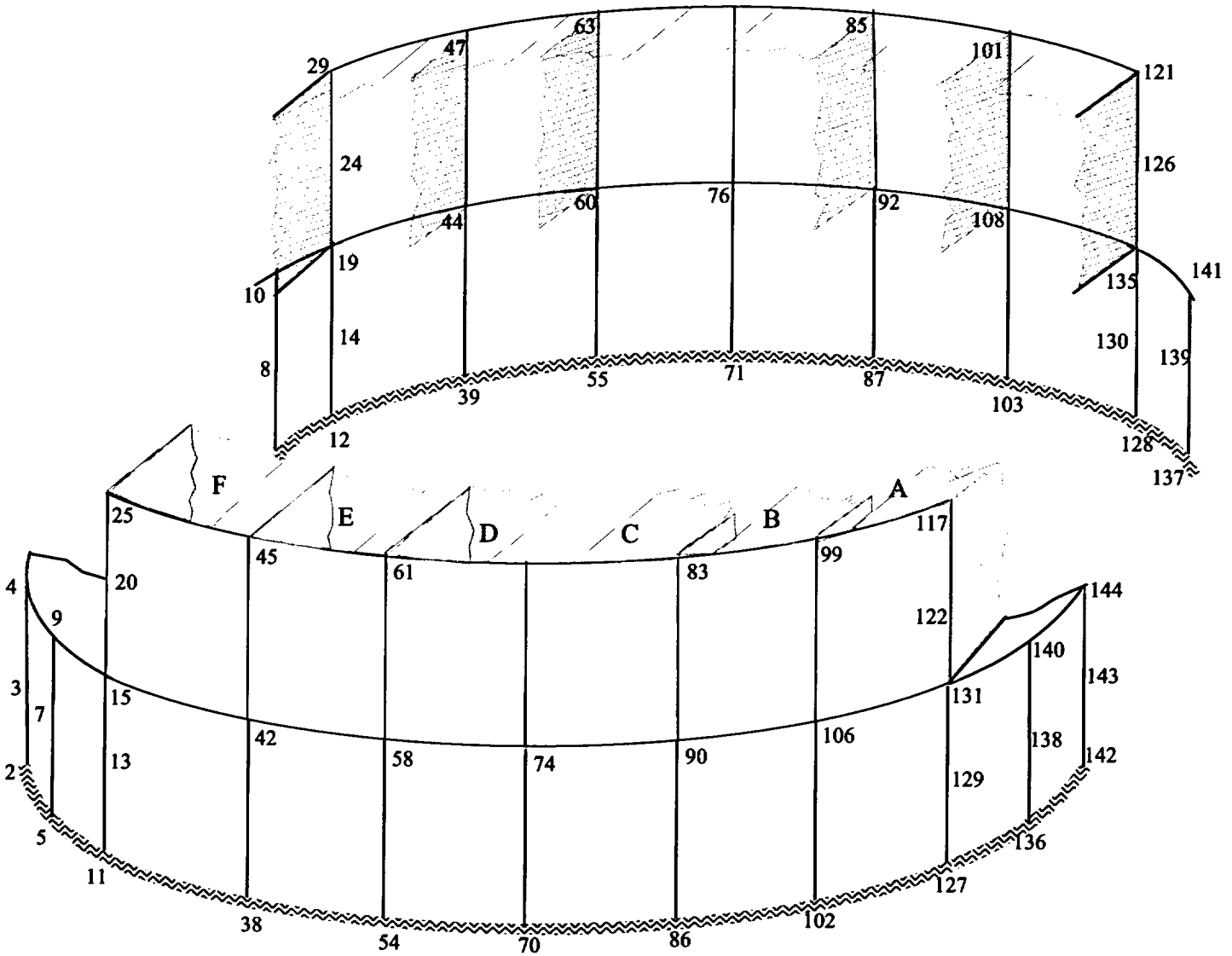

Figure 8.1d. Skirt plates pressure node locations.

[[

[3]]]

Figure 8.2. Low resolution loads predicted on the QC2 replacement dryer for Modified Prediction (red curve), Minimum Error (black curve), and Minimum RMS (green curve).

[[

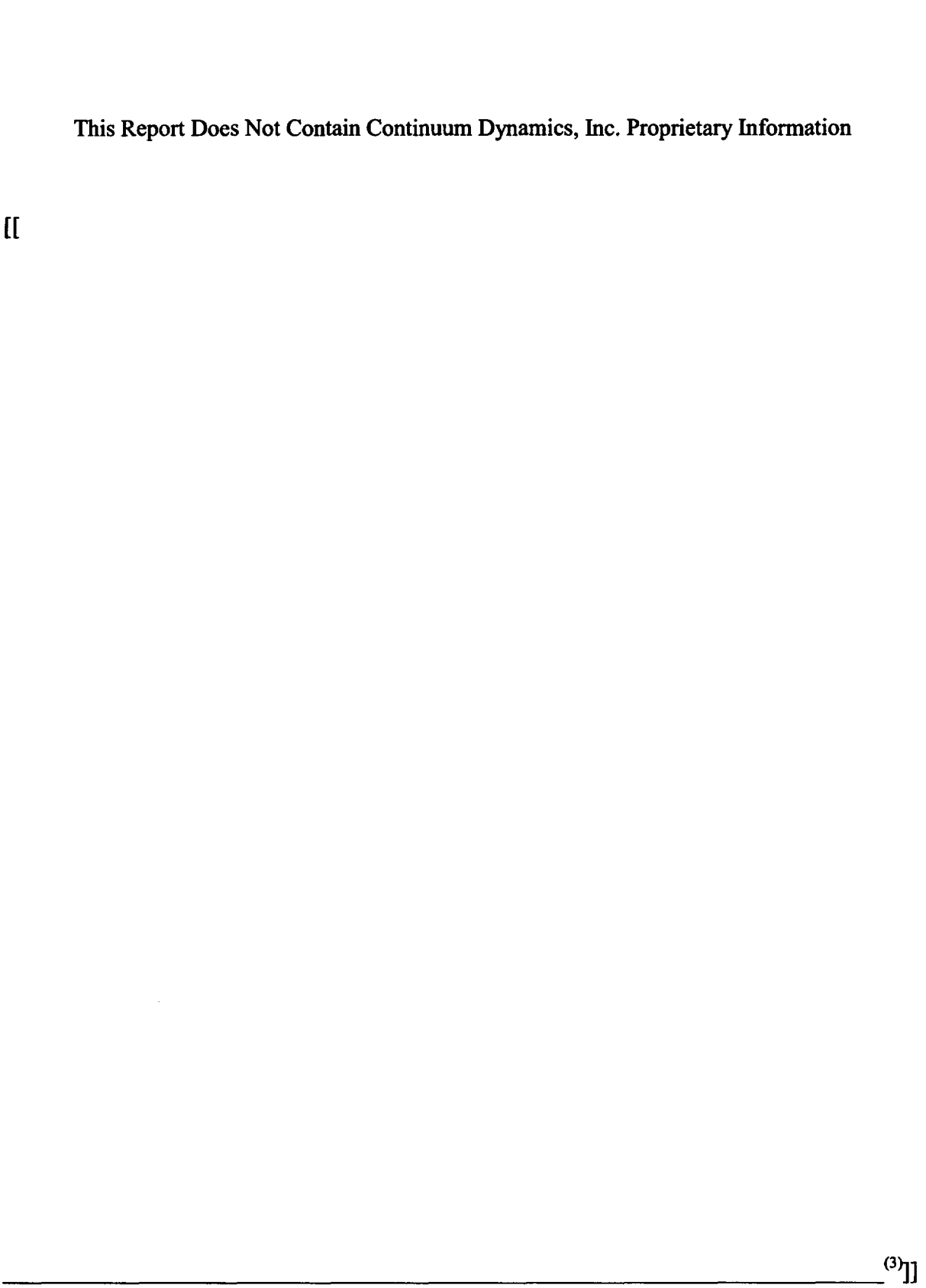

]][3]

Figure 8.3. Low resolution loads predicted on the QC2 replacement dryer for Bounding Pressure (red curve), Bounding RMS (black curve), and Bounding PSD (green curve).

IX. Reduction of Noise in Measured Main Steam Line Data

[[

]][3]

[[

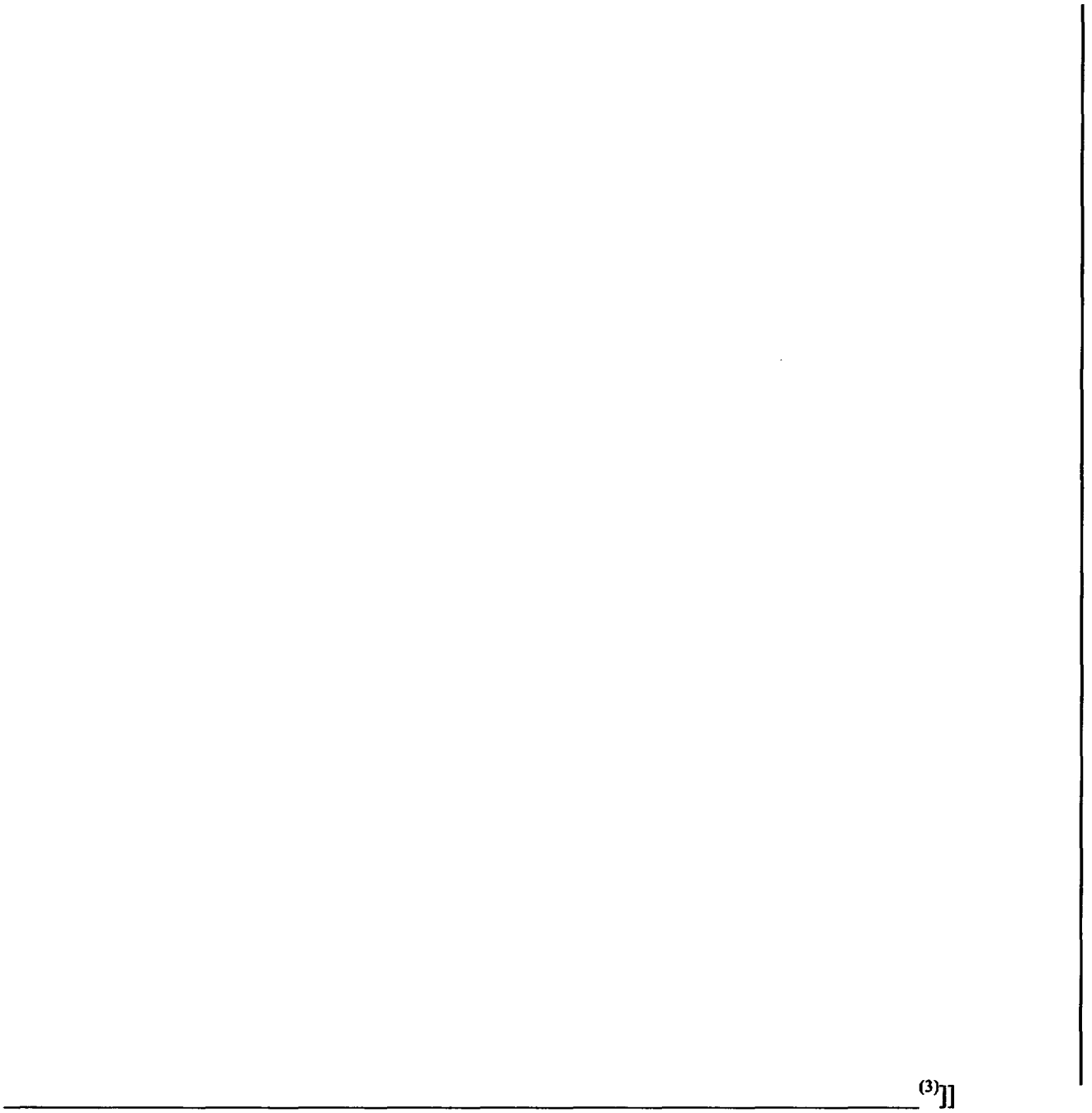

]][3]

Figure 9.1 PSDs of measure main steam line pressures and the signal after noise conditioning.

[[

]][3]

Figure 9.1 (continued)

[[

[redacted]

[redacted][(3)]]

Figure 9.1 (continued)

[[

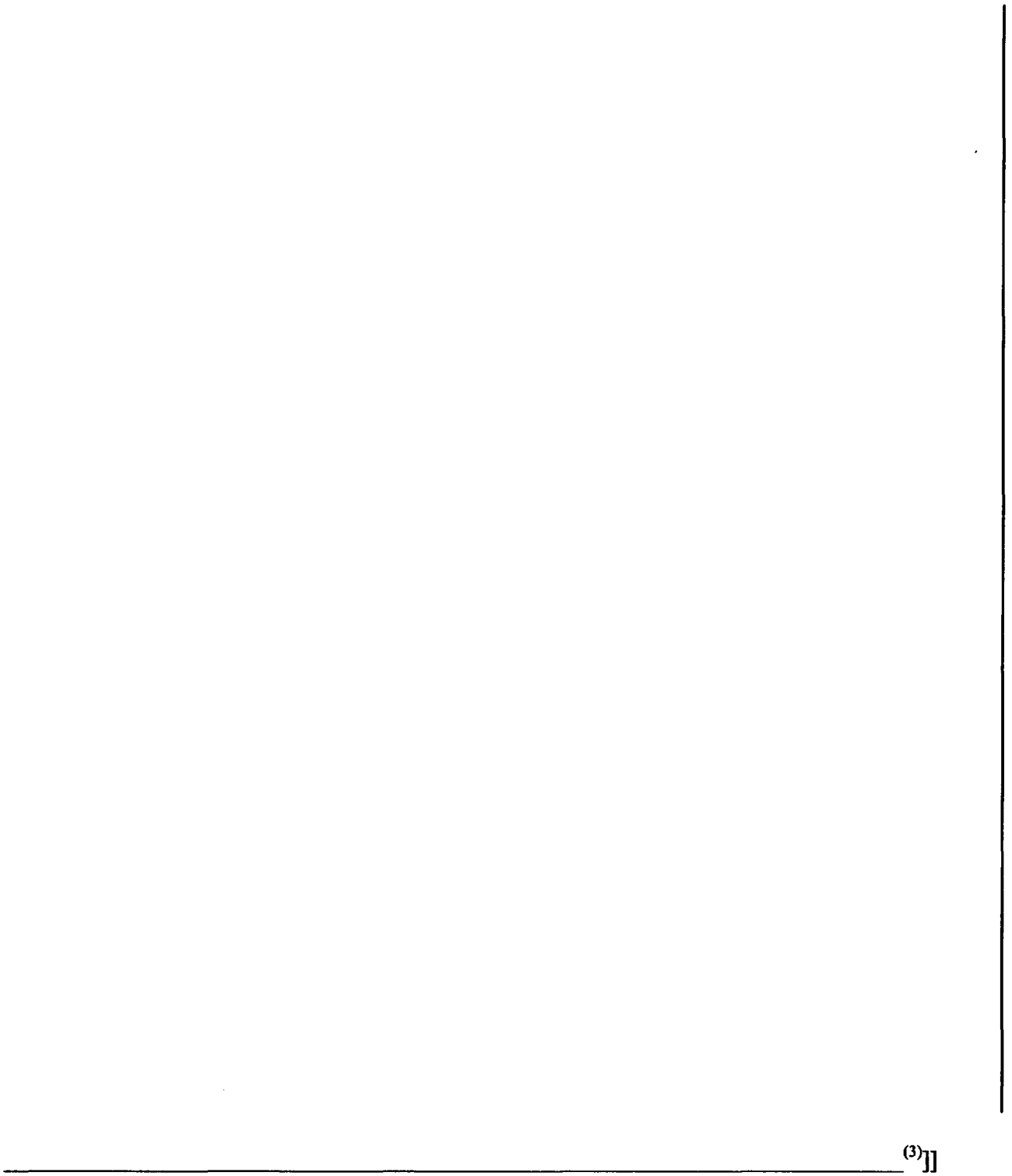

[3]]]

Figure 9.1 (continued)

[[

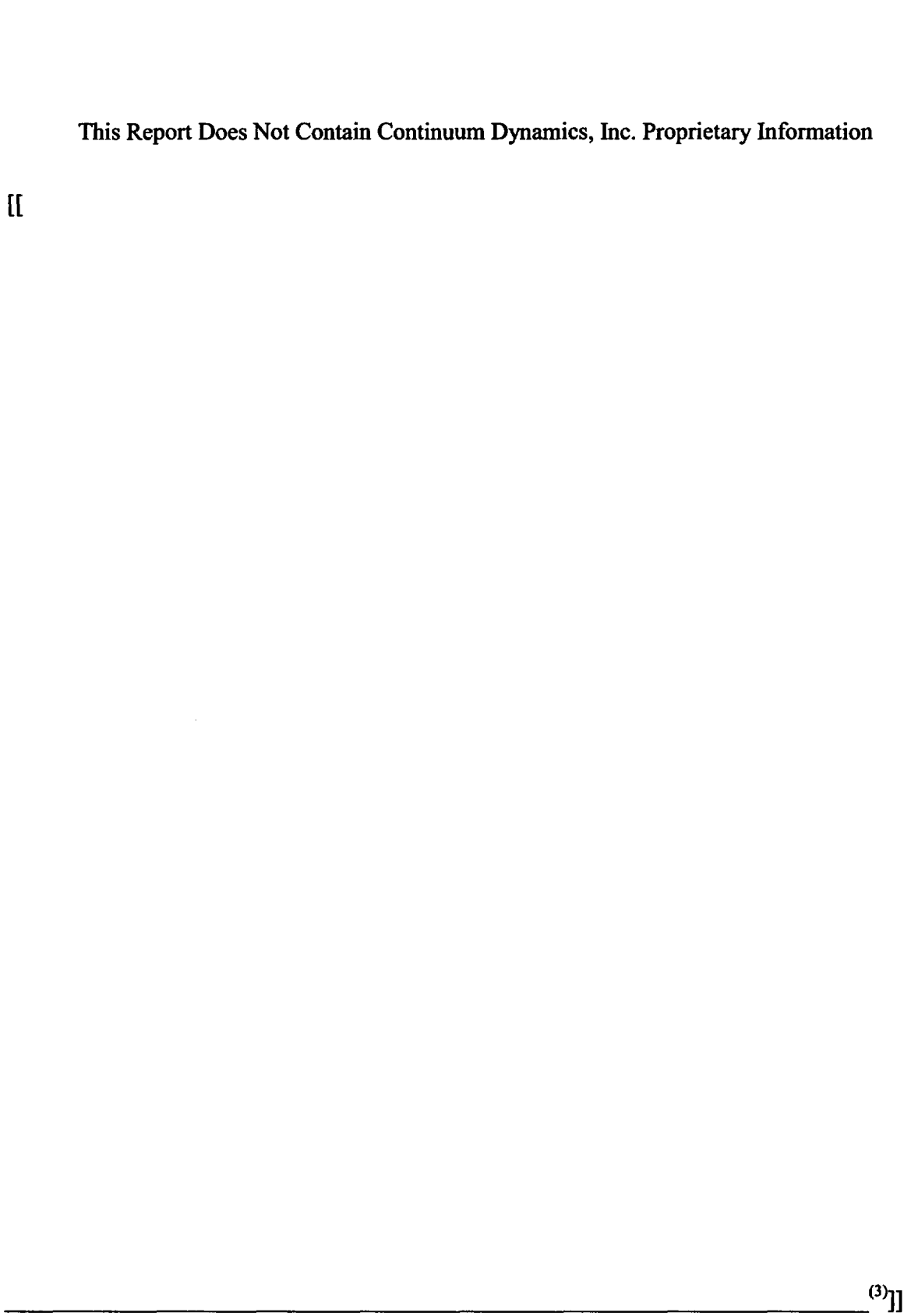

]]$^{(3)}$

Figure 9.2 The coherence function between main steam line pressure measurements made of each steam line.

[[

[3]]]

Figure 9.2 (continued)

[[

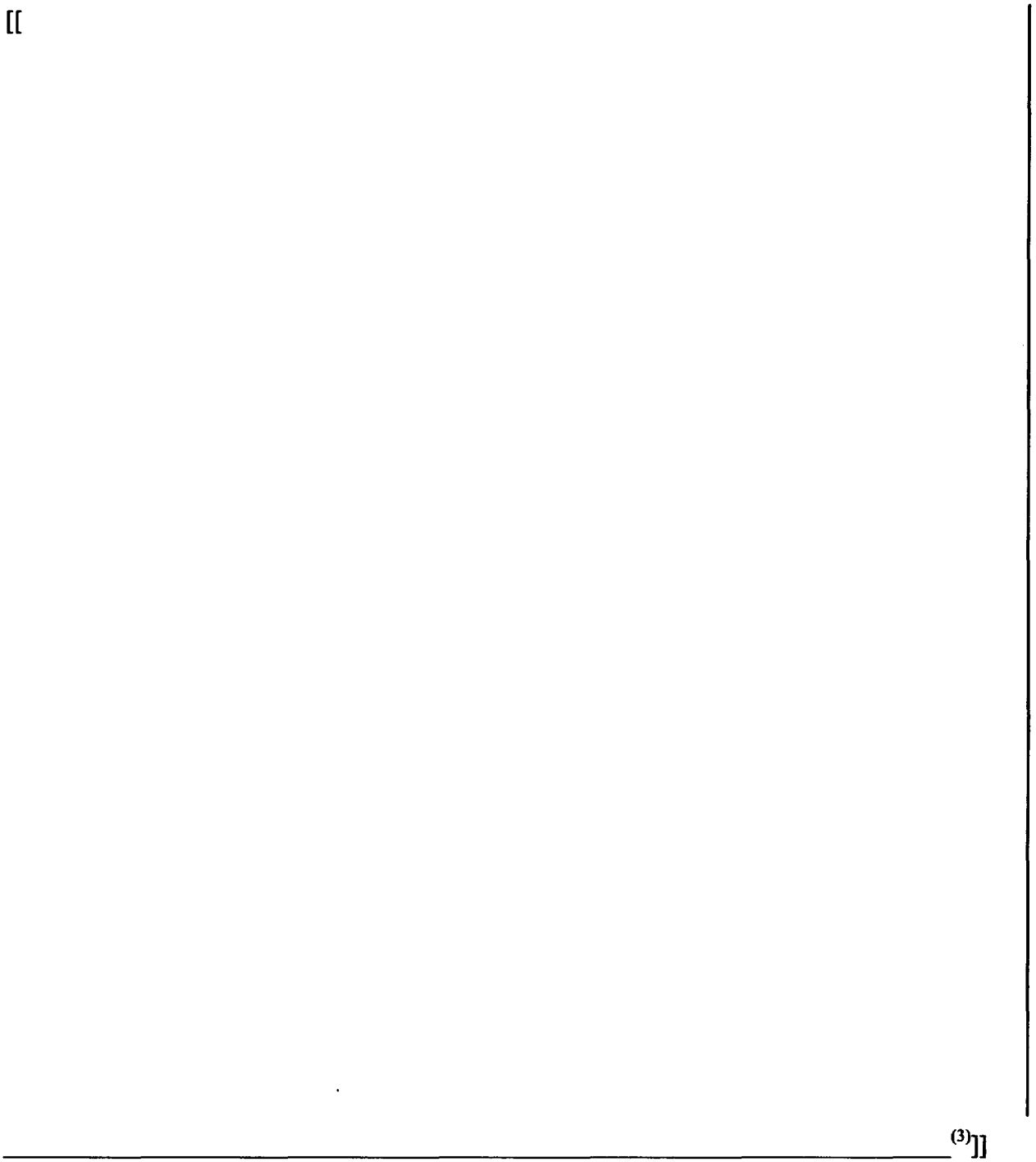

(3)]]

Figure 9.3 Comparisons between the data and the Bounding Pressure Model with and without noise conditioning at selected dryer pressure transducers.

[[

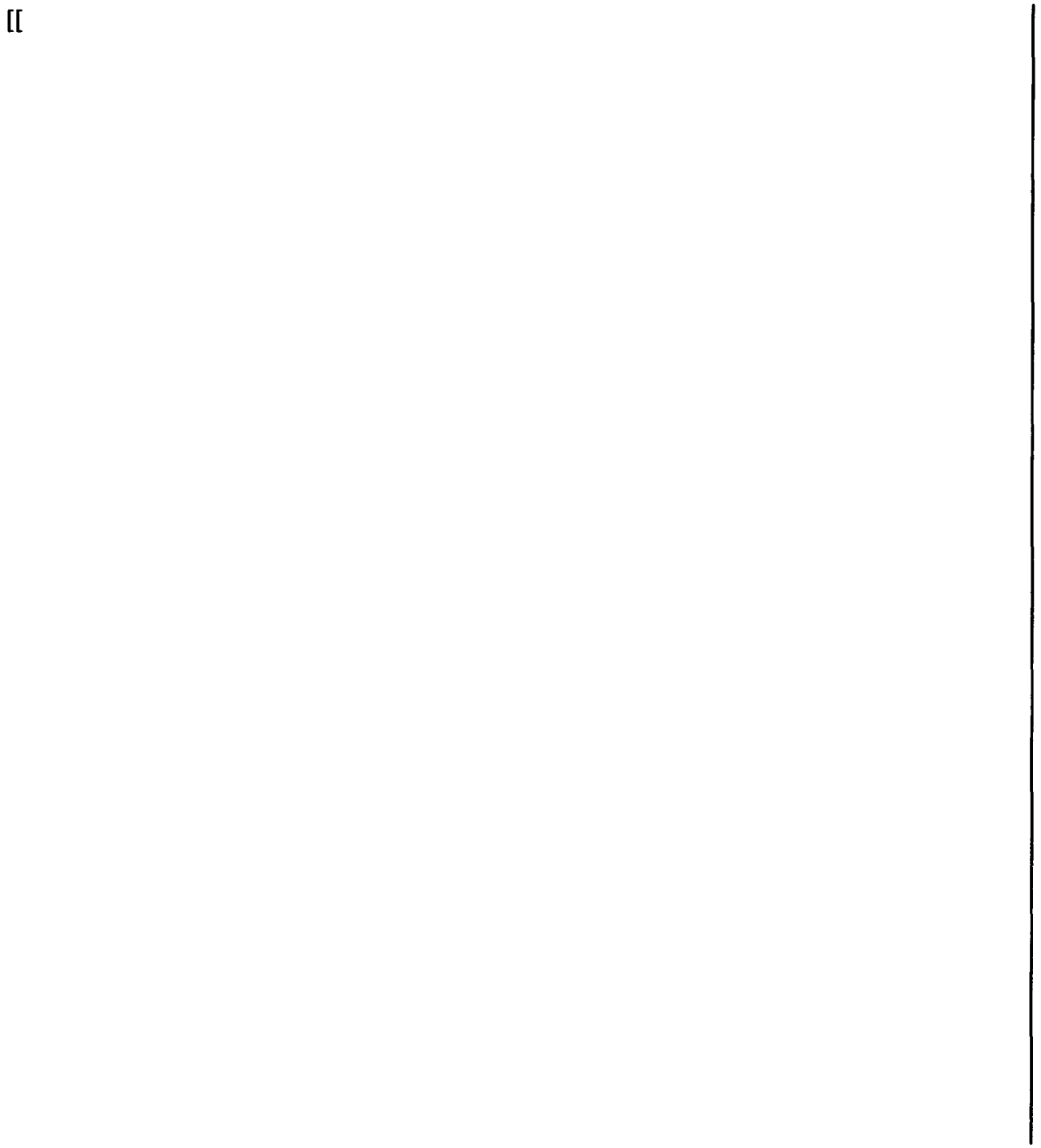

[3]]]

Figure 9.3 (continued)

[[

[3]]]

Figure 9.3 (continued)

Table 9.1 Comparison between the 790 MWe data and the Bounding Pressure predictions for minimum pressure, with the addition of the results when noise conditioning is applied to the main steam line data. The data have been filtered to include the frequencies from 0 Hz to 200 Hz only. Standard deviation and relative standard deviation do not include P13, P14, P16, P23, P26, or P27.

[[

]]$^{(3)}$

Table 9.2. Comparison between the 790 MWe data and the Bounding Pressure predictions for maximum pressure, with the addition of the results when noise conditioning is applied to the main steam line data. The data have been filtered to include the frequencies from 0 Hz to 200 Hz only. Standard deviation and relative standard deviation do not include P13, P14, P16, P23, P26, or P27.

[[

(3)]]

Table 9.3. Comparison between the 790 MWe data and the Bounding Pressure predictions for RMS pressure, with the addition of the results when noise conditioning is applied to the main steam line data. The data have been filtered to include the frequencies from 0 Hz to 200 Hz only. Standard deviation and relative standard deviation do not include P13, P14, P16, P23, P26, or P27.

[[

(3)]]

Table 9.4. Comparison between the 790 MWe data and the Bounding Pressure predictions for maximum PSD, with the addition of the results when noise conditioning is applied to the main steam line data. The data have been filtered to include the frequencies from 0 Hz to 200 Hz only. Standard deviation and relative standard deviation do not include P13, P14, P16, P23, P26, or P27.

[[

]]$^{(3)}$

X. Conclusions

The further model evaluation examined here confirms the applicability of the C.D.I. acoustic circuit analysis for use with in-plant strain gage data collected on the main steam lines. The model with "locked" modeling parameters can now be used with other steam dryer geometries and other main steam line configurations to provide a representative pressure loading on the steam dryer.

Instrumenting the main steam lines at locations similar to QC2 would minimize the uncertainty with regard to instrument placement along the main steam lines. Since the Helmholtz solution is geometrically unique, for each steam dome dryer geometry, differences between plants are accounted for in the analysis. It is anticipated that the high quality of steam exiting the dryer and entering the main steam lines is similar between plants; thus, model parameter values should not be plant-dependent.

The results of this evaluation, in combination with the blind evaluations and modified evaluations given in [3], [4], and [5], illustrate the following:

1. The C.D.I. acoustic circuit model predictions improved as its modeling parameters were refined.

2. The model accurately predicts the peak frequency spike in all pressure sensors, not only in frequency location but also in PSD magnitude, depending on the model selected.

3. [[

_____ (3)]]

XI. References

1. Continuum Dynamics, Inc. 2005. Quad Cities 2 New Dryer Vulnerability Loads. C.D.I. Technical Note No. 05-03.

2. Continuum Dynamics, Inc. 2005. Quad Cities 2 New Dryer SMT Loads. C.D.I. Technical Note No. 05-04.

3. Continuum Dynamics, Inc. 2005. Evaluation of Continuum Dynamics, Inc. Steam Dryer Load Methodology against Quad Cities Unit 2 In-Plant Data. C.D.I. Report No. 05-10.

4. Continuum Dynamics, Inc. 2005. Blind Evaluation of Continuum Dynamics, Inc. Steam Dryer Load Methodology against Quad Cities Unit 2 In-Plant Data at 2831 MWe. C.D.I. Technical Note No. 05-37.

5. Continuum Dynamics, Inc. 2005. Improved Methodology to Predict Full Scale Steam Dryer Loads from In-Plant Measurements. C.D.I. Report No. 05-23.

6. Continuum Dynamics, Inc. 2005. Methodology to Determine Unsteady Pressure Loading on Components in Reactor Steam Domes (Rev. 5). C.D.I. Report No. 04-09 (Proprietary).

7. General Electric Company (C. Hinds). 2005. Dryer Sensor Locations. Letter Report No. GE-ENG-DRY-087. Dated 18 May 2005.

8. Exelon Nuclear Generating Company. 2005. An Assessment of the Uncertainty in the Application of the Modified 930 MWe Acoustic Circuit Model Predictions for the Replacement Quad Cities Units 1 and 2 Steam Dryers. Document No. AM-2005-012.

Appendix A: Bounding Model Comparisons at 790 MWe

[[

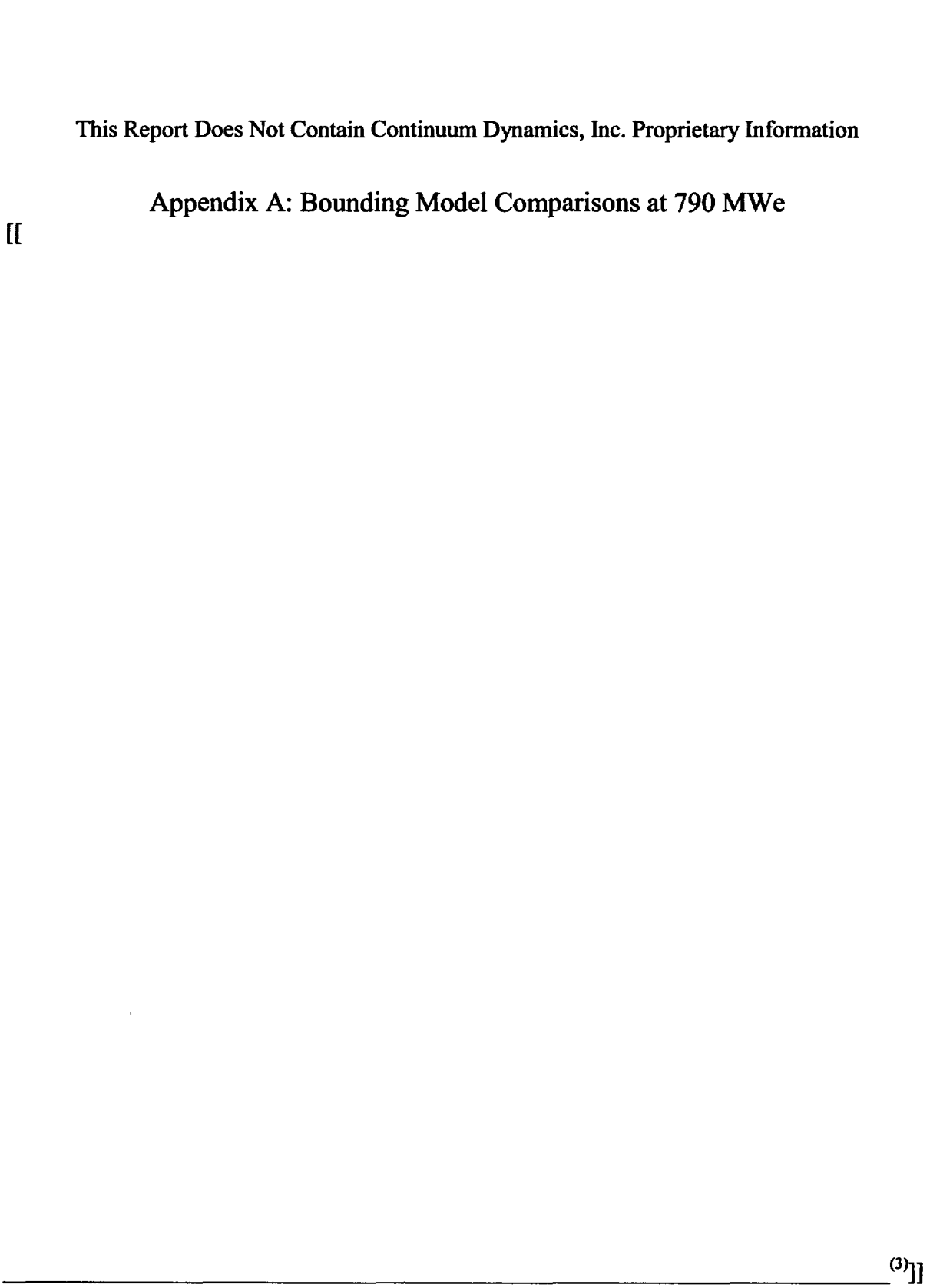

(3)]]

Figure A.1. PSD comparison at 790 MWe for pressure sensor data (blue curve) and Bounding Pressure prediction (red curve), for P1: 0 to 200 Hz (top), 125 to 165 Hz (bottom).

[[

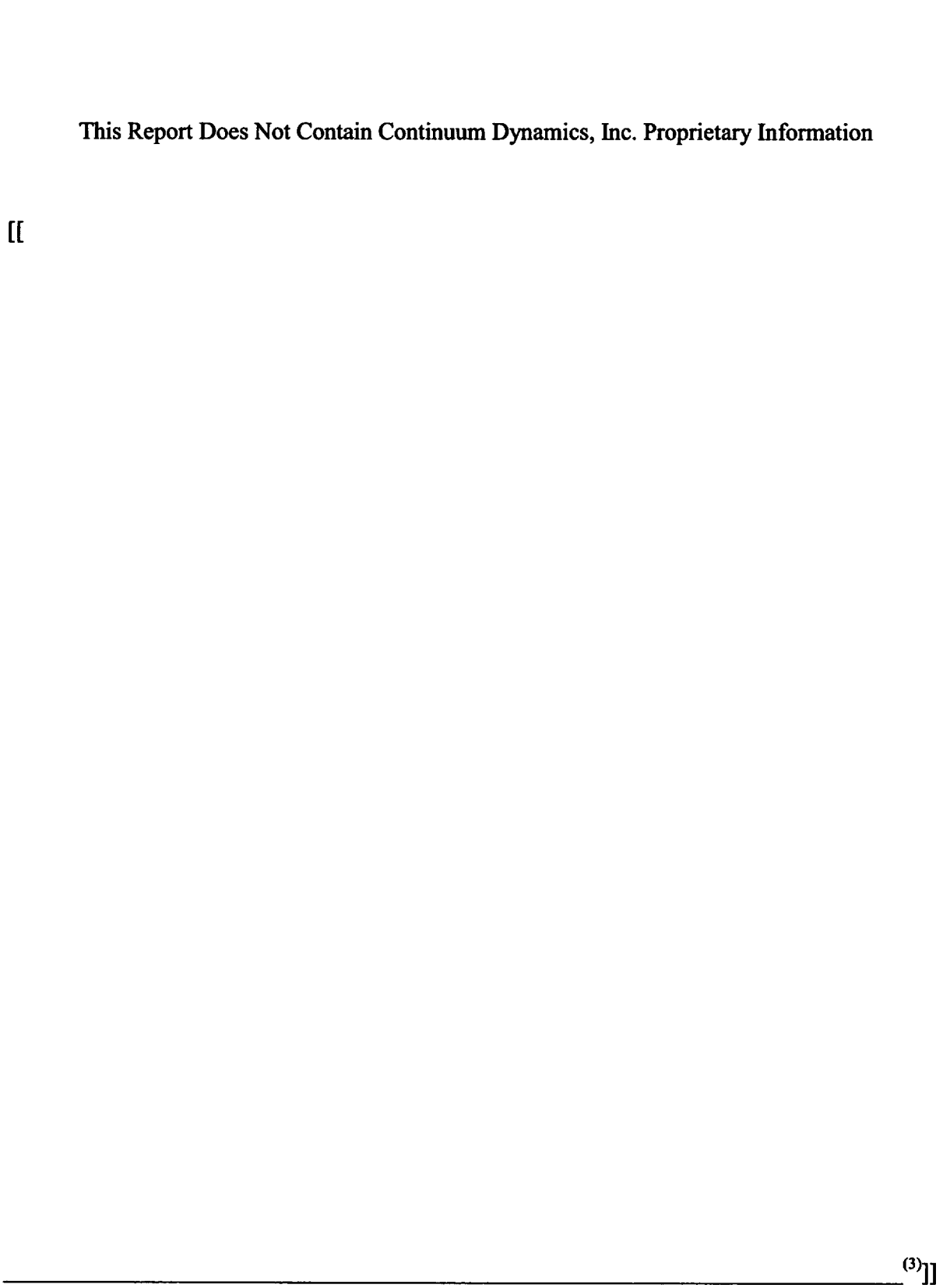

(3)]]

Figure A.2. PSD comparison for 790 MWe for pressure sensor data (blue curve) and Bounding Pressure prediction (red curve), for P2: 0 to 200 Hz (top), 125 to 165 Hz (bottom).

[[

]][3]

Figure A.3. PSD comparison for 790 MWe for pressure sensor data (blue curve) and Bounding Pressure prediction (red curve), for P3: 0 to 200 Hz (top), 125 to 165 Hz (bottom).

[[

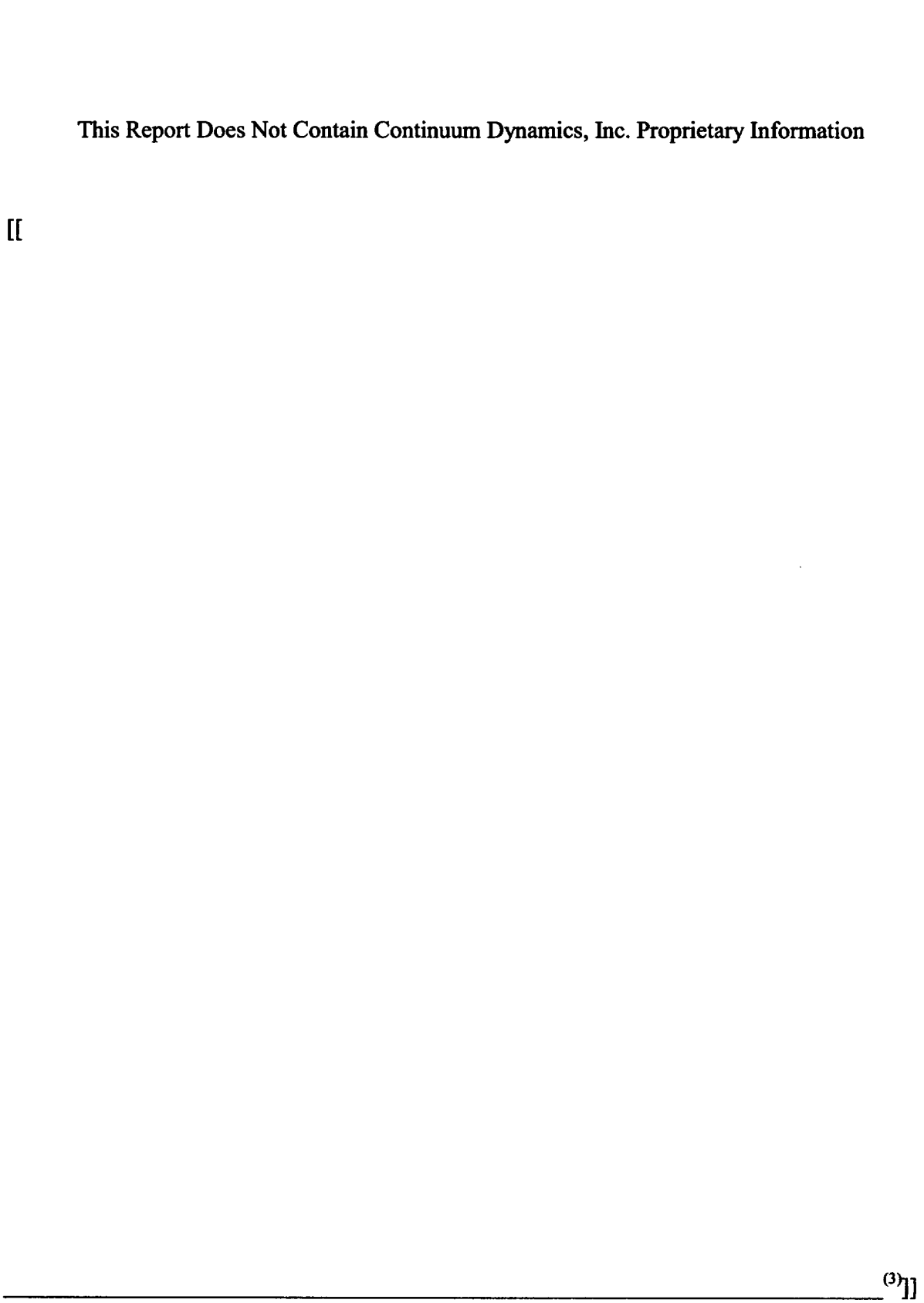

(3)]]

Figure A.4. PSD comparison at 790 MWe for pressure sensor data (blue curve) and Bounding Pressure prediction (red curve), for P4: 0 to 200 Hz (top), 125 to 165 Hz (bottom).

[[

]]$^{(3)}$

Figure A.5. PSD comparison at 790 MWe for pressure sensor data (blue curve) and Bounding Pressure prediction (red curve), for P5: 0 to 200 Hz (top), 125 to 165 Hz (bottom).

[[

[redacted]

[redacted]$^{(3)}$]]

Figure A.6. PSD comparison at 790 MWe for pressure sensor data (blue curve) and Bounding Pressure prediction (red curve), for P6: 0 to 200 Hz (top), 125 to 165 Hz (bottom).

[[

]][3]

Figure A.7. PSD comparison at 790 MWe for pressure sensor data (blue curve) and Bounding Pressure prediction (red curve), for P7: 0 to 200 Hz (top), 125 to 165 Hz (bottom).

[[

]]$^{(3)}$

Figure A.8. PSD comparison at 790 MWe for pressure sensor data (blue curve) and Bounding Pressure prediction (red curve), for P8: 0 to 200 Hz (top), 125 to 165 Hz (bottom).

[[

[3]]]

Figure A.9. PSD comparison at 790 MWe for pressure sensor data (blue curve) and Bounding Pressure prediction (red curve), for P9: 0 to 200 Hz (top), 125 to 165 Hz (bottom).

[[

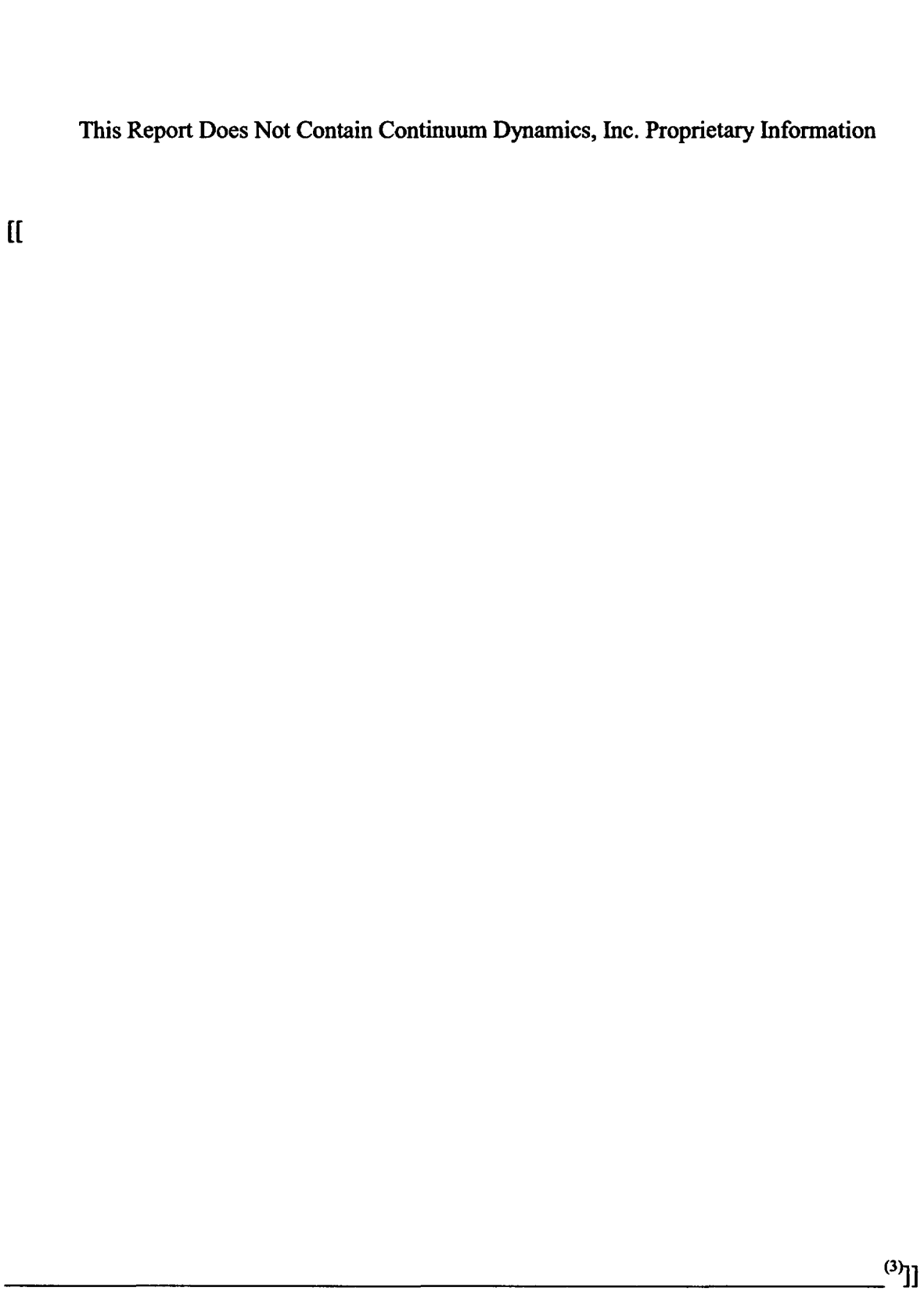

(3)]]

Figure A.10. PSD comparison at 790 MWe for pressure sensor data (blue curve) and Bounding Pressure prediction (red curve), for P10: 0 to 200 Hz (top), 125 to 165 Hz (bottom).

[[

[3]]]

Figure A.11. PSD comparison at 790 MWe for pressure sensor data (blue curve) and Bounding Pressure prediction (red curve), for P11: 0 to 200 Hz (top), 125 to 165 Hz (bottom).

[[

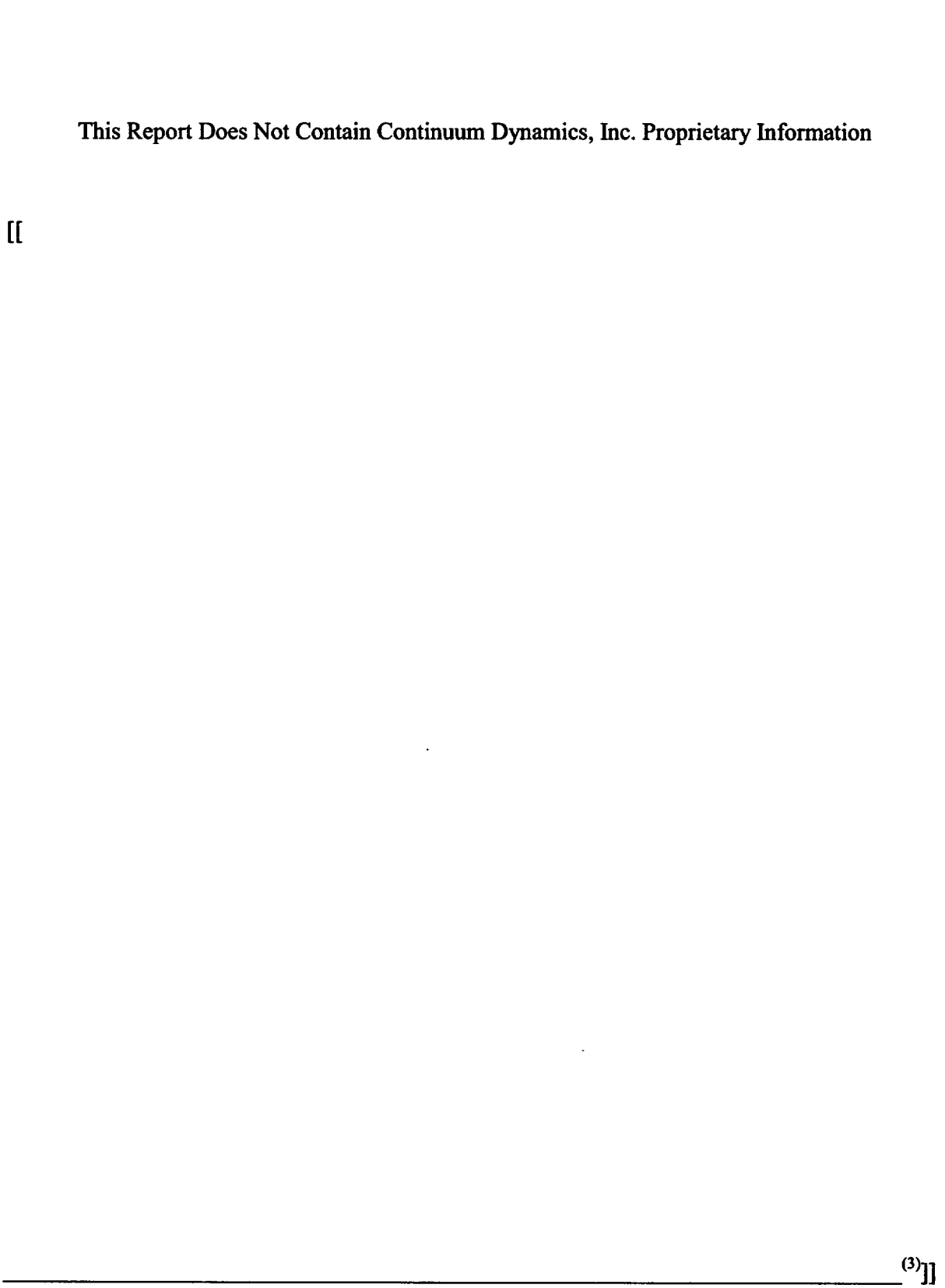

]][3]

Figure A.12. PSD comparison at 790 MWe for pressure sensor data (blue curve) and Bounding Pressure prediction (red curve), for P12: 0 to 200 Hz (top), 125 to 165 Hz (bottom).

[[

]][3]

Figure A.13. PSD comparison at 790 MWe for pressure sensor data (blue curve) and Bounding Pressure prediction (red curve), for P13: 0 to 200 Hz (top), 125 to 165 Hz (bottom).

[[

]][3]

Figure A.14. PSD comparison at 790 MWe for pressure sensor data (blue curve) and Bounding Pressure prediction (red curve), for P14: 0 to 200 Hz (top), 125 to 165 Hz (bottom).

[[

]] [3]

Figure A.15. PSD comparison at 790 MWe for pressure sensor data (blue curve) and Bounding Pressure prediction (red curve), for P15: 0 to 200 Hz (top), 125 to 165 Hz (bottom).

[[

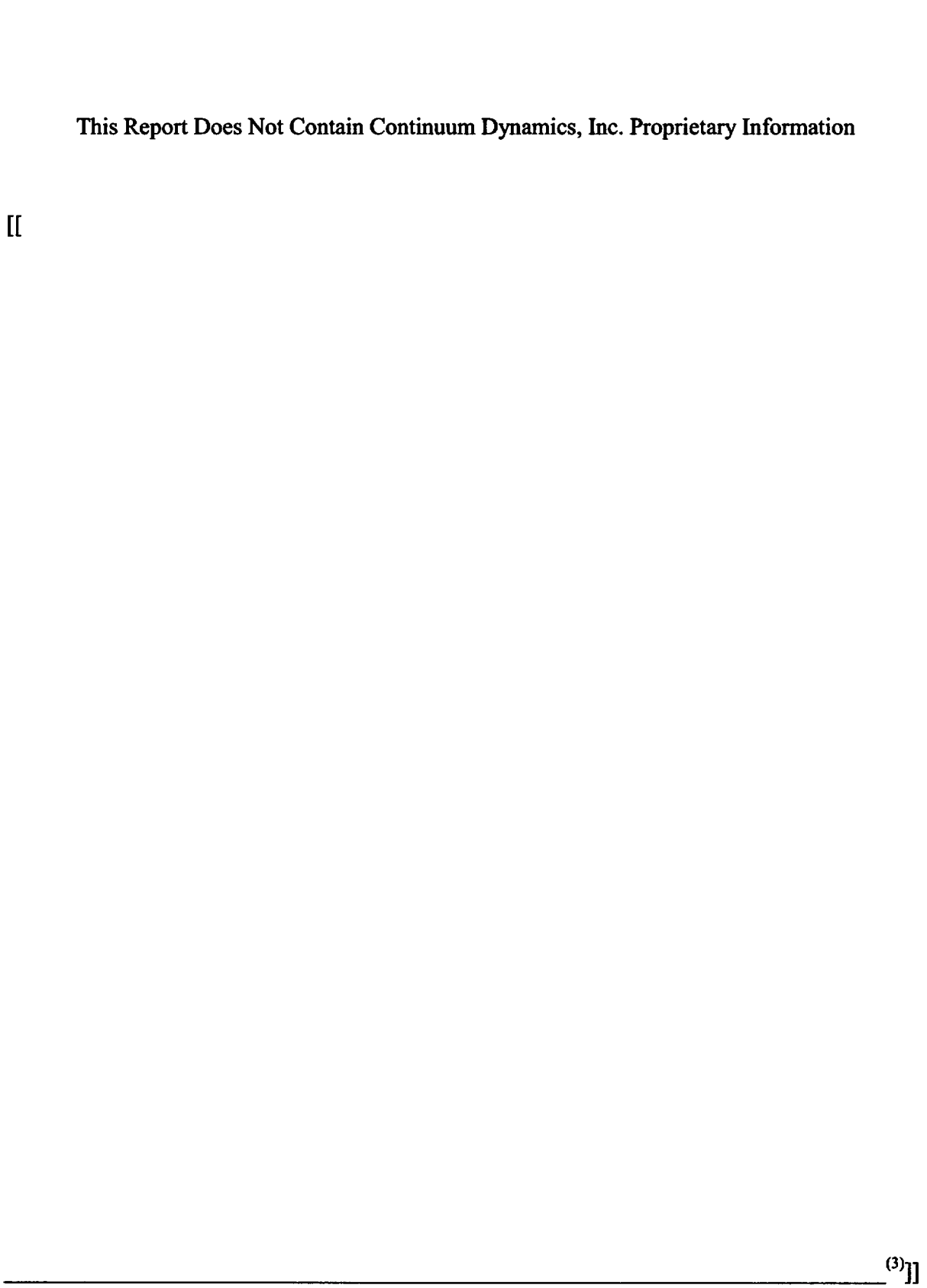

[3]]]

Figure A.16. PSD comparison at 790 MWe for pressure sensor data (blue curve) and Bounding Pressure prediction (red curve), for P16: 0 to 200 Hz (top), 125 to 165 Hz (bottom).

[[

[3]]]

Figure A.17. PSD comparison at 790 MWe for pressure sensor data (blue curve) and Bounding Pressure prediction (red curve), for P17: 0 to 200 Hz (top), 125 to 165 Hz (bottom).

[[

[3]]]

Figure A.18. PSD comparison at 790 MWe for pressure sensor data (blue curve) and Bounding Pressure prediction (red curve), for P18: 0 to 200 Hz (top), 125 to 165 Hz (bottom).

[[

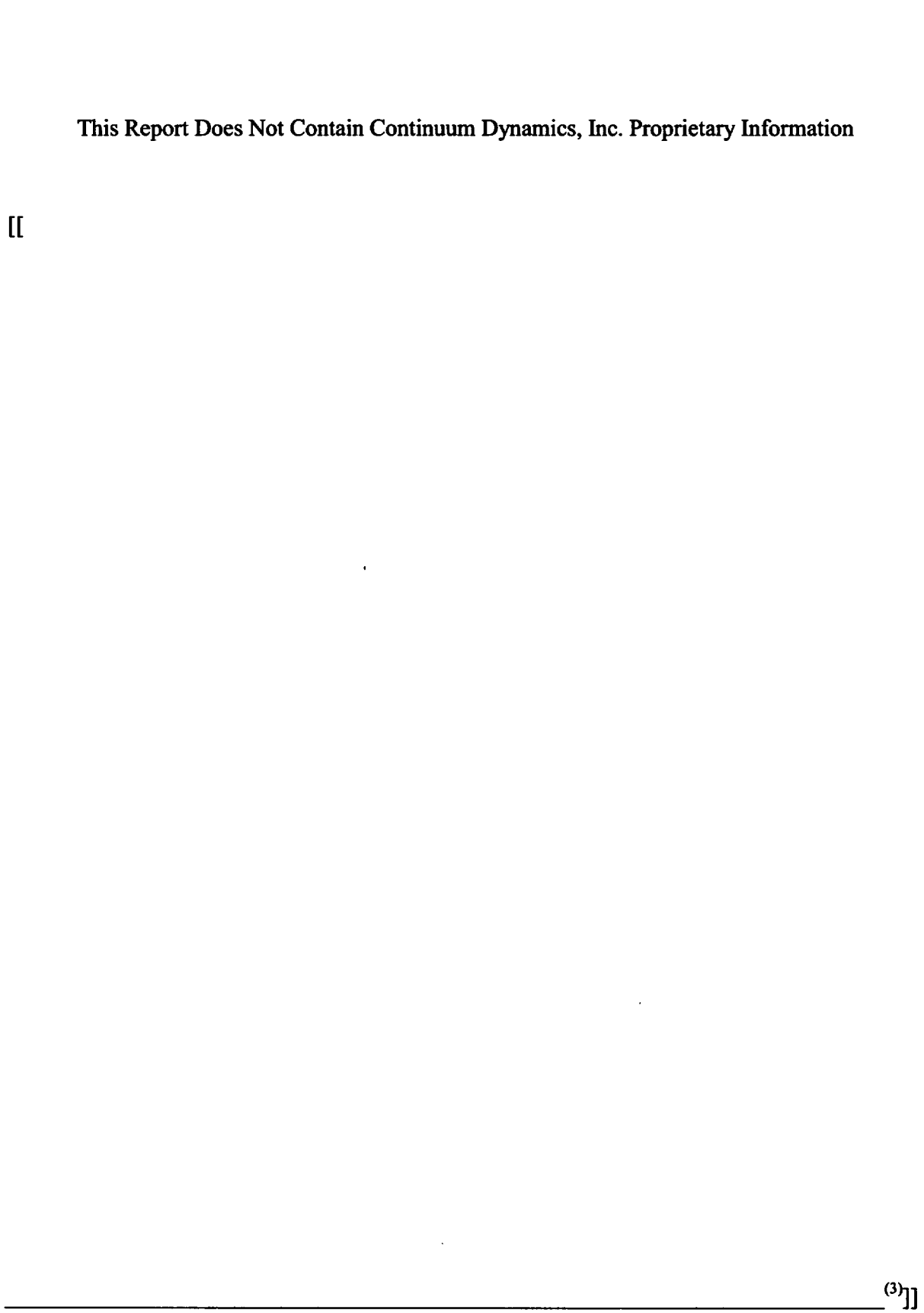

(3)]]

Figure A.19. PSD comparison at 790 MWe for pressure sensor data (blue curve) and Bounding Pressure prediction (red curve), for P20: 0 to 200 Hz (top), 125 to 165 Hz (bottom).

[[

]]$^{(3)}$

Figure A.20. PSD comparison at 790 MWe for pressure sensor data (blue curve) and Bounding Pressure prediction (red curve), for P21: 0 to 200 Hz (top), 125 to 165 Hz (bottom).

[[

]][3]

Figure A.21. PSD comparison at 790 MWe for pressure sensor data (blue curve) and Bounding Pressure prediction (red curve), for P22: 0 to 200 Hz (top), 125 to 165 Hz (bottom).

[[

]]$^{(3)}$

Figure A.22. PSD comparison at 790 MWe for pressure sensor data (blue curve) and Bounding Pressure prediction (red curve), for P23: 0 to 200 Hz (top), 125 to 165 Hz (bottom).

[[

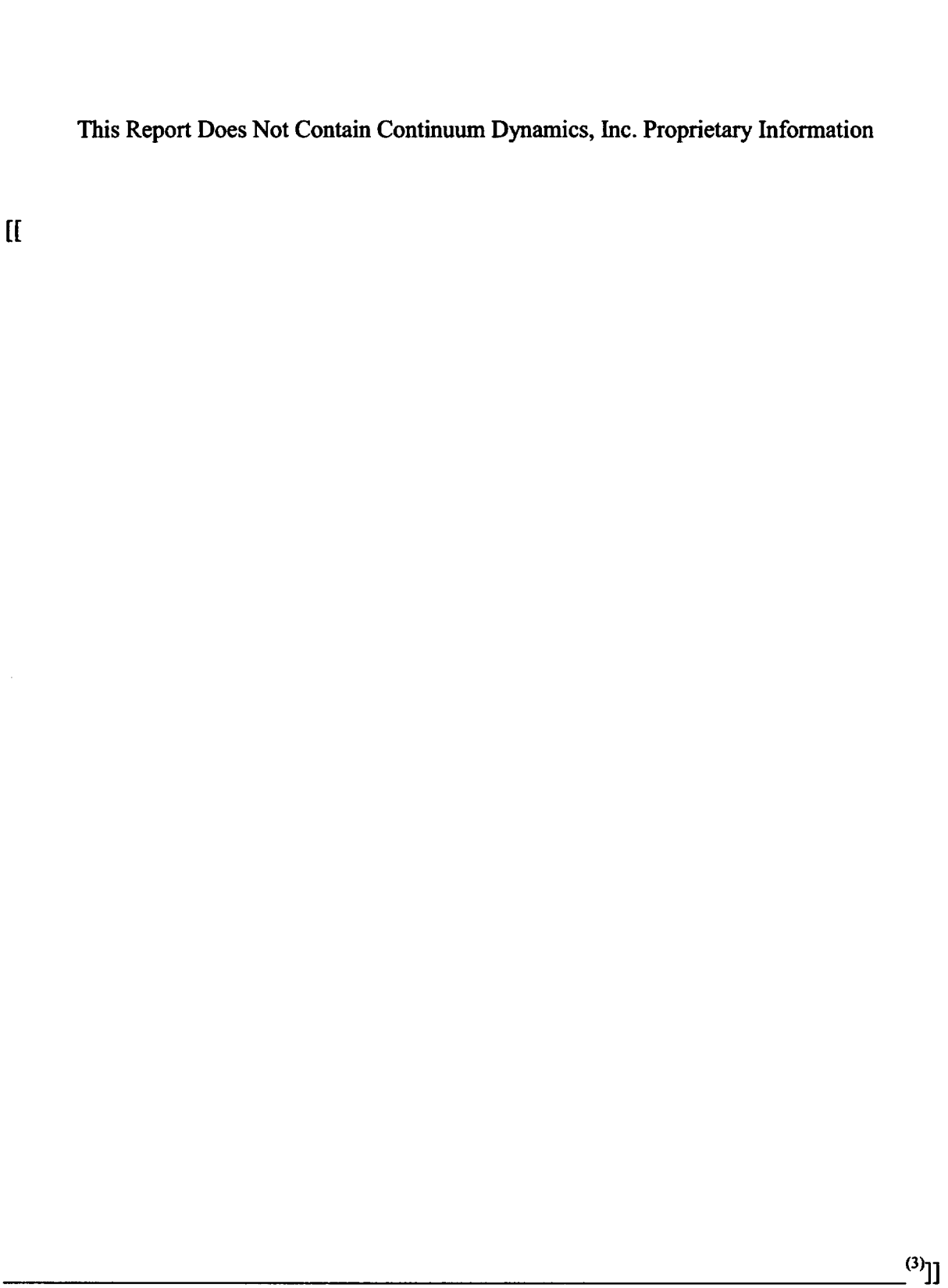

(3)]]

Figure A.23. PSD comparison at 790 MWe for pressure sensor data (blue curve) and Bounding Pressure prediction (red curve), for P24: 0 to 200 Hz (top), 125 to 165 Hz (bottom).

[[

]]$^{(3)}$

Figure A.24. PSD comparison at 790 MWe for pressure sensor data (blue curve) and Bounding Pressure prediction (red curve), for P25: 0 to 200 Hz (top), 125 to 165 Hz (bottom).

[[

]]$^{(3)}$

Figure A.25. PSD comparison at 790 MWe for pressure sensor data (blue curve) and Bounding Pressure prediction (red curve), for P26: 0 to 200 Hz (top), 125 to 165 Hz (bottom).

[[

[3]]]

Figure A.26. PSD comparison at 790 MWe for pressure sensor data (blue curve) and Bounding Pressure prediction (red curve), for P27: 0 to 200 Hz (top), 125 to 165 Hz (bottom).

Appendix B: Bounding Model Comparisons at 842 MWe

[[

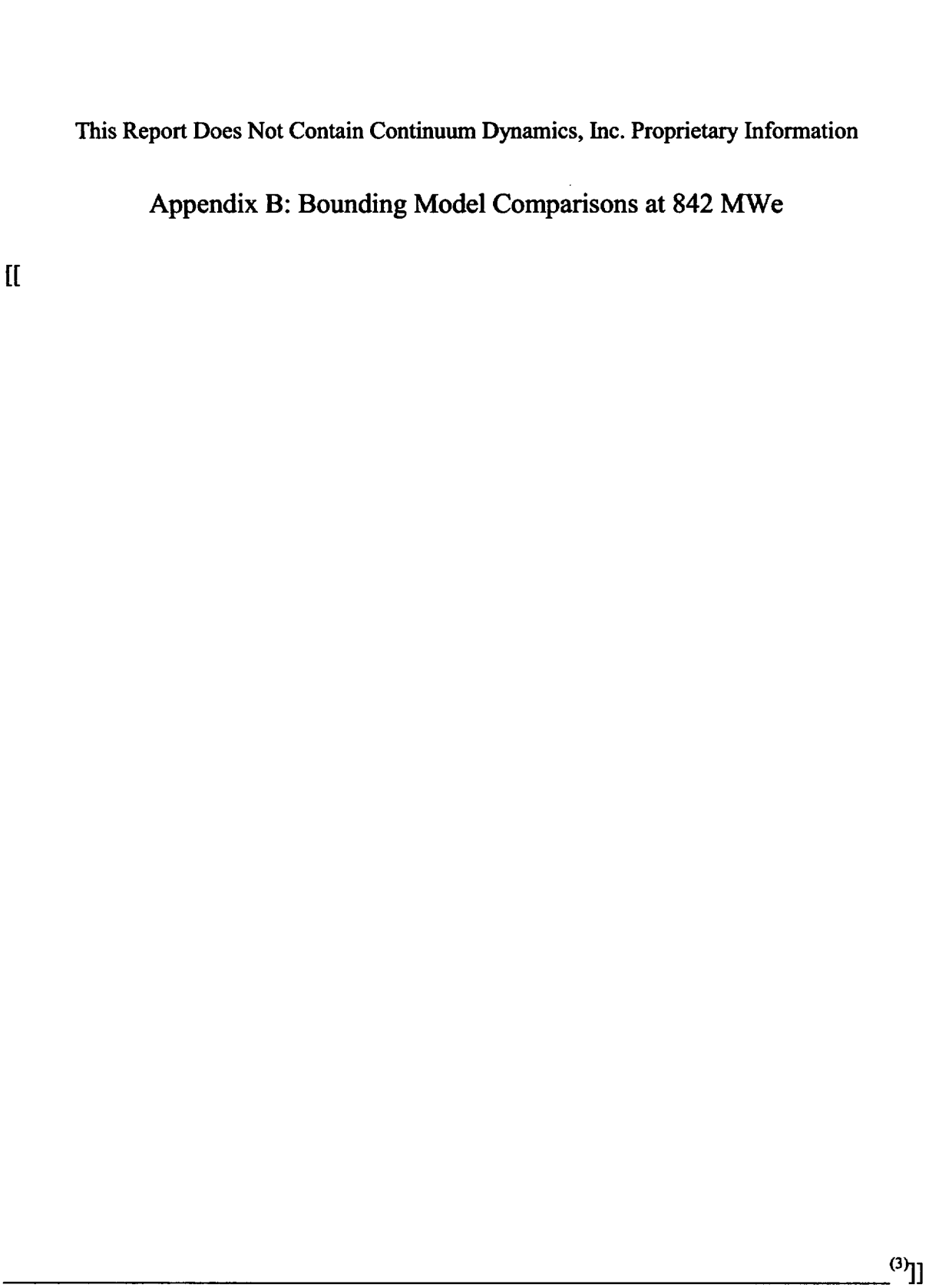

]]^(3)

Figure B.1. PSD comparison at 842 MWe for pressure sensor data (blue curve), Bounding Pressure prediction (red curve), and Bounding RMS prediction (black curve), for P1: 0 to 200 Hz (top), 130 to 165 Hz (bottom).

[[

]]$^{(3)}$

Figure B.2. PSD comparison at 842 MWe for pressure sensor data (blue curve), Bounding Pressure prediction (red curve), and Bounding RMS prediction (black curve), for P2: 0 to 200 Hz (top), 130 to 165 Hz (bottom).

[[

[3]]]

Figure B.3. PSD comparison at 842 MWe for pressure sensor data (blue curve), Bounding Pressure prediction (red curve), and Bounding RMS prediction (black curve), for P3: 0 to 200 Hz (top), 130 to 165 Hz (bottom).

[[

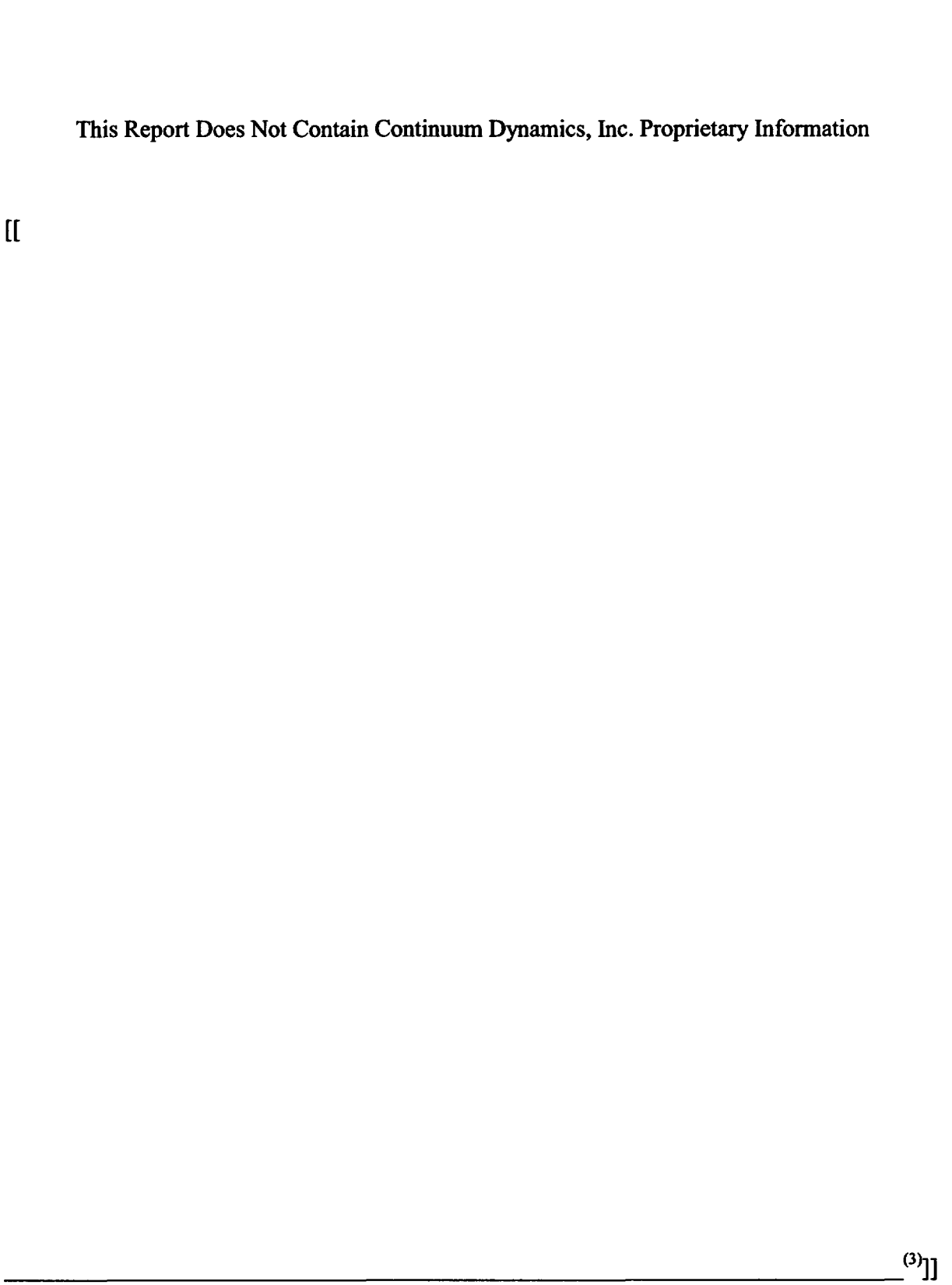

[3]]]

Figure B.4. PSD comparison at 842 MWe for pressure sensor data (blue curve), Bounding Pressure prediction (red curve), and Bounding RMS prediction (black curve), for P4: 0 to 200 Hz (top), 130 to 165 Hz (bottom).

[[

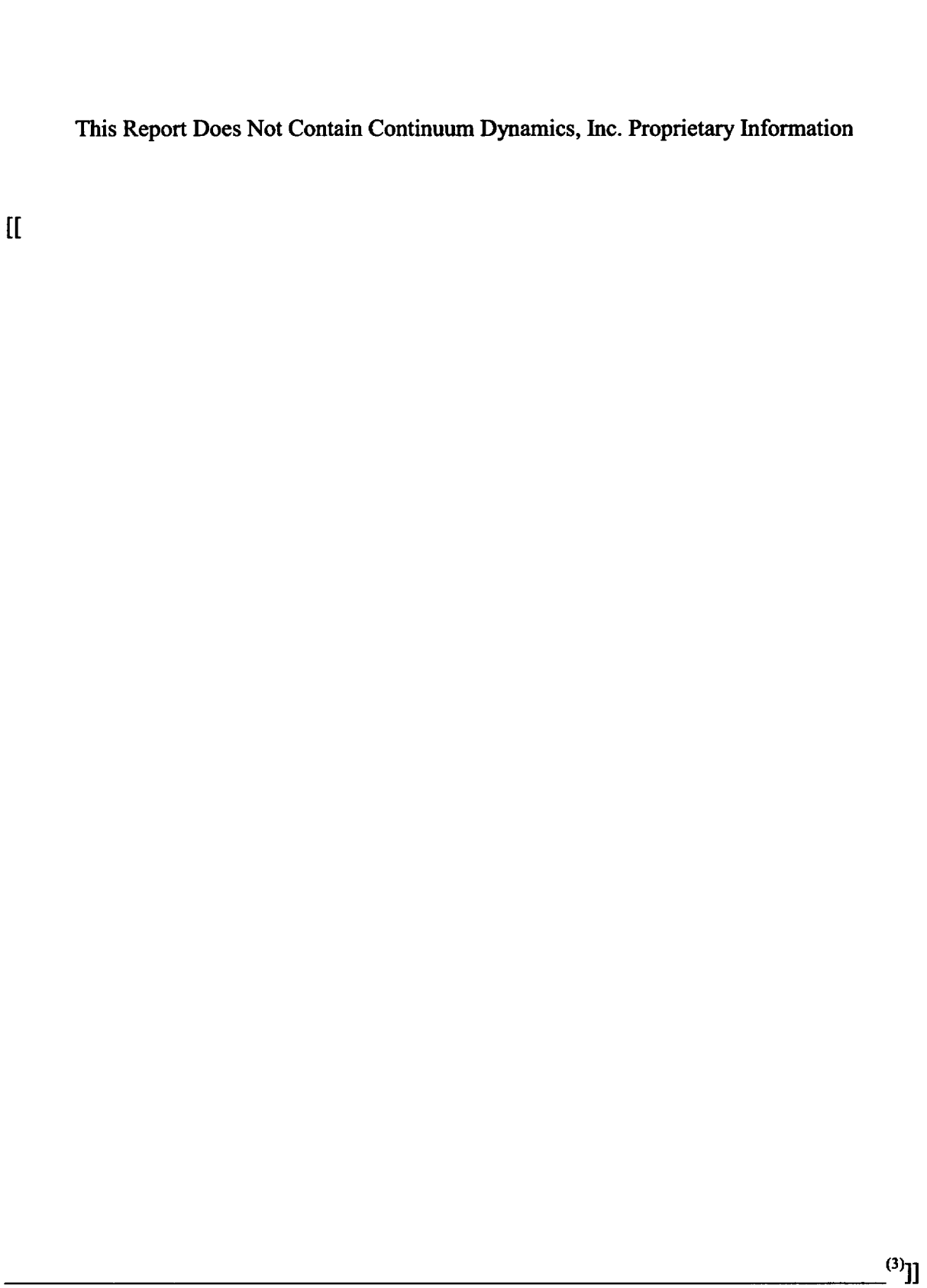

]][3]

Figure B.5. PSD comparison at 842 MWe for pressure sensor data (blue curve), Bounding Pressure prediction (red curve), and Bounding RMS prediction (black curve), for P5: 0 to 200 Hz (top), 130 to 165 Hz (bottom).

[[

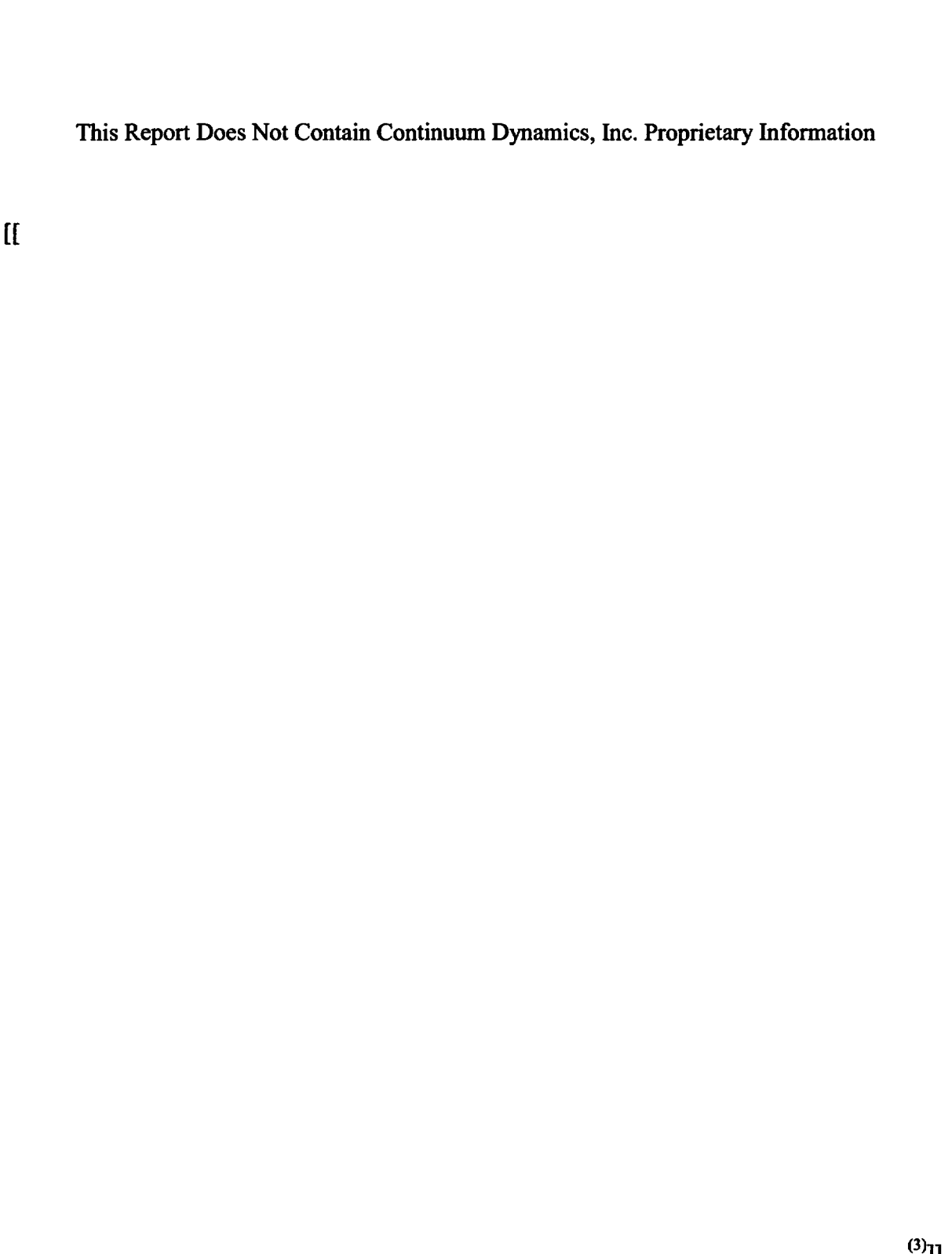

]] [3]

Figure B.6. PSD comparison at 842 MWe for pressure sensor data (blue curve), Bounding Pressure prediction (red curve), and Bounding RMS prediction (black curve), for P6: 0 to 200 Hz (top), 130 to 165 Hz (bottom).

[[

]][3]

Figure B.7. PSD comparison at 842 MWe for pressure sensor data (blue curve), Bounding Pressure prediction (red curve), and Bounding RMS prediction (black curve), for P7: 0 to 200 Hz (top), 130 to 165 Hz (bottom).

[[

[3]]]

Figure B.8. PSD comparison at 842 MWe for pressure sensor data (blue curve), Bounding Pressure prediction (red curve), and Bounding RMS prediction (black curve), for P8: 0 to 200 Hz (top), 130 to 165 Hz (bottom).

[[

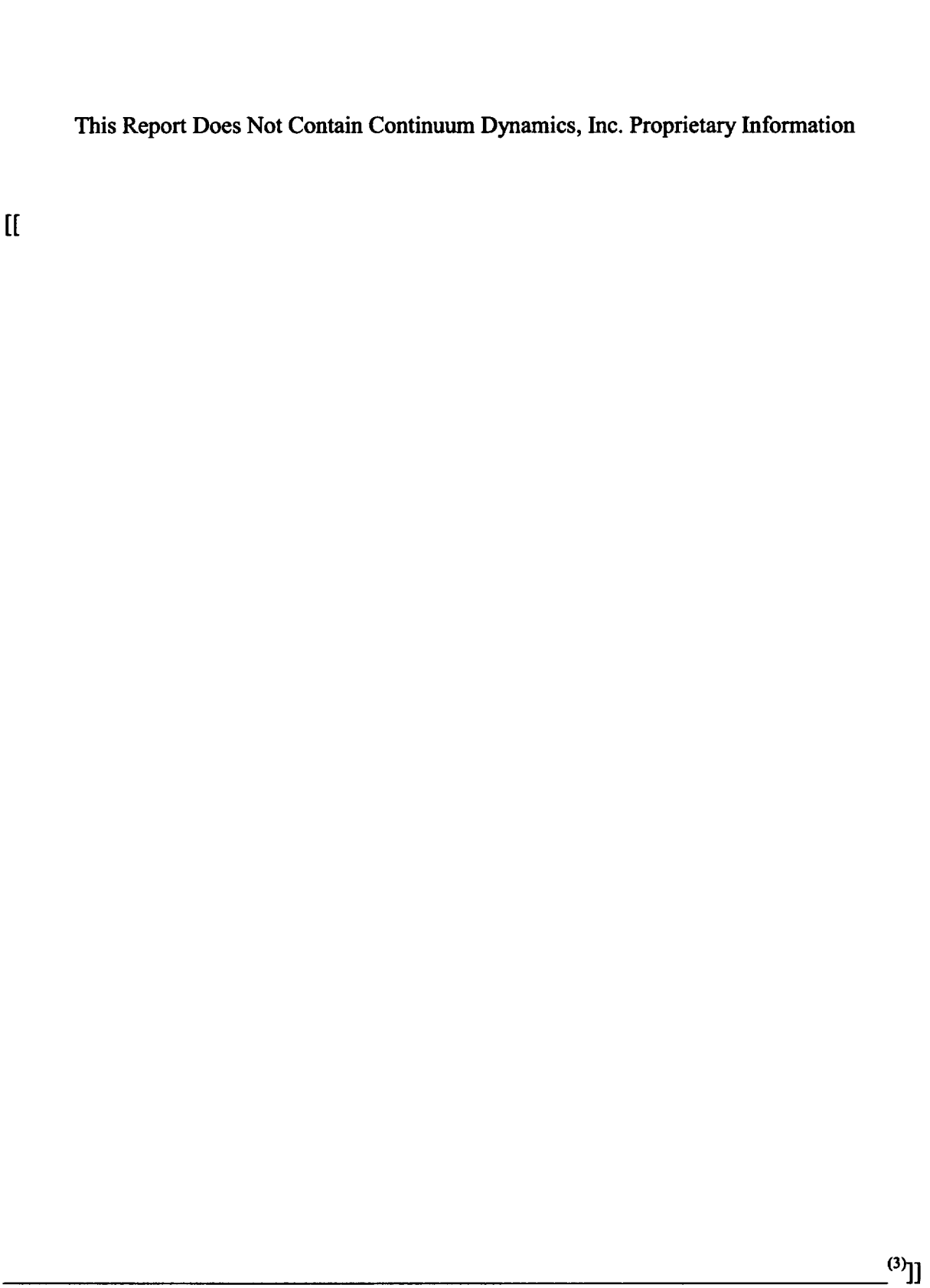

[3]]

Figure B.9. PSD comparison at 842 MWe for pressure sensor data (blue curve), Bounding Pressure prediction (red curve), and Bounding RMS prediction (black curve), for P9: 0 to 200 Hz (top), 130 to 165 Hz (bottom).

[[

[3]]]

Figure B.10. PSD comparison at 842 MWe for pressure sensor data (blue curve), Bounding Pressure prediction (red curve), and Bounding RMS prediction (black curve), for P10: 0 to 200 Hz (top), 130 to 165 Hz (bottom).

[[

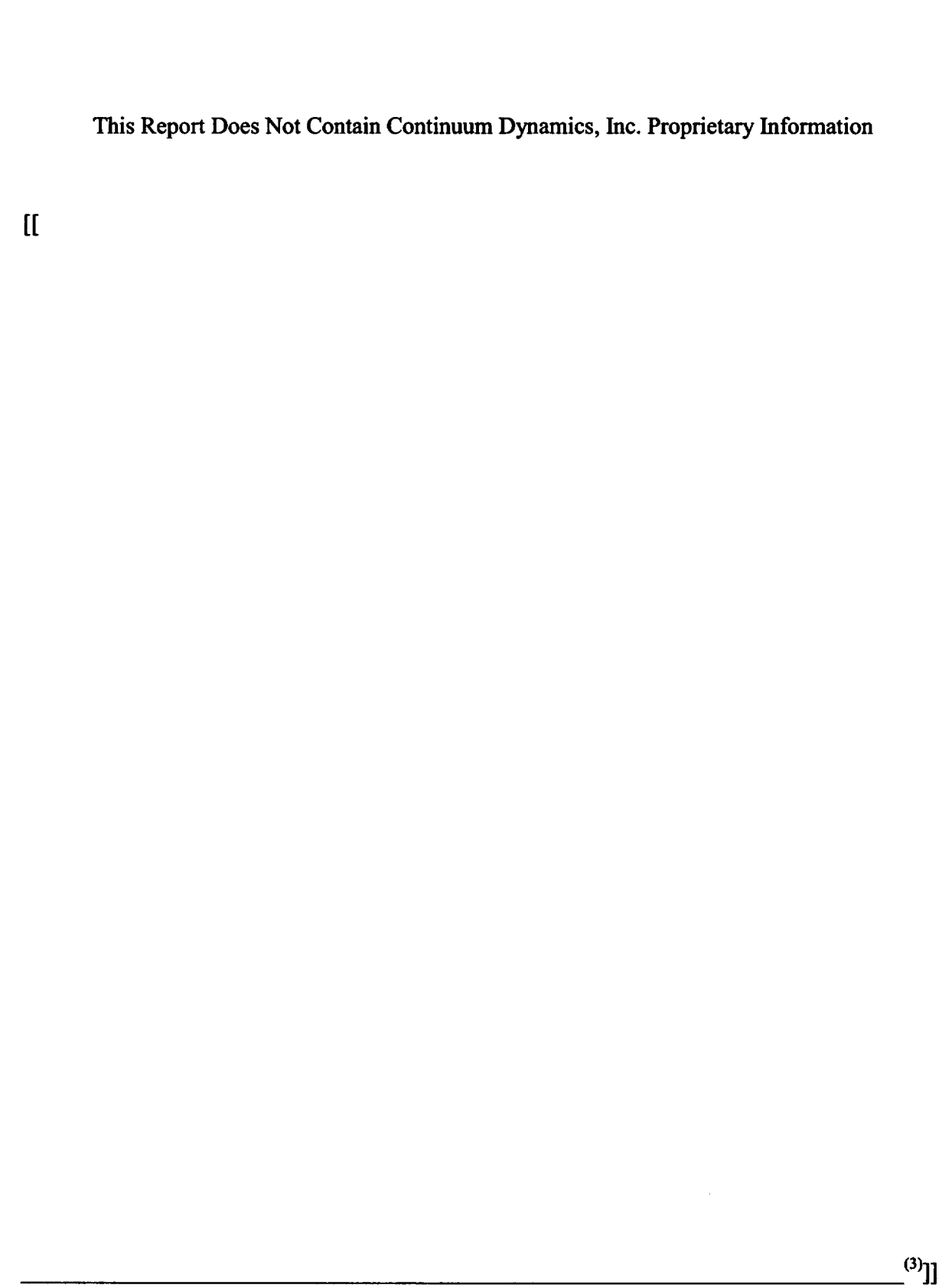

(3)]]

Figure B.11. PSD comparison at 842 MWe for pressure sensor data (blue curve), Bounding Pressure prediction (red curve), and Bounding RMS prediction (black curve), for P11: 0 to 200 Hz (top), 130 to 165 Hz (bottom).

[[

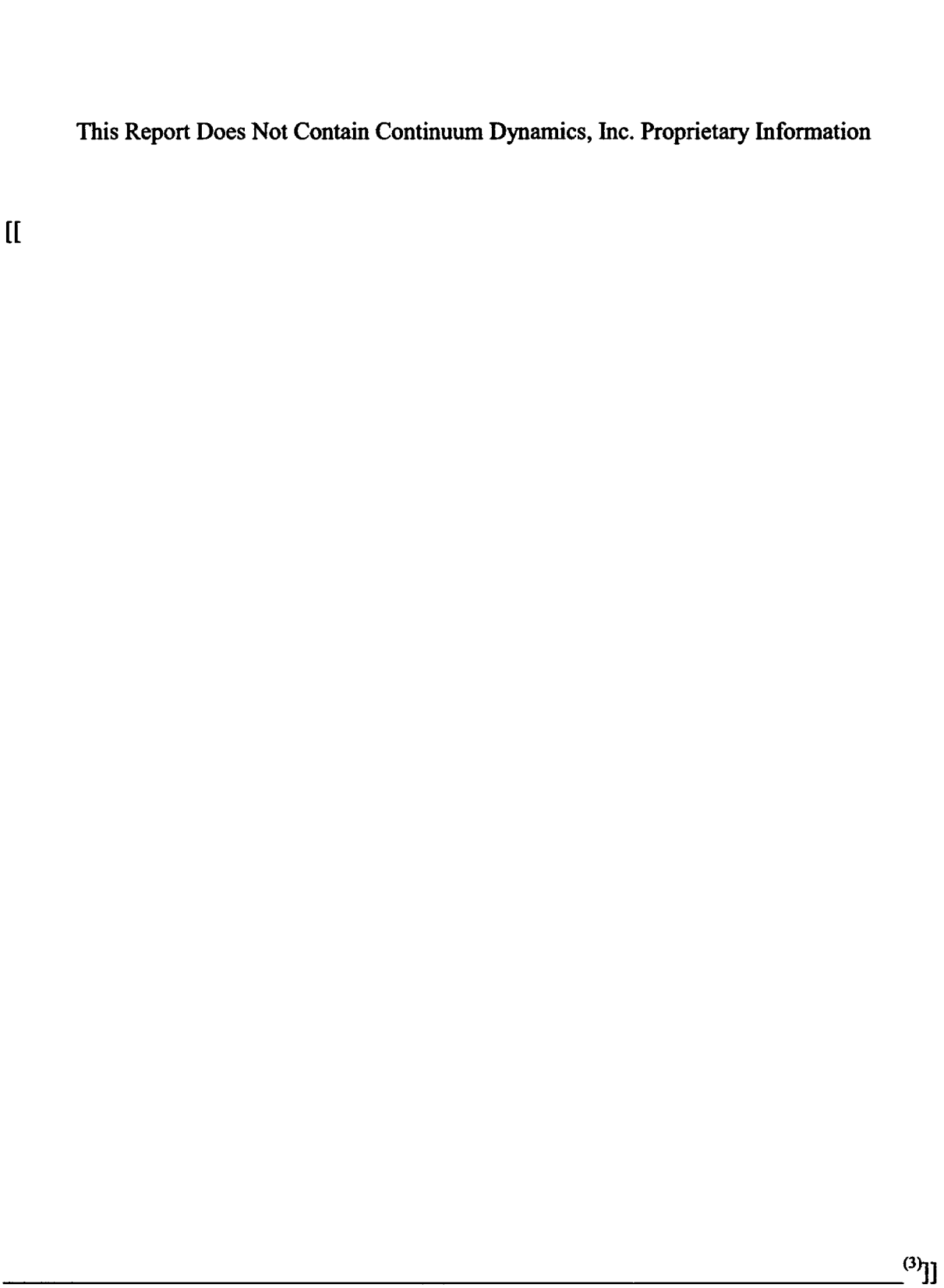

]]^(3)

Figure B.12. PSD comparison at 842 MWe for pressure sensor data (blue curve), Bounding Pressure prediction (red curve), and Bounding RMS prediction (black curve), for P12: 0 to 200 Hz (top), 130 to 165 Hz (bottom).

[[

[3]]]

Figure B.13. PSD comparison at 842 MWe for pressure sensor data (blue curve), Bounding Pressure prediction (red curve), and Bounding RMS prediction (black curve), for P13: 0 to 200 Hz (top), 130 to 165 Hz (bottom).

[[

(3)]]

Figure B.14. PSD comparison at 842 MWe for pressure sensor data (blue curve), Bounding Pressure prediction (red curve), and Bounding RMS prediction (black curve), for P14: 0 to 200 Hz (top), 130 to 165 Hz (bottom).

[[

]][3]

Figure B.15. PSD comparison at 842 MWe for pressure sensor data (blue curve), Bounding Pressure prediction (red curve), and Bounding RMS prediction (black curve), for P15: 0 to 200 Hz (top), 130 to 165 Hz (bottom).

[[

[3]]]

Figure B.16. PSD comparison at 842 MWe for pressure sensor data (blue curve), Bounding Pressure prediction (red curve), and Bounding RMS prediction (black curve), for P16: 0 to 200 Hz (top), 130 to 165 Hz (bottom).

[[

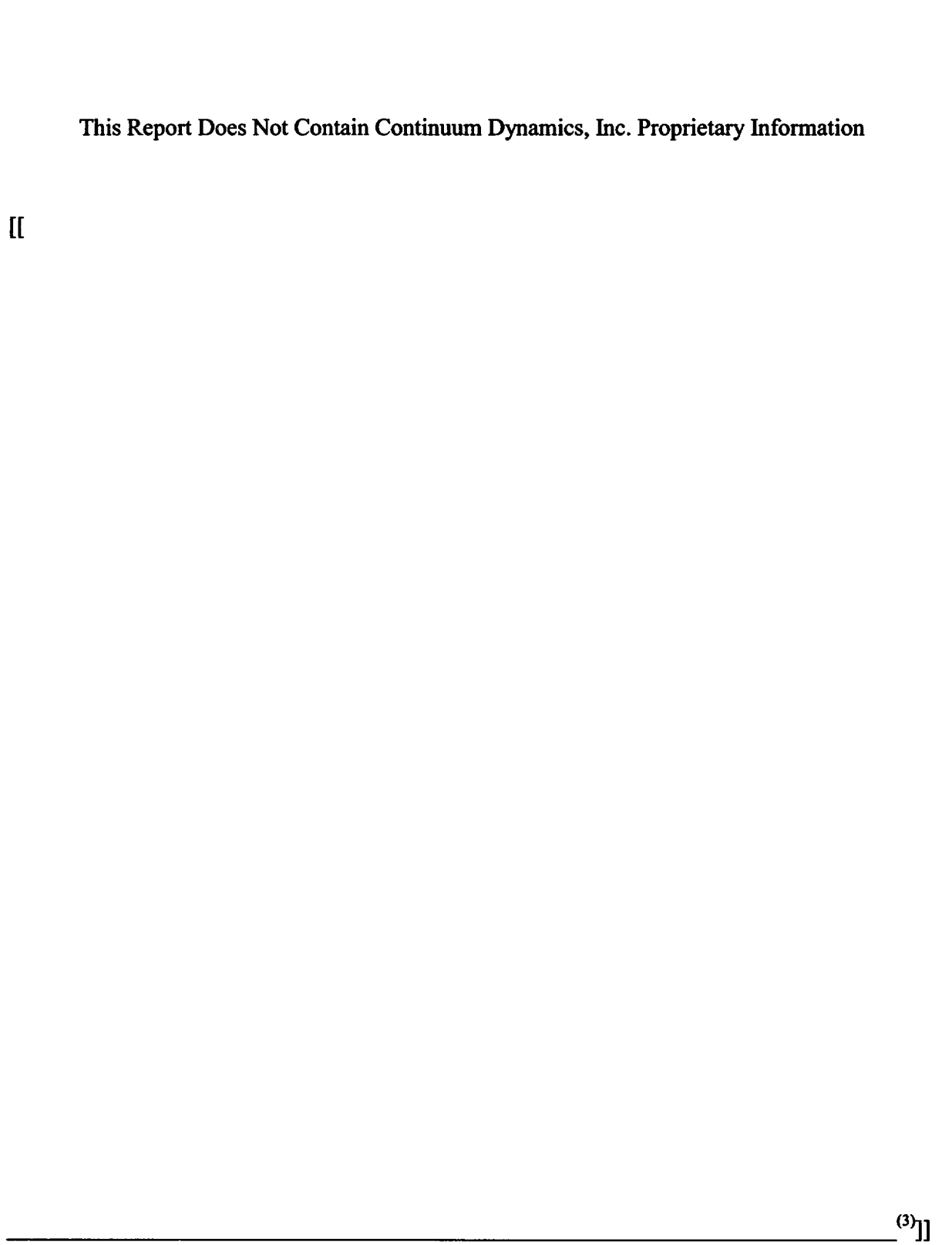

[3]]]

Figure B.17. PSD comparison at 842 MWe for pressure sensor data (blue curve), Bounding Pressure prediction (red curve), and Bounding RMS prediction (black curve), for P17: 0 to 200 Hz (top), 130 to 165 Hz (bottom).

[[

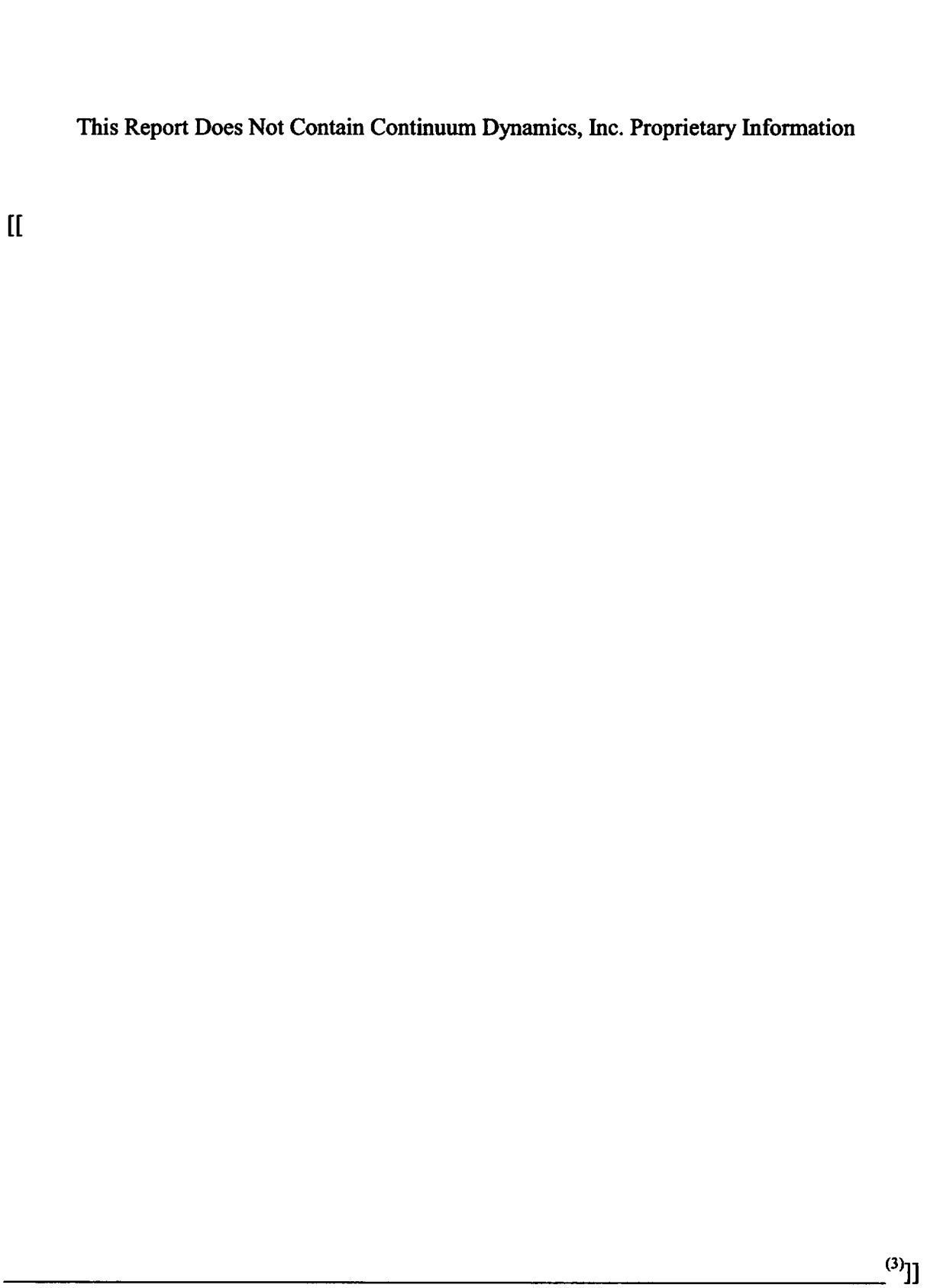

(3)]]

Figure B.18. PSD comparison at 842 MWe for pressure sensor data (blue curve), Bounding Pressure prediction (red curve), and Bounding RMS prediction (black curve), for P18: 0 to 200 Hz (top), 130 to 165 Hz (bottom).

[[

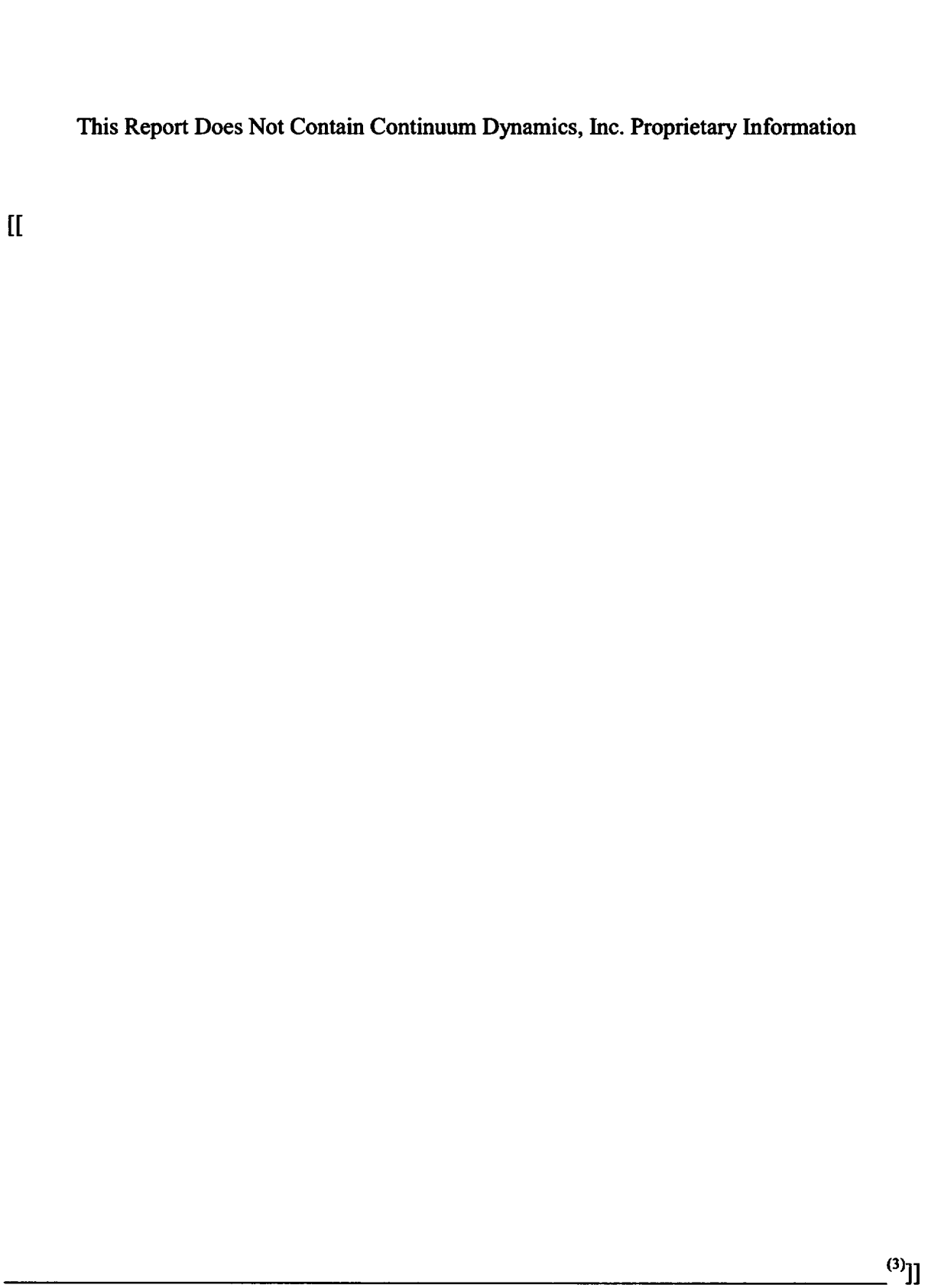

]] [3]

Figure B.19. PSD comparison at 842 MWe for pressure sensor data (blue curve), Bounding Pressure prediction (red curve), and Bounding RMS prediction (black curve), for P20: 0 to 200 Hz (top), 130 to 165 Hz (bottom).

[[

[3]]]

Figure B.20. PSD comparison at 842 MWe for pressure sensor data (blue curve), Bounding Pressure prediction (red curve), and Bounding RMS prediction (black curve), for P21: 0 to 200 Hz (top), 130 to 165 Hz (bottom).

[[

[3]]]

Figure B.21. PSD comparison at 842 MWe for pressure sensor data (blue curve), Bounding Pressure prediction (red curve), and Bounding RMS prediction (black curve), for P22: 0 to 200 Hz (top), 130 to 165 Hz (bottom).

[[

(3)]]

Figure B.22. PSD comparison at 842 MWe for pressure sensor data (blue curve), Bounding Pressure prediction (red curve), and Bounding RMS prediction (black curve), for P23: 0 to 200 Hz (top), 130 to 165 Hz (bottom).

[[

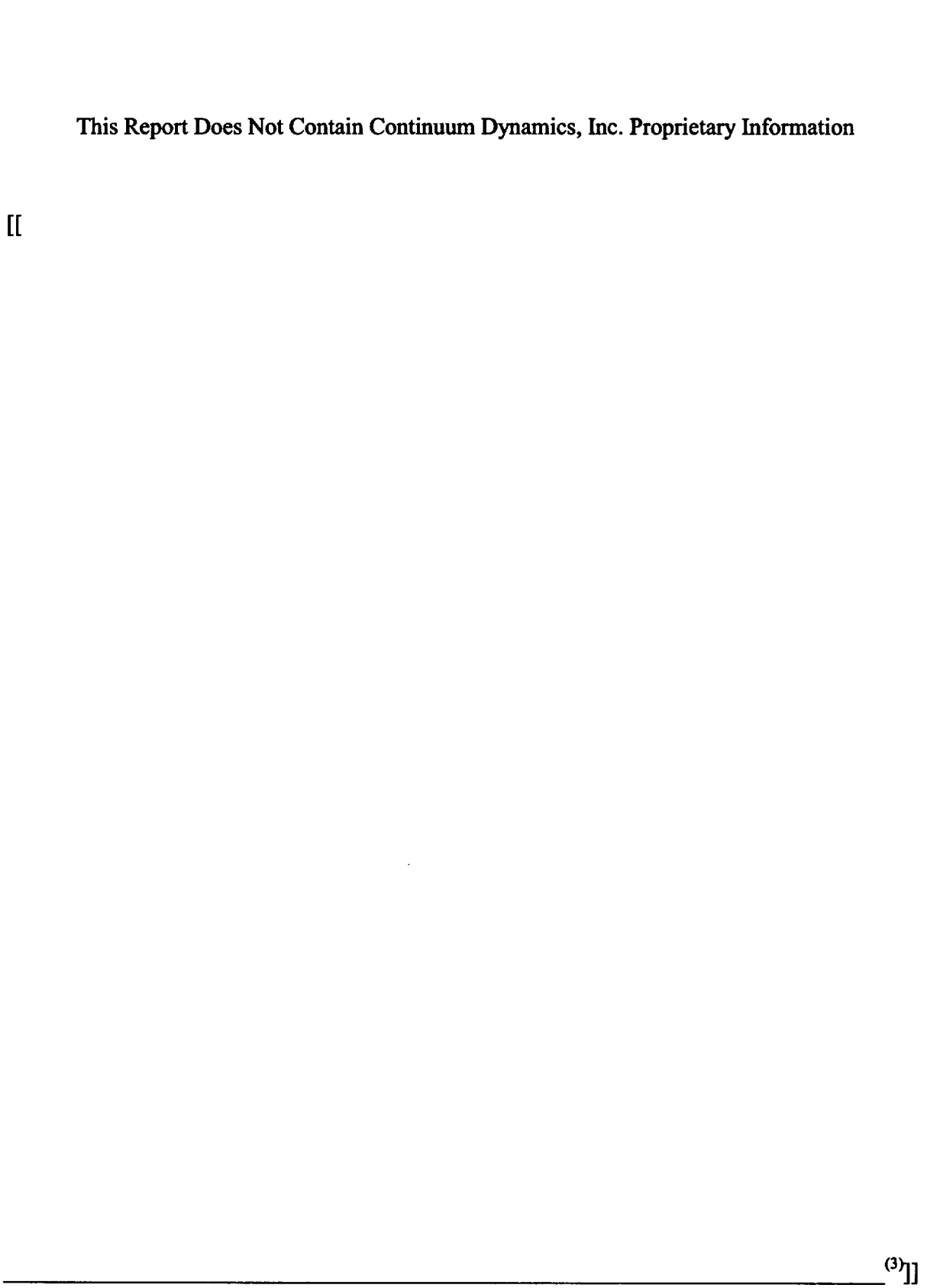

]]$^{(3)}$

Figure B.23. PSD comparison at 842 MWe for pressure sensor data (blue curve), Bounding Pressure prediction (red curve), and Bounding RMS prediction (black curve), for P24: 0 to 200 Hz (top), 130 to 165 Hz (bottom).

[[

]]^(3)

Figure B.24. PSD comparison at 842 MWe for pressure sensor data (blue curve), Bounding Pressure prediction (red curve), and Bounding RMS prediction (black curve), for P25: 0 to 200 Hz (top), 130 to 165 Hz (bottom).

[[

[3]]]

Figure B.25. PSD comparison at 842 MWe for pressure sensor data (blue curve), Bounding Pressure prediction (red curve), and Bounding RMS prediction (black curve), for P26: 0 to 200 Hz (top), 130 to 165 Hz (bottom).

[[

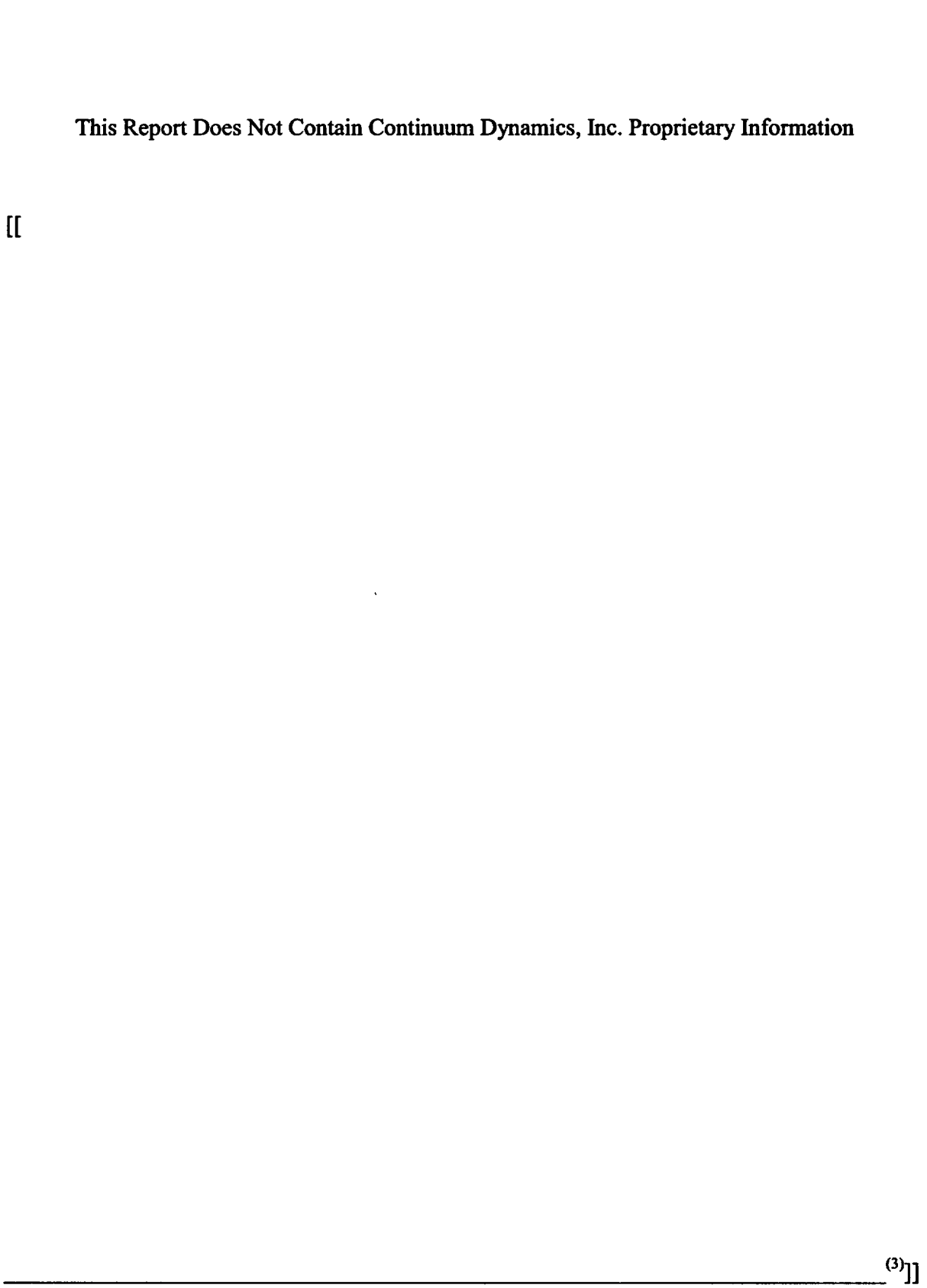

]]^(3)

Figure B.26. PSD comparison at 842 MWe for pressure sensor data (blue curve), Bounding Pressure prediction (red curve), and Bounding RMS prediction (black curve), for P27: 0 to 200 Hz (top), 130 to 165 Hz (bottom).

Appendix C: Bounding Model Comparisons at 930 MWe

[[

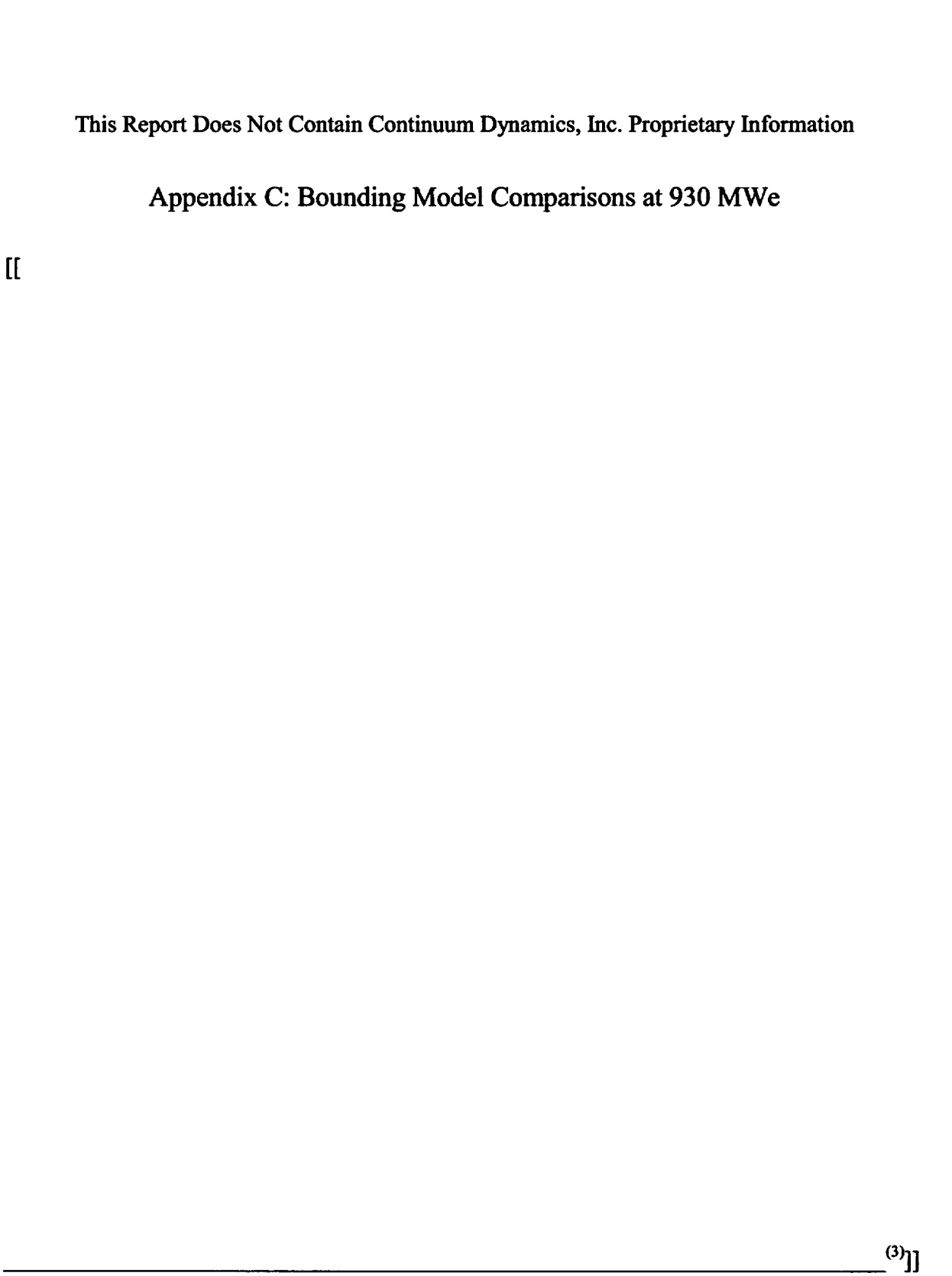

$^{(3)}$]]

Figure C.1. PSD comparison at 930 MWe for pressure sensor data (blue curve), Bounding Pressure prediction (red curve), Bounding RMS prediction (black curve), and Bounding PSD prediction (green curve), for P1: 0 to 200 Hz (top), 135 to 165 Hz (bottom).

[[

]]$^{(3)}$

Figure C.2. PSD comparison at 930 MWe for pressure sensor data (blue curve), Bounding Pressure prediction (red curve), Bounding RMS prediction (black curve), and Bounding PSD prediction (green curve), for P2: 0 to 200 Hz (top), 135 to 165 Hz (bottom).

[[

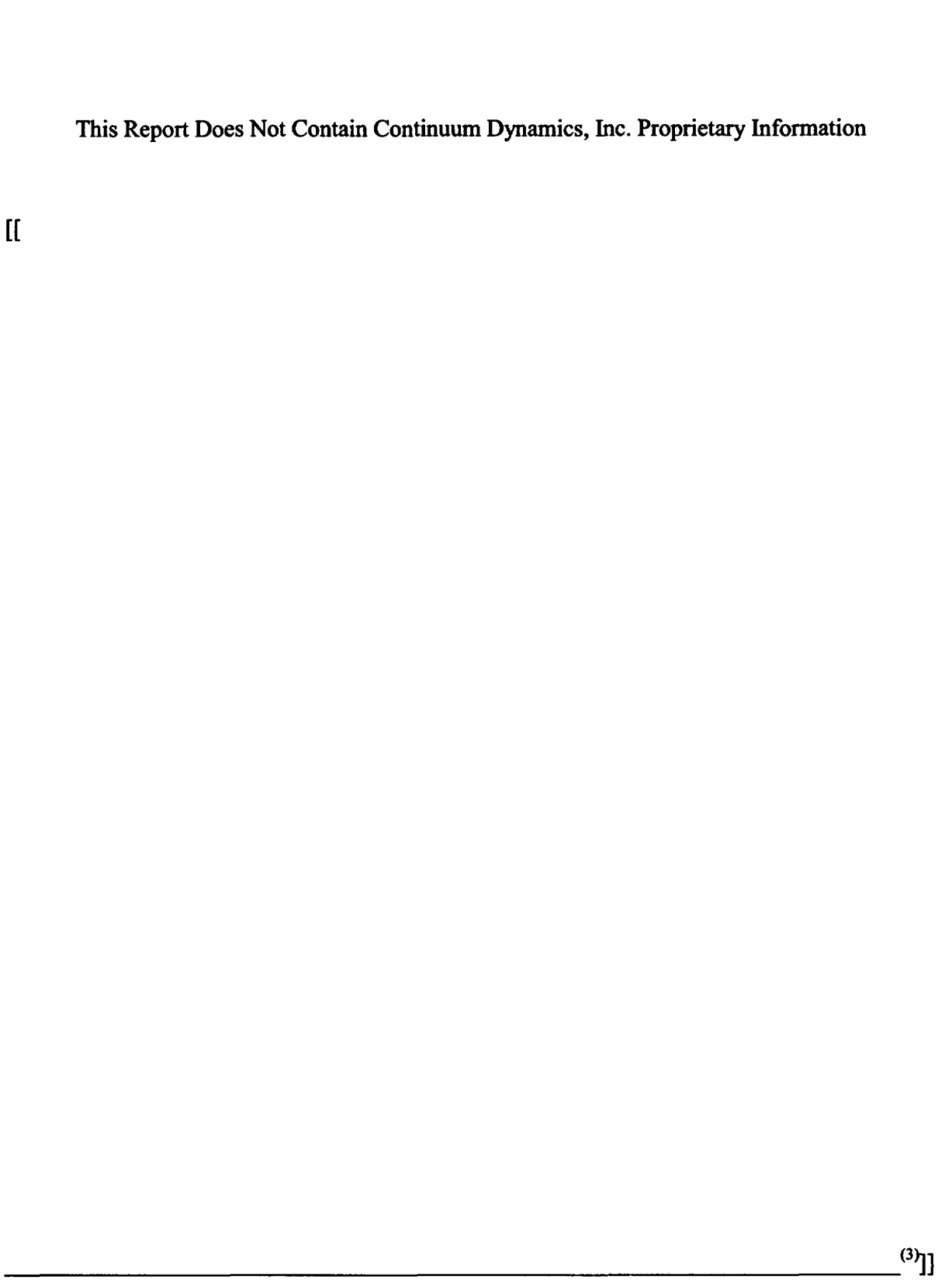

[3]]]

Figure C.3. PSD comparison at 930 MWe for pressure sensor data (blue curve), Bounding Pressure prediction (red curve), Bounding RMS prediction (black curve), and Bounding PSD prediction (green curve), for P3: 0 to 200 Hz (top), 135 to 165 Hz (bottom).

[[

$^{(3)}$]]

Figure C.4. PSD comparison at 930 MWe for pressure sensor data (blue curve), Bounding Pressure prediction (red curve), Bounding RMS prediction (black curve), and Bounding PSD prediction (green curve), for P4: 0 to 200 Hz (top), 135 to 165 Hz (bottom).

[[

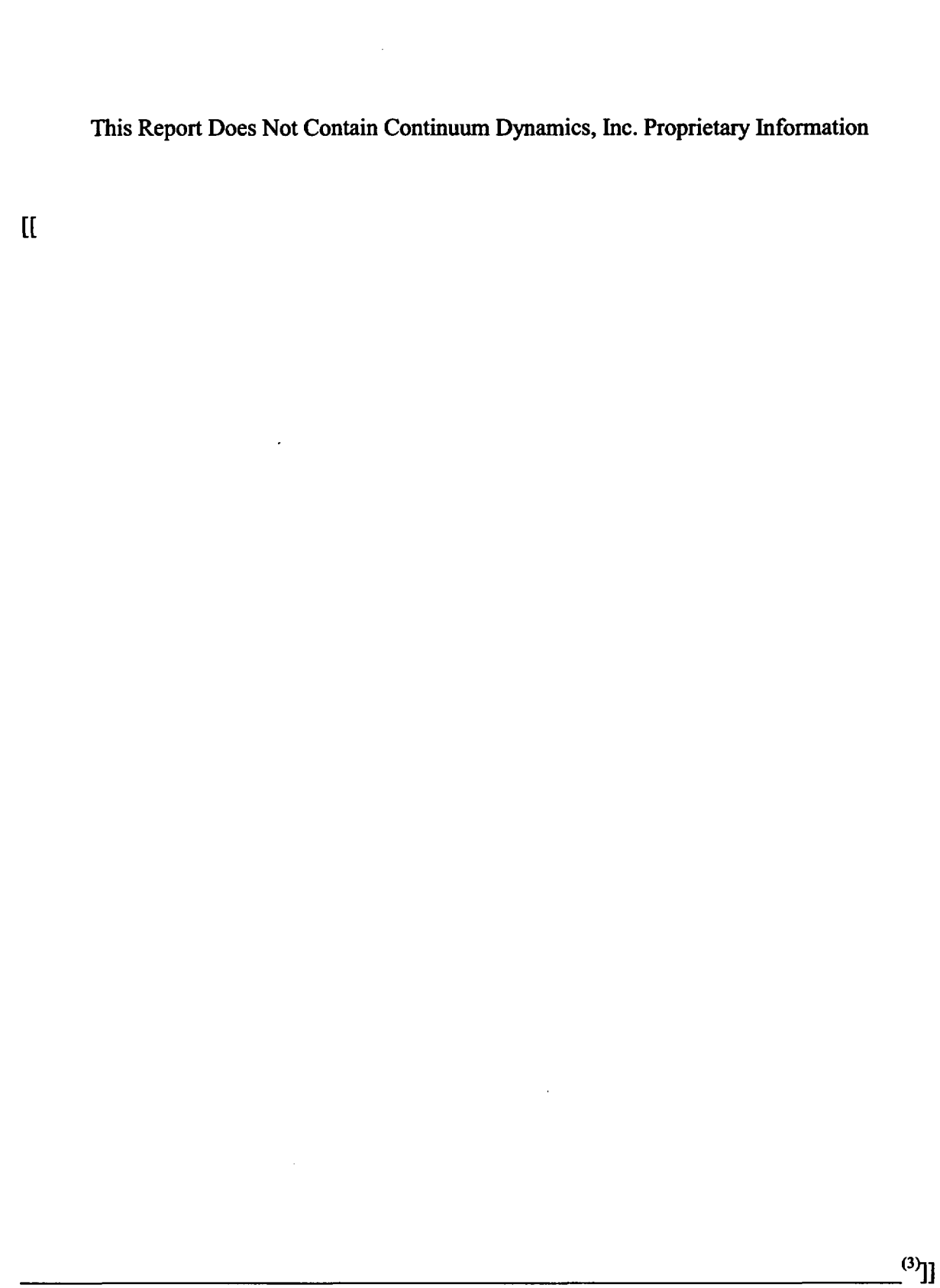

]]$^{(3)}$

Figure C.5. PSD comparison at 930 MWe for pressure sensor data (blue curve), Bounding Pressure prediction (red curve), Bounding RMS prediction (black curve), and Bounding PSD prediction (green curve), for P5: 0 to 200 Hz (top), 135 to 165 Hz (bottom).

[[

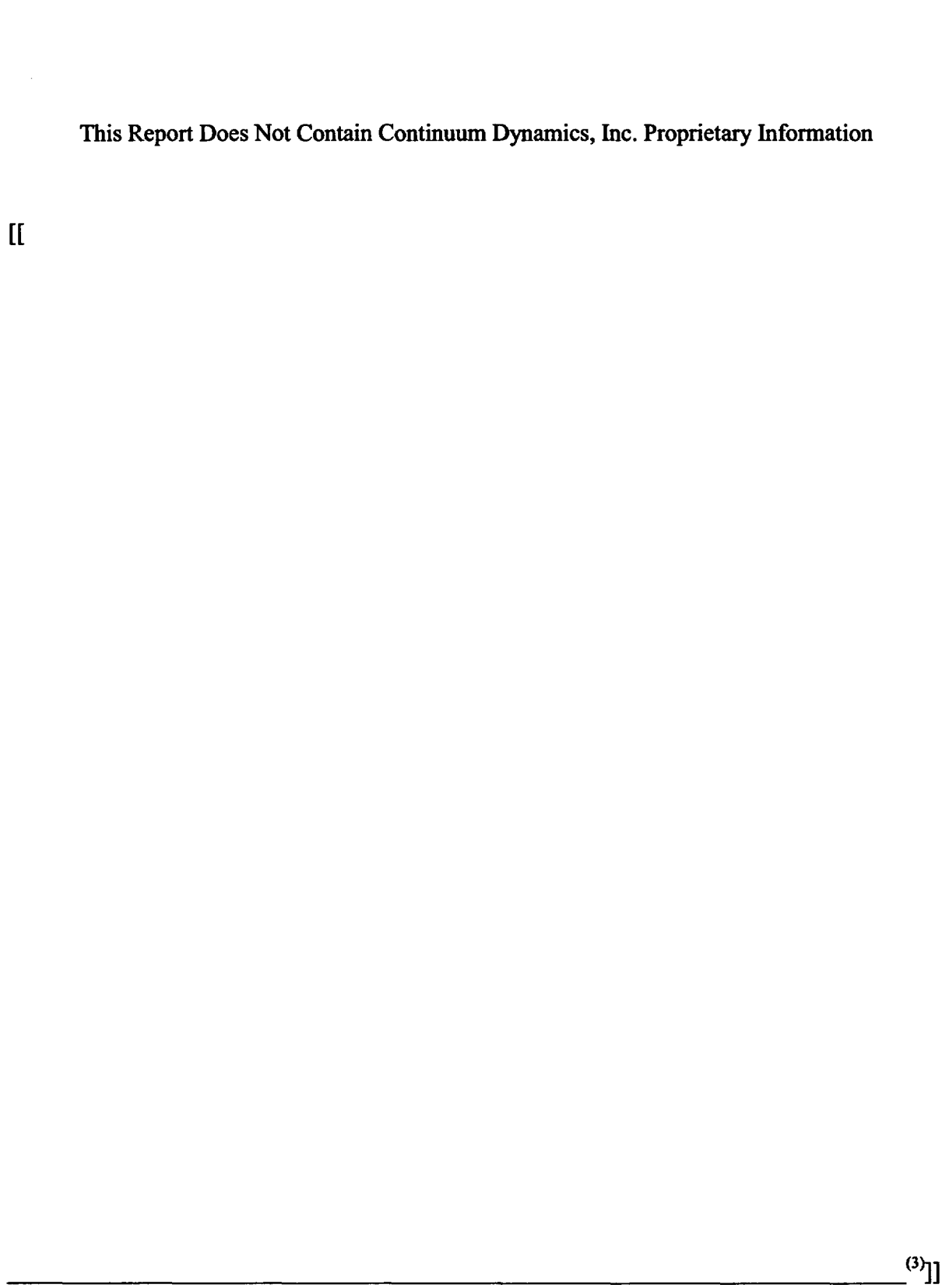

]]^(3)

Figure C.6. PSD comparison at 930 MWe for pressure sensor data (blue curve), Bounding Pressure prediction (red curve), Bounding RMS prediction (black curve), and Bounding PSD prediction (green curve), for P6: 0 to 200 Hz (top), 135 to 165 Hz (bottom).

[[

[3]]]

Figure C.7. PSD comparison at 930 MWe for pressure sensor data (blue curve), Bounding Pressure prediction (red curve), Bounding RMS prediction (black curve), and Bounding PSD prediction (green curve), for P7: 0 to 200 Hz (top), 135 to 165 Hz (bottom).

[[

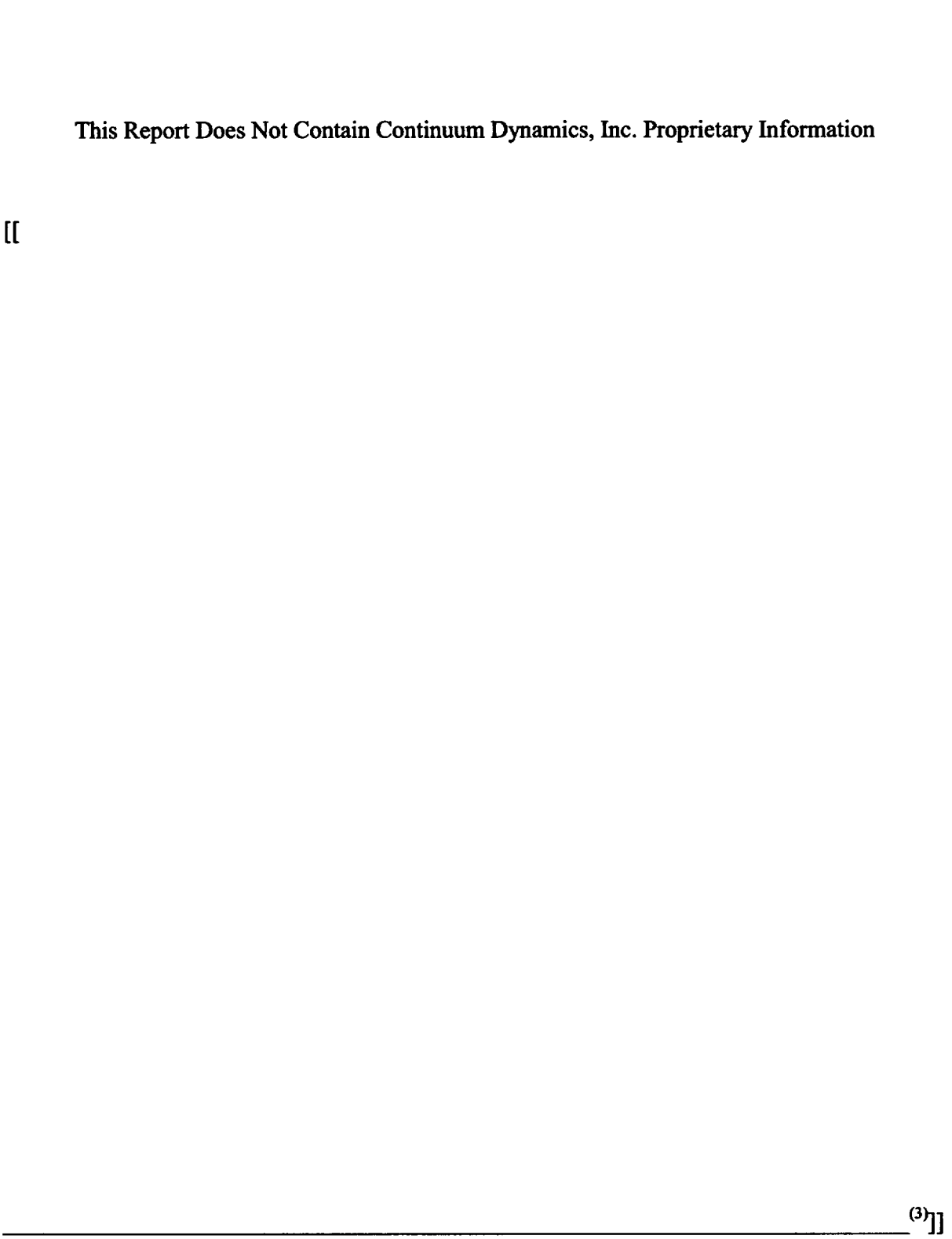

]]$^{(3)}$

Figure C.8. PSD comparison at 930 MWe for pressure sensor data (blue curve), Bounding Pressure prediction (red curve), Bounding RMS prediction (black curve), and Bounding PSD prediction (green curve), for P8: 0 to 200 Hz (top), 135 to 165 Hz (bottom).

[[

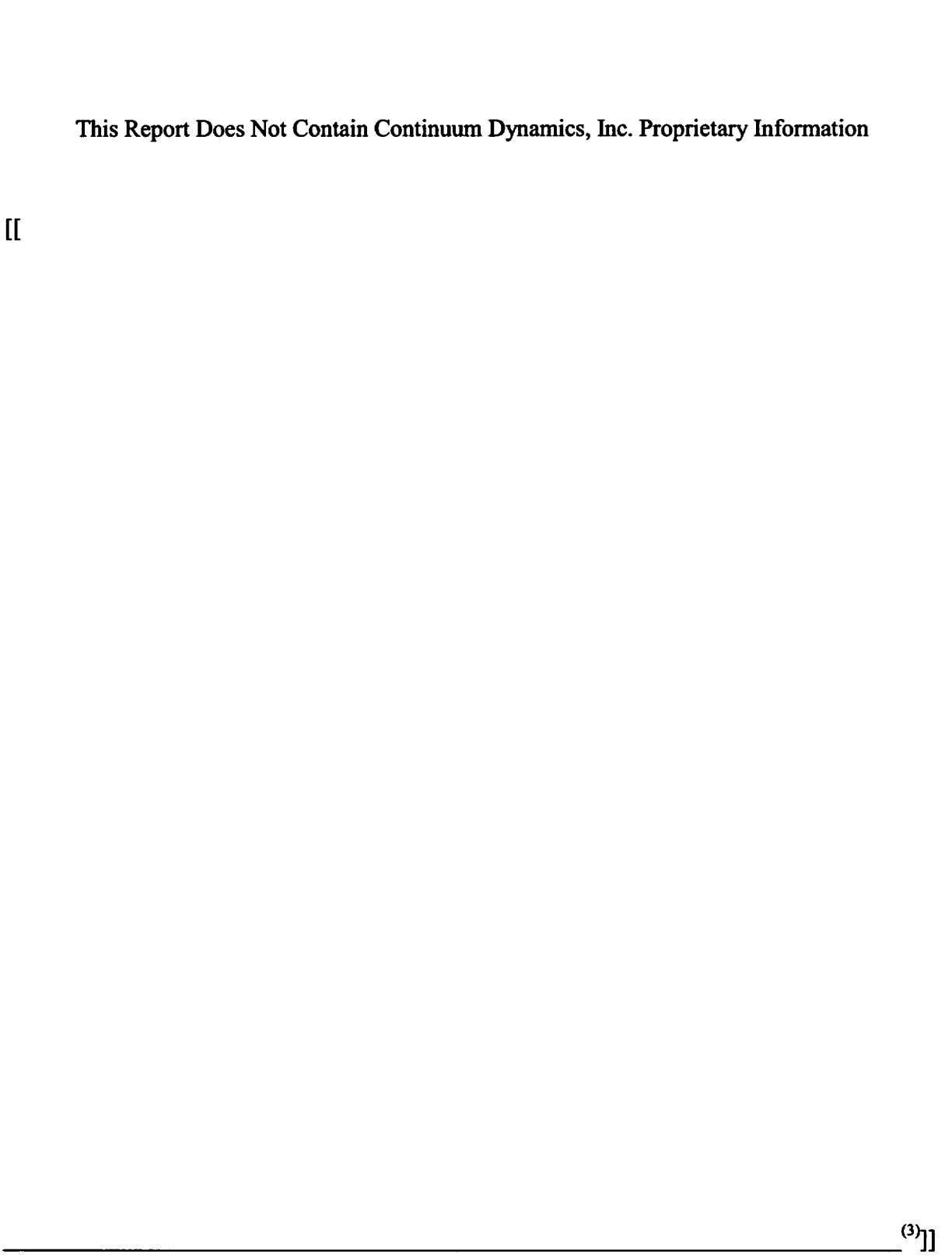

[3]]]

Figure C.9. PSD comparison at 930 MWe for pressure sensor data (blue curve), Bounding Pressure prediction (red curve), Bounding RMS prediction (black curve), and Bounding PSD prediction (green curve), for P9: 0 to 200 Hz (top), 135 to 165 Hz (bottom).

[[

[3]]]

Figure C.10. PSD comparison at 930 MWe for pressure sensor data (blue curve), Bounding Pressure prediction (red curve), Bounding RMS prediction (black curve), and Bounding PSD prediction (green curve), for P10: 0 to 200 Hz (top), 135 to 165 Hz (bottom).

[[

[3]]]

Figure C.11. PSD comparison at 930 MWe for pressure sensor data (blue curve), Bounding Pressure prediction (red curve), Bounding RMS prediction (black curve), and Bounding PSD prediction (green curve), for P11: 0 to 200 Hz (top), 135 to 165 Hz (bottom).

[[

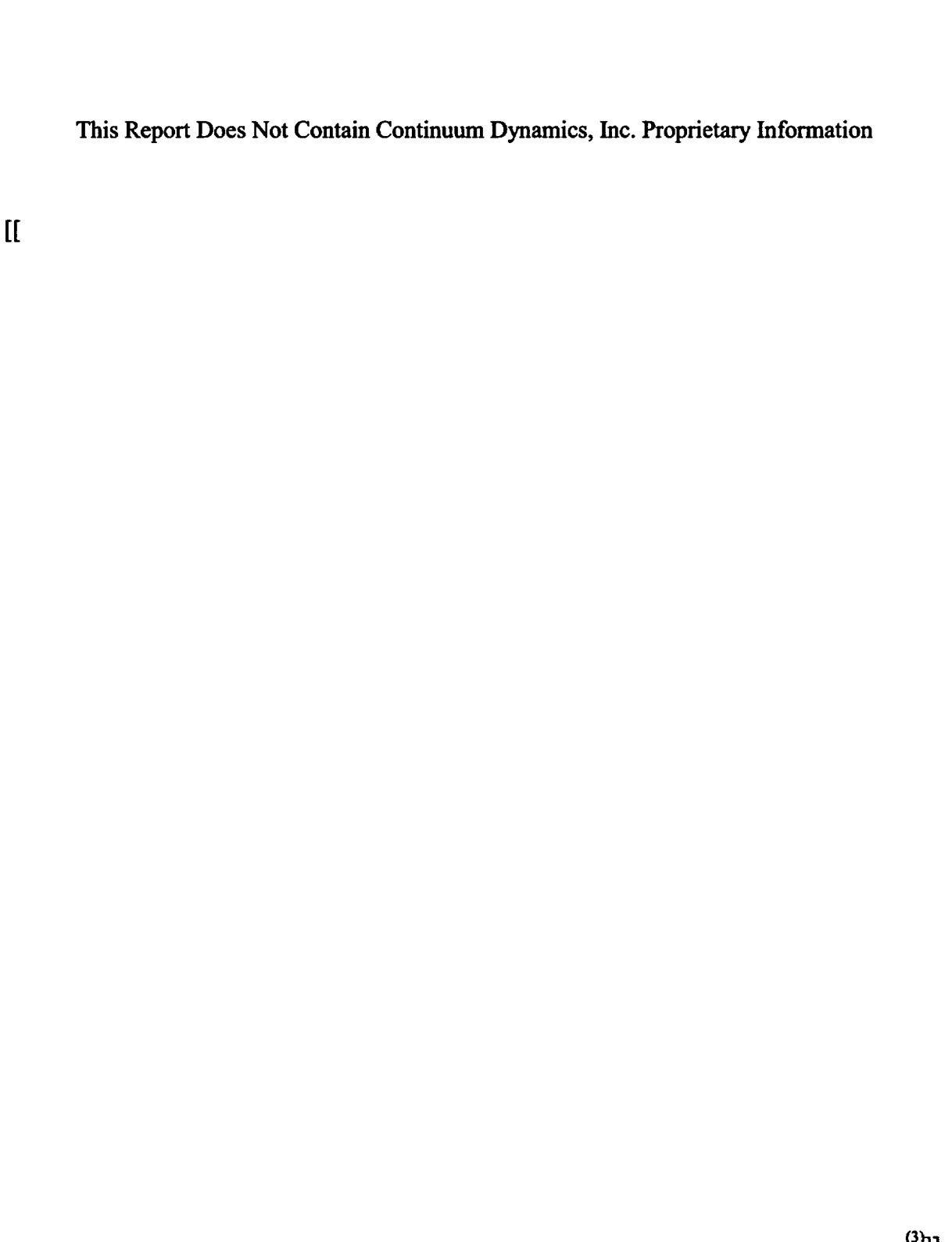

[3]]]

Figure C.12. PSD comparison at 930 MWe for pressure sensor data (blue curve), Bounding Pressure prediction (red curve), Bounding RMS prediction (black curve), and Bounding PSD prediction (green curve), for P12: 0 to 200 Hz (top), 135 to 165 Hz (bottom).

[[

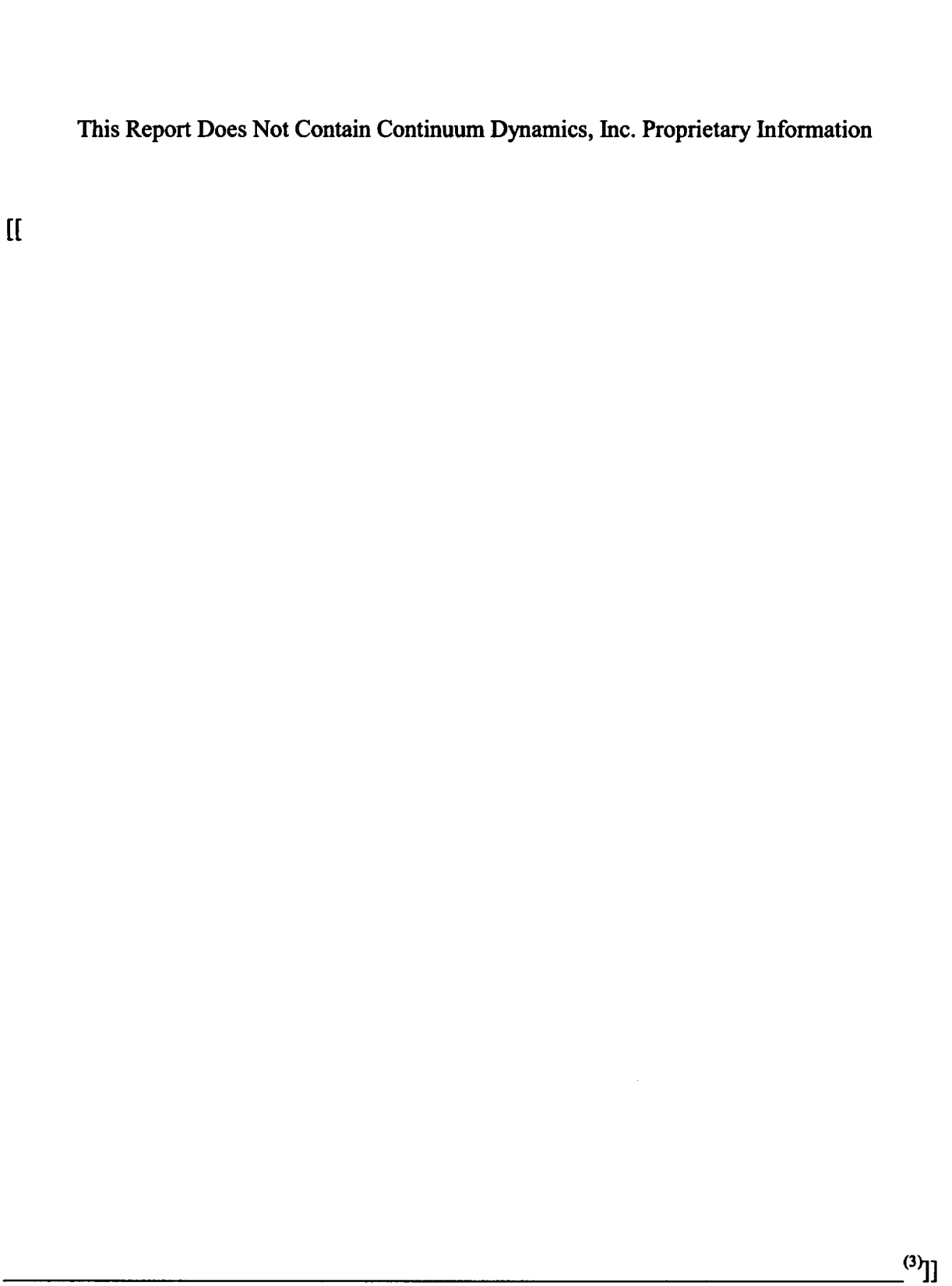

(3)]]

Figure C.13. PSD comparison at 930 MWe for pressure sensor data (blue curve), Bounding Pressure prediction (red curve), Bounding RMS prediction (black curve), and Bounding PSD prediction (green curve), for P13: 0 to 200 Hz (top), 135 to 165 Hz (bottom).

[[

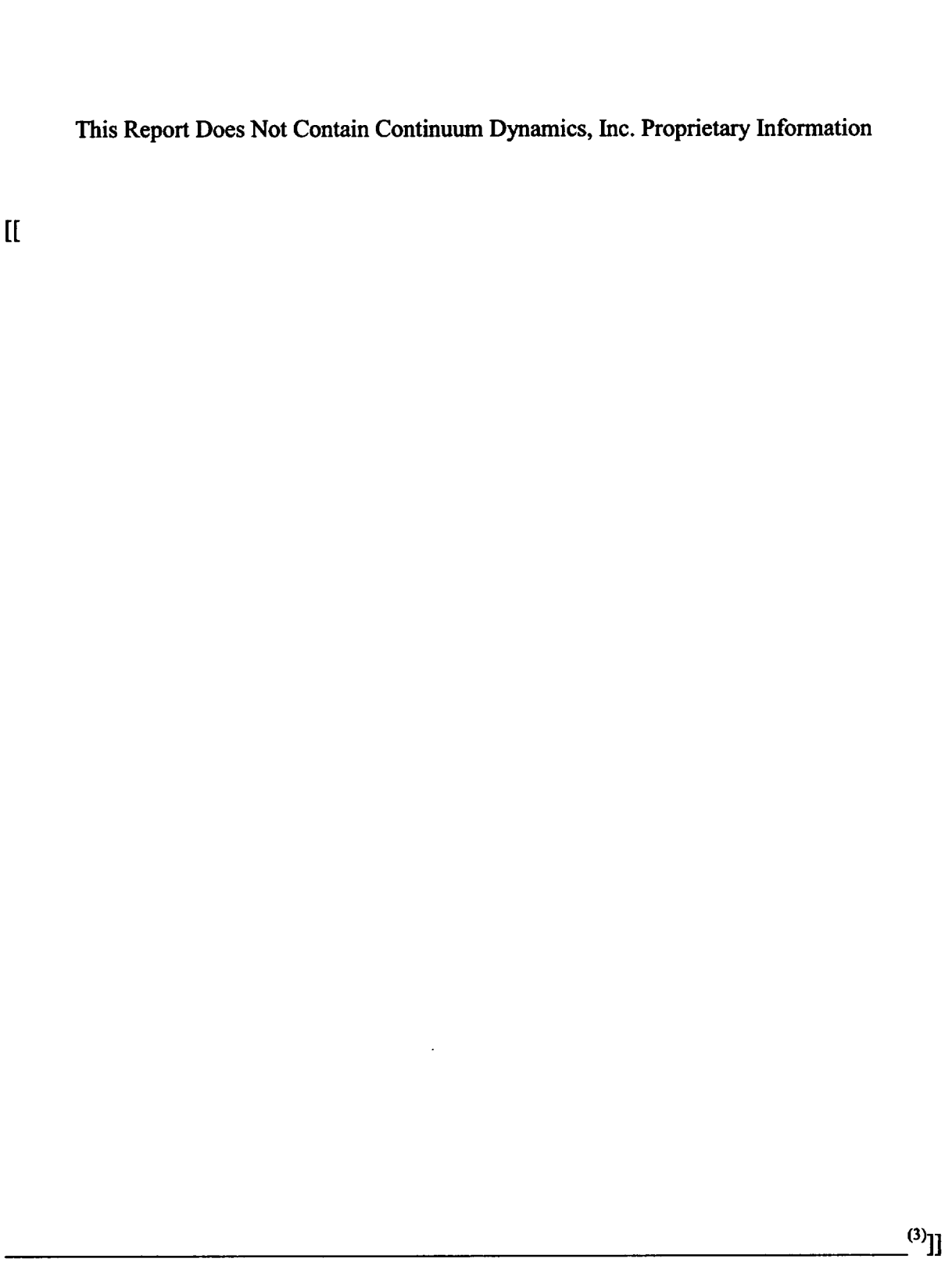

]][3]

Figure C.14. PSD comparison at 930 MWe for pressure sensor data (blue curve), Bounding Pressure prediction (red curve), Bounding RMS prediction (black curve), and Bounding PSD prediction (green curve), for P14: 0 to 200 Hz (top), 135 to 165 Hz (bottom).

[[

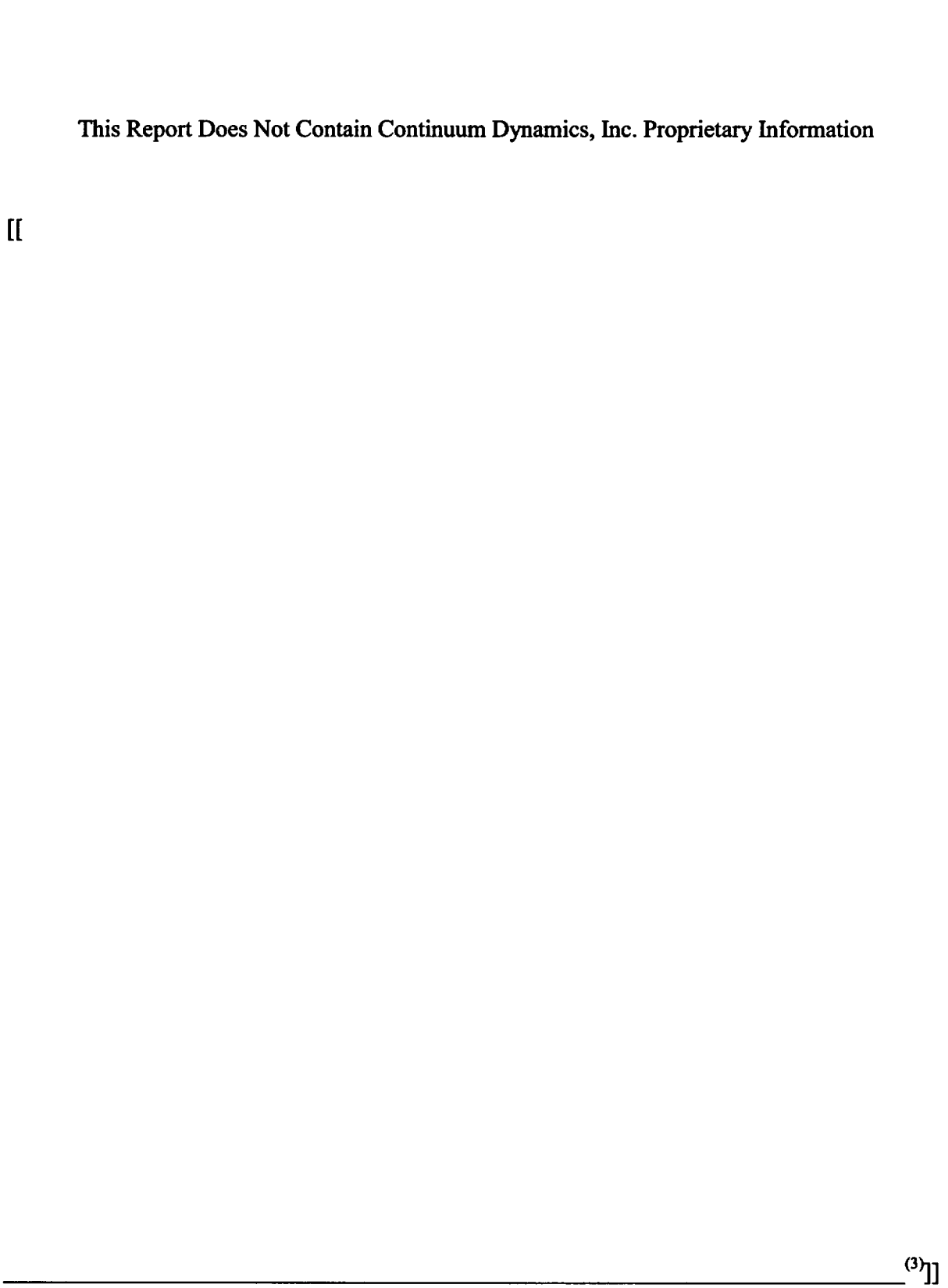

(3)]]

Figure C.15. PSD comparison at 930 MWe for pressure sensor data (blue curve), Bounding Pressure prediction (red curve), Bounding RMS prediction (black curve), and Bounding PSD prediction (green curve), for P15: 0 to 200 Hz (top), 135 to 165 Hz (bottom).

[[

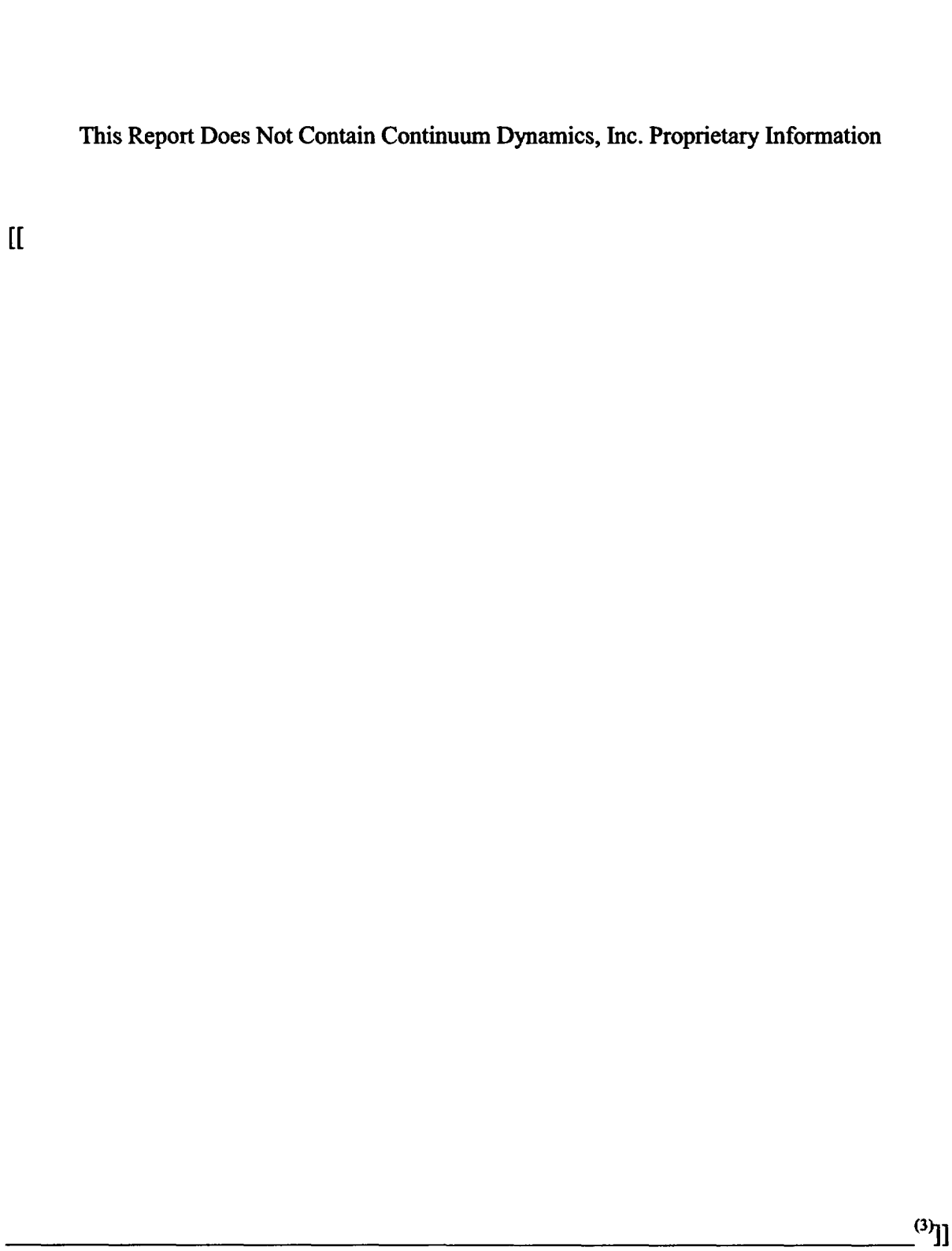

]]^(3)

Figure C.16. PSD comparison at 930 MWe for pressure sensor data (blue curve), Bounding Pressure prediction (red curve), Bounding RMS prediction (black curve), and Bounding PSD prediction (green curve), for P16: 0 to 200 Hz (top), 135 to 165 Hz (bottom).

[[

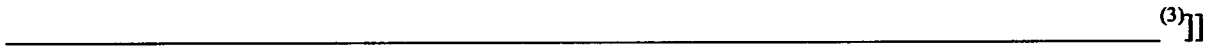

]]$^{(3)}$

Figure C.17. PSD comparison at 930 MWe for pressure sensor data (blue curve), Bounding Pressure prediction (red curve), Bounding RMS prediction (black curve), and Bounding PSD prediction (green curve), for P17: 0 to 200 Hz (top), 135 to 165 Hz (bottom).

[[

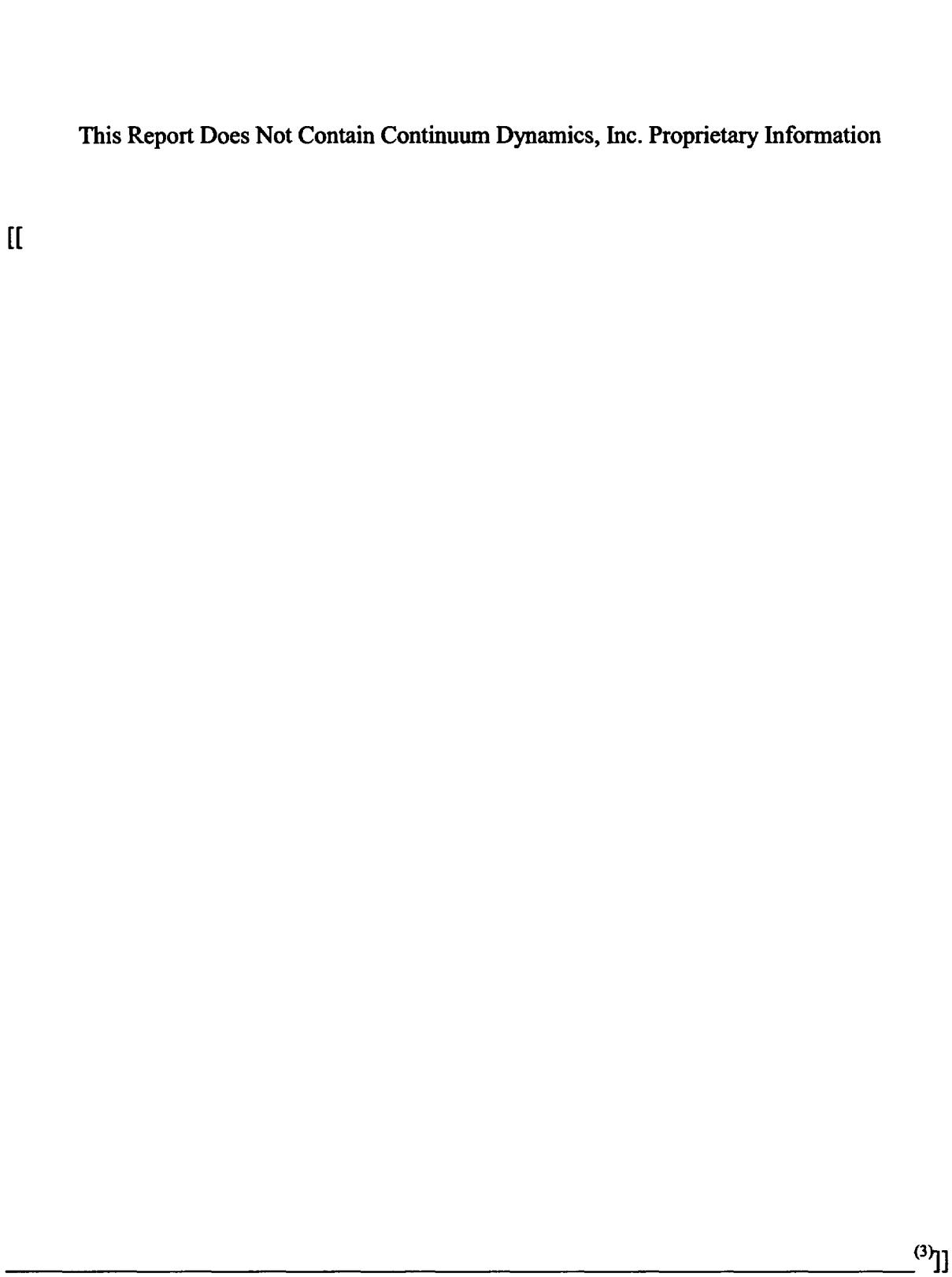

(3)]]

Figure C.18. PSD comparison at 930 MWe for pressure sensor data (blue curve), Bounding Pressure prediction (red curve), Bounding RMS prediction (black curve), and Bounding PSD prediction (green curve), for P18: 0 to 200 Hz (top), 135 to 165 Hz (bottom).

[[

]][3]

Figure C.19. PSD comparison at 930 MWe for pressure sensor data (blue curve), Bounding Pressure prediction (red curve), Bounding RMS prediction (black curve), and Bounding PSD prediction (green curve), for P20: 0 to 200 Hz (top), 135 to 165 Hz (bottom).

[[

[3]]]

Figure C.20. PSD comparison at 930 MWe for pressure sensor data (blue curve), Bounding Pressure prediction (red curve), Bounding RMS prediction (black curve), and Bounding PSD prediction (green curve), for P21: 0 to 200 Hz (top), 135 to 165 Hz (bottom).

[[

$^{(3)}$]]

Figure C.21. PSD comparison at 930 MWe for pressure sensor data (blue curve), Bounding Pressure prediction (red curve), Bounding RMS prediction (black curve), and Bounding PSD prediction (green curve), for P22: 0 to 200 Hz (top), 135 to 165 Hz (bottom).

[[

[3]]]

Figure C.22. PSD comparison at 930 MWe for pressure sensor data (blue curve), Bounding Pressure prediction (red curve), Bounding RMS prediction (black curve), and Bounding PSD prediction (green curve), for P23: 0 to 200 Hz (top), 135 to 165 Hz (bottom).

[[

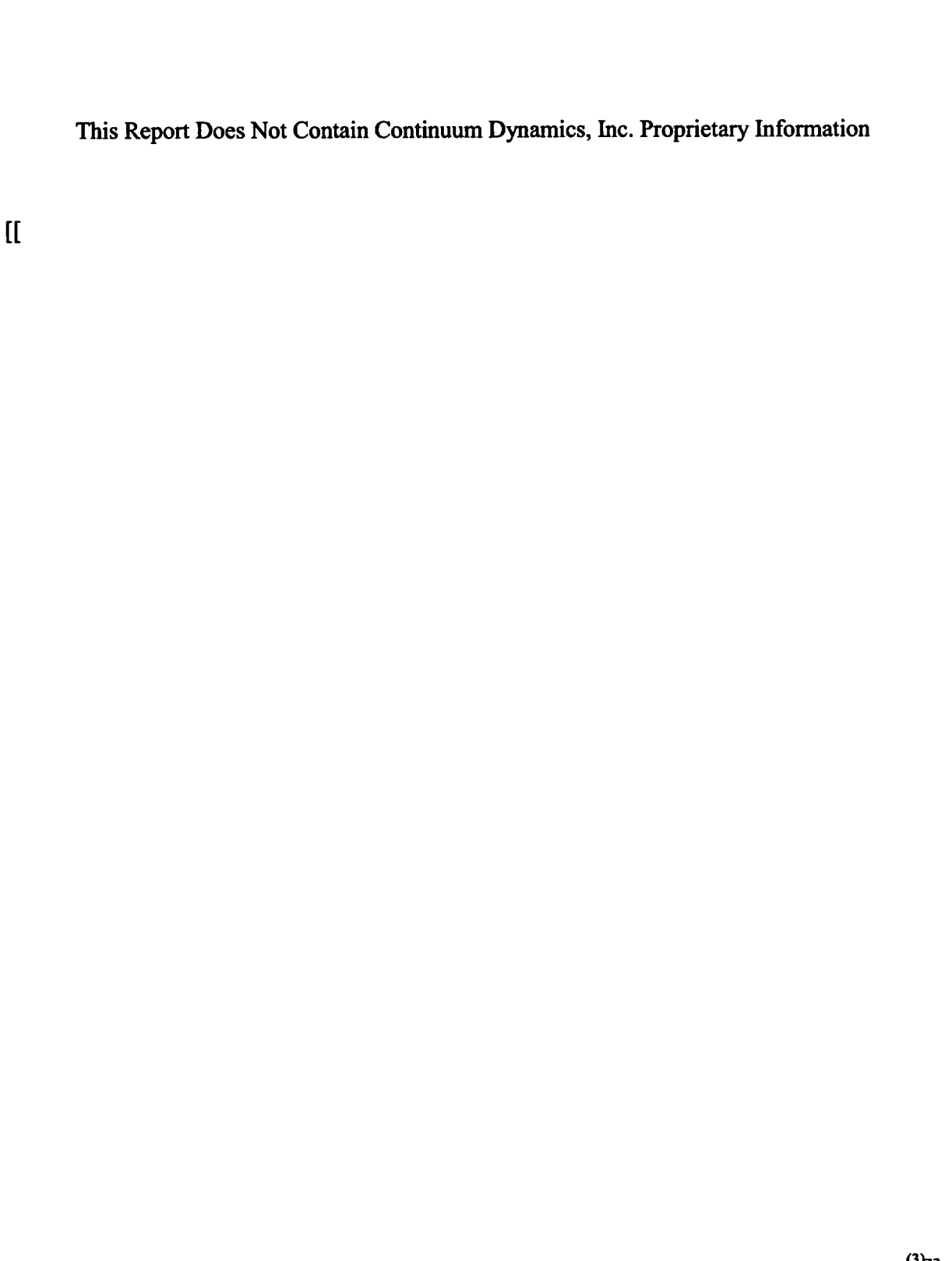

[3]]]

Figure C.23. PSD comparison at 930 MWe for pressure sensor data (blue curve), Bounding Pressure prediction (red curve), Bounding RMS prediction (black curve), and Bounding PSD prediction (green curve), for P24: 0 to 200 Hz (top), 135 to 165 Hz (bottom).

[[

]][3]

Figure C.24. PSD comparison at 930 MWe for pressure sensor data (blue curve), Bounding Pressure prediction (red curve), Bounding RMS prediction (black curve), and Bounding PSD prediction (green curve), for P25: 0 to 200 Hz (top), 135 to 165 Hz (bottom).

[[

(3)]]

Figure C.25. PSD comparison at 930 MWe for pressure sensor data (blue curve), Bounding Pressure prediction (red curve), Bounding RMS prediction (black curve), and Bounding PSD prediction (green curve), for P26: 0 to 200 Hz (top), 135 to 165 Hz (bottom).

[[

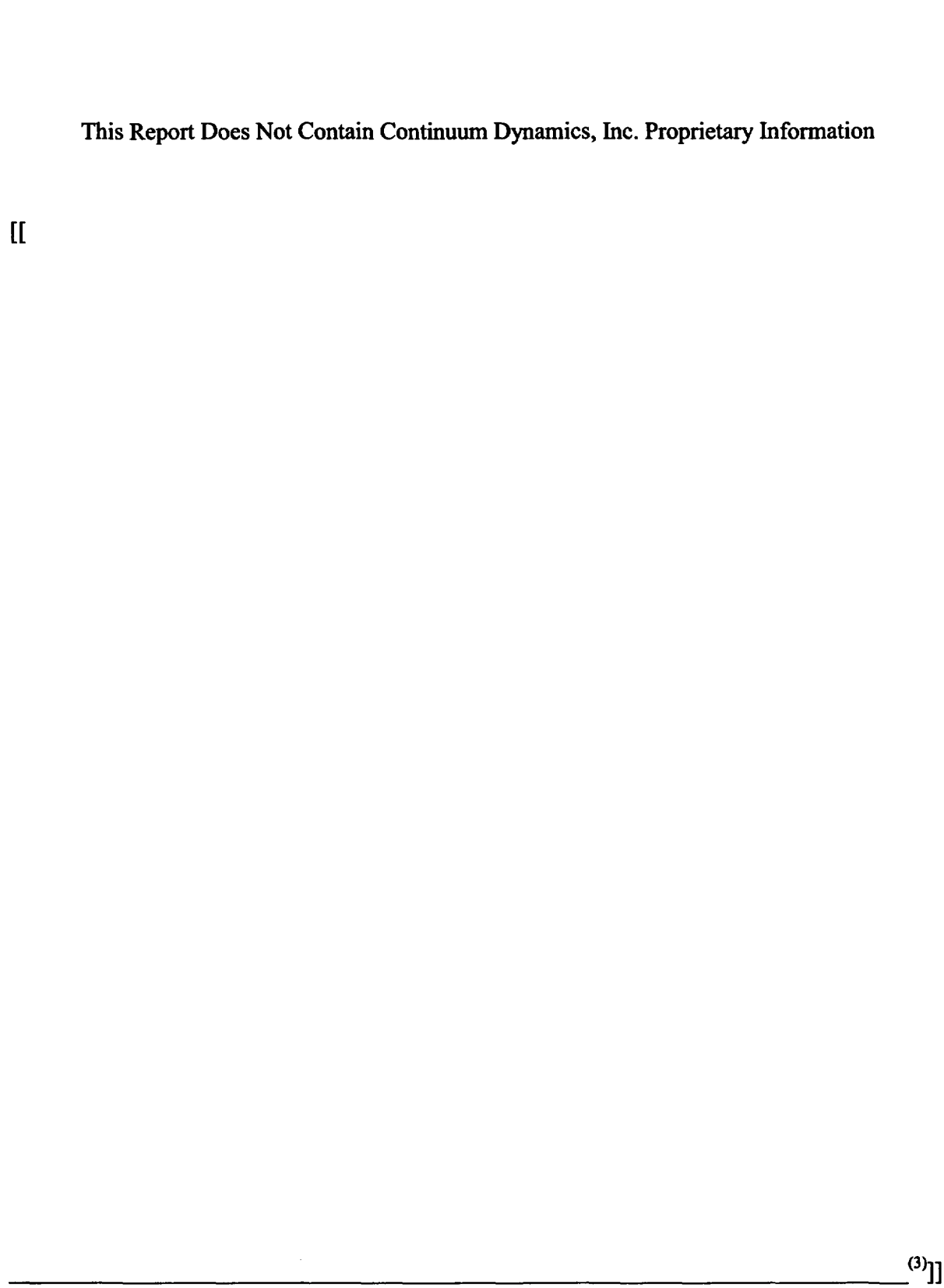

(3)]]

Figure C.26. PSD comparison at 930 MWe for pressure sensor data (blue curve), Bounding Pressure prediction (red curve), Bounding RMS prediction (black curve), and Bounding PSD prediction (green curve), for P27: 0 to 200 Hz (top), 135 to 165 Hz (bottom).

Appendix D: Reduction of Noise from In-Pipe Pressure Measurements

[[

]][3]

[[

]][3]

[[

[3]]]

[[

[3]]]

[[

]][3]